# Dynamic Modeling, Analysis, and Control of Integrated Electricity and District Heating Systems

by

Muhammad Abuelhamd Mahmoud Muhammad

A thesis
presented to the University of Waterloo
in fulfillment of the
thesis requirement for the degree of
Doctor of Philosophy
in
Electrical and Computer Engineering

Waterloo, Ontario, Canada, 2025

© Muhammad Abuelhamd Mahmoud Muhammad 2025

**Examining Committee Membership**

The following served on the Examining Committee for this thesis. The decision of the Examining Committee is by majority vote.

| | |
|---|---|
| Supervisor: | Claudio Cañizares<br>University Professor<br>Dept. of Electrical and Computer Engineering<br>University of Waterloo |
| Internal Member: | Mehrdad Kazerani<br>Professor<br>Dept. of Electrical and Computer Engineering<br>University of Waterloo |
| Internal Member: | Michael Fisher<br>Professor<br>Dept. of Electrical and Computer Engineering<br>University of Waterloo |
| Internal–External Member: | Roydon Fraser<br>Professor<br>Dept. of Mechanical and Mechatronics Engineering<br>University of Waterloo |
| External Examiner: | Chongqing Kang<br>Professor<br>Dept. of Electrical Engineering<br>Tsinghua University |

## Author's Declaration

I hereby declare that I am the sole author of this thesis. This is a true copy of the thesis, including any required final revisions, as accepted by my examiners.

I understand that my thesis may be made electronically available to the public.

# Abstract

Some of the main challenges with more efficient and cleaner energy systems include the development of Integrated Electricity and Heating Systems (IEHSs). Thus, the proposed research explores IEHSs in the context of Microgrids (MGs) and Bulk Power System (BPS), including the integration of Small Modular Reactors (SMRs) to provide both electricity and heat. In this context, the main goal is to study dynamics and control of IEHSs, with an emphasis on District Heating Networks (DHNs) for efficient energy use. Thus, the proposed work aims to support a cleaner energy transition in both remote communities and urban areas through the use of IEHSs, focusing on two key objectives, namely, developing a comprehensive dynamic models of a combined DHN and Electric Power Network (EPN) to study energy exchanges between these systems, and the provision of ancillary services for power grids for both BPSs and MGs.

A dynamic DHN and EPN model is first developed for MGs, considering all relevant heating and electricity system details, but especially soil limitations, extreme low temperatures, and piping insulation to minimize heat loss. The accurate sizing of the Heat Pumps (HPs) based on thermal load requirements, weather conditions, and consumer profiles is also discussed, proposing a demand management control to enhance MG primary frequency regulation, which facilitates the integration of variable Renewable Energy Sources (RESs) in power grids. The proposed dynamic models are applied, tested, and validated in a realistic community MG based on a remote community EPN located at Kasabonika Lake First Nation (KLFN) in Northern Ontario. It is shown that the DHN facilitates the proper integration of RESs in isolated MGs through the development of novel EPN control systems.

The presented research also studies IEHSs to serve a broader geographical region beyond MGs. Thus, it proposes to investigate the impacts of IEHSs on the dynamic operation of the BPS in collaboration with Ontario's Independent Electricity System Operator (IESO), using SMRs as the primary source for both electricity and thermal energy demand. For this purpose, a comprehensive dynamic model of a boiling water SMR power plant, incorporating all essential components, including the reactor, steam turbine, and steam flow control system, is first developed to evaluate its practical application in power grids. Unlike previous studies that focus on individual elements, this work proposes the first full-system model with direct steam expansion, capturing key thermal-hydraulic dynamics of the reactor, such as pressure variations and two-phase drift velocity, to improve simulation accuracy. The incorporation of a DHN is then studied, demonstrating that the reactor efficiency can be improved by enabling combined heat and power generation and the provision of ancillary services, which collectively would increase the overall performance and efficiency of the BPS.

The proposed SMR dynamic models are integrated into a widely used power system analysis tool to assess their dynamic performance and impact on Ontario's BPS. The results highlight the operational flexibility and frequency regulation potential of the BWRX-300, demonstrating its feasibility for practical deployment in modern power grids while also discussing the potential challenges of integrating it within large-scale power networks. Furthermore, the results of the SMR-based DHN models highlight the strong potential of SMRs for cogeneration applications, demonstrating their operational flexibility in practical settings and illustrating a significant reduction in energy consumption compared to heating systems based solely on HPs, which is the current trend.

# Acknowledgments

I would first like to express my sincere gratitude to my supervisor, Professor Claudio Cañizares, for his continuous support, guidance, and encouragement throughout my PhD journey at the University of Waterloo. His mentorship, both academically and personally, has been instrumental in shaping my research and professional growth. I am truly honored to have worked under his supervision and learned from his wealth of experience. I would also like to extend my appreciation to all the instructors who taught me during my coursework at the University of Waterloo. Their dedication and expertise provided a strong academic foundation that supported my research journey.

My heartfelt thanks go to my colleagues and friends who have made this journey more meaningful: Pablo, Ivan, Samuel, Carlos, Hediyeh, and many others whose support and camaraderie I will always cherish. I am especially grateful to my fellow researchers at the University of Waterloo for their collaboration and friendship.

I am especially thankful to my friends who have supported me along the way. In Canada, I am grateful to Mohsen and Aboelsood for their constant encouragement and companionship. In Egypt, my heartfelt thanks go to M. Elghazaly and M. Ibrahim, whose support from afar has meant a great deal to me. To my close friends back home, your encouragement and belief in me have been deeply appreciated, even across the distance. Special thanks to those who stood by me through the most difficult times.

I gratefully acknowledge the financial support provided by the Egyptian Cultural Office in Montreal, the Government of Egypt, and the University of Waterloo, which has made this research possible.

Above all, I dedicate this thesis to my family for their unwavering love and sacrifice. To the memory of my late parents, your values, strength, and prayers continue to guide me every day. To my beloved wife, Fatma, for her endless patience, encouragement, and strength. To my children, Kenan and Yazan, may this work one day inspire you to pursue your own dreams with passion and integrity. I am also deeply grateful to my brother and sisters for their unconditional love and continuous support throughout this journey.

## Dedication

To the memory of my mother and father.

# Table of Contents

**List of Figures** **xii**

**List of Tables** **xv**

**List of Abbreviations** **xvi**

**1 Introduction** **1**

1.1 Motivation . . . . . 1

1.2 Literature Review . . . . . 2

1.2.1 IEHS Dynamic Modeling of Microgrids . . . . . 3

1.2.2 BPS Dynamic Analysis and Control with SMRs . . . . . 6

1.2.3 SMR-based Cogeneration Dynamic Modeling and Control . . . . . 9

1.3 Objectives . . . . . 11

1.3.1 IEHS Modeling in MGs . . . . . 11

1.3.2 SMR Modeling . . . . . 11

1.3.3 SMR-based DHN Modeling . . . . . 12

1.4 Content . . . . . 12

**2 Background** **14**

2.1 Microgrids . . . . . 14

2.1.1 Components and Architecture . . . . . 15

2.1.2 Modeling and Control . . . . . 18

2.2 District Heating Network . . . . . 20
2.2.1 Components and Architecture . . . . . 20
2.2.2 Modeling and Control . . . . . 23
2.3 Integrated Electricity and Heating System . . . . . 24
2.3.1 Components and Architecture . . . . . 25
2.3.2 Modeling and Control . . . . . 27
2.4 Small Modular Reactors . . . . . 28
2.4.1 Natural Circulation BWSMR . . . . . 29
2.4.2 BWSMR Steam Turbine and Heat Extraction . . . . . 29
2.4.3 Control Strategies in SMRs . . . . . 31
2.5 NPP-based Cogeneration Systems . . . . . 32
2.6 Summary . . . . . 32

**3 Dynamic Model of Integrated Electricity and District Heating for Remote Communities 34**

Nomenclature . . . . . 34
3.1 DHN Model . . . . . 38
3.1.1 Household Model . . . . . 38
3.1.2 Pipeline Heat Loss . . . . . 40
3.1.3 Heat Exchanger . . . . . 42
3.1.4 Thermal Power Plant . . . . . 42
3.1.5 KLFN Community Example . . . . . 44
3.2 EPN Model . . . . . 54
3.2.1 Isolated Microgrid Dynamic Model . . . . . 54
3.2.2 Kasabonika Lake First Nation (KLFN) Community Example . . . . 57
3.3 Summary . . . . . 71

**4 Dynamic Modeling and Practical Application of Boiling Water Small Modular Reactor Power Plants 73**

Nomenclature . . . . . 74

4.1 BWSMR Modeling . . . . . 77

4.1.1 Point Kinetic Equations . . . . . 79

4.1.2 Thermodynamic Equations . . . . . 80

4.1.3 Mixture Void Formation . . . . . 80

4.1.4 Thermohydraulic Equations . . . . . 81

4.2 Steam Turbine . . . . . 82

4.2.1 High Pressure Turbine . . . . . 82

4.2.2 Moisture Separator . . . . . 83

4.2.3 Low Pressure Turbine . . . . . 83

4.3 Steam Flow Control . . . . . 84

4.4 Results and Discussion . . . . . 85

4.4.1 BWRX-300 Example . . . . . 85

4.4.2 BWRX-300 Primary Frequency Control . . . . . 89

4.4.3 SMR Versus Existing NPP Units . . . . . 95

4.5 Summary . . . . . 97

**5 Modeling and Control of a Boiling Water Small Modular Reactor Cogeneration System for District Heating Applications 100**

Nomenclature . . . . . 101

5.1 Dynamic Modeling of a Cogeneration System . . . . . 103

5.1.1 Steam Extraction . . . . . 103

5.1.2 Thermal Energy Storage . . . . . 104

5.1.3 Controls . . . . . 105

5.2 Results and Discussion . . . . . 107

5.2.1 DHN Near Darlington NPP . . . . . 109

5.2.2 Electrical Analysis . . . . . 112

5.2.3 Thermal Analysis . . . . . 114
5.2.4 Distributed HPs . . . . . 121
5.3 Summary . . . . . 122

**6 Conclusion and Future Work** **125**
6.1 Summary and Conclusions . . . . . 125
6.2 Contributions . . . . . 127
6.2.1 IEHS Modeling in MGs . . . . . 127
6.2.2 SMR Modeling . . . . . 128
6.2.3 SMR-based DHN Modeling . . . . . 128
6.3 Future Work . . . . . 129

**References** **130**

# List of Figures


2.1 MG architecture. . . . . 16
2.2 Architecture of MG hierarchical control. . . . . 19
2.3 DHN architecture. . . . . 21
2.4 IEHS architecture. . . . . 26
2.5 Schematic of natural circulation BWR. . . . . 30
2.6 Schematic of a BWSMR steam cycle with steam extraction for DHN and TES. . . . . 31

3.1 Electric equivalent circuit of the pipeline control volume. . . . . 41
3.2 Cross-sectional design of a DHN pipeline. . . . . 48
3.3 (a) Ambient temperature and temperature response of the thermal group located at the far end of the DHN, and (b) temperature response of the thermal power plant and the HP. . . . . 51
3.4 Thermal power demand, EG recovered power, piping heat loss, and HP generated power. . . . . 52
3.5 Heat balance between the thermal supply and demand of the KLFN DHN. 53
3.6 Power fluctuation of PV panels, with a sudden trip at about 50 s. . . . . 58
3.7 KLFN Community IEHS. . . . . 59
3.8 Droop control for DGU and HP IM. . . . . 61
3.9 Comparison of frequency response with and without DHN and HP droop control. . . . . 63
3.10 Generator power, HP shaft power, and shaft speed with frequency changes. 64

3.11 Generator power, HP shaft and thermal powers, base electric load, and HP's COP. . . . . 64
3.12 Temperature response of the thermal group located at the far end of the DHN after HP thermal power reduction imposed by the secondary frequency control. . . . . 65
3.13 Schematic of building heating with ETS unit. . . . . 67
3.14 Comparison between DHN and ETS units for thermal demand provision. . 68
3.15 Comparison of frequency response between IEHS and EPN with ETS units. 69
3.16 Comparison of primary frequency control response between IEHS and EPN with ETS units for a step load increase: (a) electrical power and (b) frequency. 70
3.17 IEHS secondary frequency control under overlapping RES and load fluctuations. . . . . 71

4.1 Schematic of BWRX-300 power plant. . . . . 86
4.2 Thermal and electrical power output of the simulated 300 MW BWRX-300 power plant under varying load conditions. . . . . 90
4.3 Frequency response under varying load conditions. . . . . 91
4.4 Fuel temperature response under varying load conditions. . . . . 92
4.5 Generated steam pressure and temperature response under varying load conditions. . . . . 93
4.6 Reactivity response under varying load conditions. . . . . 93
4.7 HPT and reheater temperature response under varying load conditions. . . 94
4.8 The mass flow rates of the MSI valve, the BP valve, and the RPV inlet mass flow rate under varying load conditions. . . . . 94
4.9 Frequency response of BWSMR and existing NPP units during a three-phase fault contingency near the Darlington plant. . . . . 96
4.10 Voltage response of BWSMR and existing NPP units during a three-phase fault contingency near the Darlington plant. . . . . 97
4.11 Power response of BWSMR and existing NPP units during a three-phase fault contingency. . . . . 98
4.12 Turbine mechanical power for the BWSMR units during a three-phase fault contingency. . . . . 99

5.1 Schematic representation of the proposed steam extraction-based DHN model. 104
5.2 Schematic of BWRX-300-based CHP. . . . . 108
5.3 DHN layout near Darlington NPP: (a) Baseline Area and (b) expanded areas. 110
5.4 Dynamic response of electrical and mechanical power output of the BWRX-300 power plant during dispatch transitions. . . . . 113
5.5 ES and BP valve mass flow rates during dispatch reduction in the BWRX-300 power plant. . . . . 114
5.6 Stability of steam pressure and temperature in the BWRX-300 reactor under fluctuating dispatch conditions. . . . . 114
5.7 Temperature profiles of four rooms in a household supplied by the DHN. . 115
5.8 DHN supply and return water temperatures variation. . . . . 116
5.9 Thermal power demand and central aggregated HP operation under different ambient temperature conditions. . . . . 116
5.10 TES temperature and energy variation during charging and discharging cycles. 117
5.11 Mass flow rate of ES directed to the DHN and TES under varying dispatch conditions. . . . . 117
5.12 Thermal power profiles: (a) Power components and (b) power balance. . . 119
5.13 Thermal Energy profiles: (a) Energy components and (b) energy balance. . 120
5.14 Temperature profiles of different household rooms supplied by the distributed HPs. . . . . 122
5.15 Aggregated electrical and thermal power of the distributed HPs. . . . . 123
5.16 Total electrical energy consumption comparison between the central and distributed HPs over three days. . . . . 124
5.17 Comparison of cumulative thermal demand energy supplied by the BWSMR-based DHN and distributed HPs over a 72 h period. . . . . 124

# List of Tables


2.1 Evaluation of Heating Systems . . . . . 22

3.1 Piping Network Design Parameters . . . . . 47
3.2 Pipeline Layers' Diametrical Ratios for Figure 3.2 in KLFN . . . . . 49
3.3 EG Recovery System Data for Different DGU Loadings . . . . . 49
3.4 KLFN Thermostat Temperature Setpoints . . . . . 50
3.5 HP IM Drive Parameters . . . . . 56
3.6 KLFN Generator Ratings . . . . . 60
3.7 KLFN Load Types and Powers . . . . . 60
3.8 ETS Demand Response Control Parameters . . . . . 66

4.1 Parameters for Modeling Kinetic Equations . . . . . 87
4.2 BWRX-300 Dimensions and Rated Conditions . . . . . 88
4.3 Heat Transfer Coefficients at Rated Conditions . . . . . 89
4.4 HPT and LPT Parameters . . . . . 89

5.1 House Areas in B1 . . . . . 111
5.2 Block Areas in the Baseline DHN . . . . . 112

# List of Abbreviations

| | |
|---|---|
| **ADN** | Active Distribution Network |
| **BOP** | Balance-Of-Plant |
| **BP** | Bypass |
| **BPS** | Bulk Power System |
| **BWR** | Boiling Water Reactor |
| **BWSMR** | Boiling Water Small Modular Reactor |
| **CFHX** | Counter Flow Heat eXchanger |
| **CHP** | Combined Heat and Power |
| **COP** | Coefficient Of Performance |
| **DER** | Distributed Energy Resource |
| **DG** | Distributed Generation |
| **DGU** | Diesel Generation Unit |
| **DHN** | District Heating Network |
| **EG** | Exhaust Gas |
| **EMS** | Energy Management System |
| **EPN** | Electric Power Network |

| | |
|---|---|
| **ES** | Extracted Steam |
| **ESS** | Energy Storage System |
| **ETS** | Electric Thermal Storage |
| **FMCRD** | Fine Motion Control Rod Drive |
| **GE** | General Electric |
| **GHG** | Greenhouse Gas |
| **GIS** | Geographic Information Systems |
| **HP** | Heat Pump |
| **HPT** | High Pressure Turbine |
| **HVAC** | Heating, Ventilation, and Air Conditioning |
| **HX** | Heat eXchanger |
| **IEHS** | Integrated Electricity and Heating System |
| **IESO** | Independent Electricity System Operator |
| **IM** | Induction Motor |
| **IPWR** | Integrated Pressurized Water Reactor |
| **KLFN** | Kasabonika Lake First Nation |
| **LPT** | Low Pressure Turbine |
| **LV** | Low Voltage |
| **MG** | Microgrid |
| **MGCC** | Microgrid Central Controller |
| **MSI** | Main Steam Inlet |
| **MV** | Medium Voltage |

| | |
|---|---|
| **NPP** | Nuclear Power Plant |
| **OPG** | Ontario Power Generation |
| **PCC** | Point of Common Coupling |
| **PI** | Proportional-Integral |
| **PV** | Photovoltaic |
| **PWR** | Pressurized Water Reactor |
| **QOS** | Quality Of Service |
| **RES** | Renewable Energy Source |
| **RPV** | Reactor Pressure Vessel |
| **SMR** | Small Modular Reactor |
| **SRLS** | Smart Residential Load Simulator |
| **TES** | Thermal Energy Storage |
| **TRV** | Thermostatic Radiator Valve |
| **VSC** | Voltage Source Converter |
| **WG** | Wind Generator |

# Chapter 1

# Introduction

## 1.1 Motivation

The global shift towards achieving net-zero carbon emissions is a global priority. Canada is aligning with this commitment by targeting zero $CO_2$ emissions by 2050 [1, 2]. Thus, this thesis is motivated by the role that Integrated Electricity and Heating Systems (IEHSs) can play in supporting Canada's decarbonization strategy, especially in the contexts of both remote Microgrids (MGs) and the Bulk Power Systems (BPSs). The research is centered around three interconnected components: enhancing IEHSs for remote communities, developing accurate dynamic models and control strategies for Small Modular Reactors (SMRs), and exploring the integration of SMR-based cogeneration systems within urban-scale IEHSs.

In remote northern communities, where access to clean energy is limited and thermal demand is high, the deployment of IEHSs presents a transformative opportunity. These communities typically rely on Diesel Generation Units (DGUs), which not only contribute to high Greenhouse Gas (GHG) emissions but also accelerate local environmental impacts, such as ice melting due to soot and black carbon [3]. District Heating Networks (DHNs), which provide centralized heat to multiple buildings, offer a promising solution to meet the communities' thermal needs efficiently by utilizing various energy sources [4, 5]. Although DHNs may involve higher upfront costs, their long-term benefits in terms of scalability, efficiency, and emission reduction make them an attractive option, especially in harsh climates [6–8]. In this context, this thesis focuses on developing a detailed dynamic model of the IEHS for remote MGs, considering waste heat recovery from DGUs and robust control strategies to enhance MG's stability and energy management, particularly in scenarios involving high penetration of Renewable Energy Sources (RESs).

The thesis also focuses on the development of high-fidelity dynamic models and advanced control strategies for SMR power plants, which are gaining global traction as a viable clean energy source. Unlike traditional large nuclear plants, an SMR plant offers operational flexibility, enhanced safety, and the ability to provide grid services such as frequency regulation [9]. Several recent studies have highlighted the viability of SMRs in terms of siting, carbon policy impacts, and system integration [10–12]. Thus, the Ontario Power Generation (OPG) in partnership with the Independent Electricity System Operator (IESO) is planning to deploy North America's first Boiling Water Small Modular Reactor (BWSMR) at the Darlington site by 2029 [13]. To support proper integration of these SMRs into the BPS, the presented research models the dynamics of BWSMRs and study control strategies under various operating conditions.

Finally, the thesis investigates SMR-based cogeneration as part of an urban IEHS, since integrating an SMR with a DHN can enhance system efficiency and reactor stability by supplying thermal loads alongside electricity generation [14]. In this context, the IESO is exploring the feasibility of using these units to meet local heating demands. Hence, given the potential of SMRs to improve grid flexibility and support decarbonization, this research aims to evaluate the dynamic performance and grid impact of SMR-based cogeneration within urban IEHSs.

In summary, the motivation for this thesis is address Canada's decarbonization challenges through the design, modeling, and integration of advanced IEHSs. By developing solutions for remote MGs, modeling the dynamics of SMRs, and studying the benefits of SMR-based cogeneration, the presented research contributes to the transition towards sustainable, low-carbon energy systems.

## 1.2 Literature Review

An extensive and critical examination of the relevant literature on the core subjects relevant to the research is presented here. The areas of interest include MG dynamic stability and control with RESs integration, SMR modeling and control in the context of BPS, and dynamics and control for SMR-based cogeneration systems. The main aim is to identify relevant gaps in the existing research in these areas, which will be the main focus of the thesis.

### 1.2.1 IEHS Dynamic Modeling of Microgrids

Recently, there has been a growing trend towards electrical and thermal systems integration to form IEHSs, in order to achieve optimal operation of the combined systems and minimize GHG emissions [15]. However, dynamic modeling studies of IEHSs with DHNs and Electric Power Network (EPN) are limited, especially for MGs, which are necessary to properly understand and demonstrate the viability of IEHSs for remote communities.

#### 1.2.1.1 Ancillary Service Provision with DHNs in Microgrids

There are various references in the literature discussing the DHN and its benefits for frequency regulation. For example in [16], the authors study a combined SMR and DHN to manage electric load fluctuations in isolated EPNs, enhancing RES integration and grid stability. However, the study does not consider the DHN's secondary circuit dynamics, using 15 min resolution that does not allow to consider primary frequency regulation issues. Reference [17] analyzes the dynamic operability of interconnected Combined Heat and Power (CHP) plants in DHNs, but the models utilized are not detailed enough to properly represent EPNs in the context of IEHSs. The authors in [18] propose a model-based approach to assess the potential of power-to-heat assets for frequency regulation in Active Distribution Networks (ADNs), which is relevant to MGs. However, the simplified representation of the DHN in the case study does not fully capture the necessary IEHS dynamics. In [19], a state space model is proposed to represent large-scale Heat Pumps (HPs) in DHNs, enabling performance evaluation of local frequency control methods, highlighting the HPs promising role in IEHS, but there is no proper modeling of the EPN to study the required IEHS dynamics relevant to frequency control.

#### 1.2.1.2 DHN Dynamic Modeling

While DHNs involve higher initial costs, their scalability and long-term savings make them attractive to improve energy efficiency. This is particularly true for remote, northern communities, which have significant thermal loads associated with their northern location and have a pressing need for the integration of RESs into their EPN to significantly reduce emissions, as discussed in [3]. This is an urgent concern for these communities, where the rate of warming is 3 to 4 times that of the rest of the planet, with local emission and soot from DGUs having a direct impact on ice melting. Thus, in these communities, DHNs are regarded as an attractive solution to supply their thermal needs. For example, the authors in [6] study implementing biomass-driven DHNs in northern remote and rural

communities, demonstrating that biomass-driven DHNs offer economic benefits for remote and rural energy systems. In [7], the estimated cost of delivering heat through biomass-driven DHNs is shown to be lower than the estimated price of fuel oil in rural villages. In [8], the authors analyze a CHP MG for remote communities, integrating renewable energy to reduce diesel consumption and energy costs. These papers explore the economic feasibility of implementing DHNs in remote communities; however, there is a notable gap in addressing the dynamic feasibility and challenges of DHNs in such areas, which is the focus of this thesis.

Implementing DHNs in remote communities presents unique challenges due to geographical isolation, harsh environmental conditions, and limited infrastructure. Despite these difficulties, the idea is gaining traction, with several pilot projects demonstrating its feasibility. For instance, the U.S. Department of Energy supports isolated communities with geothermal DHN projects, like the one in Nome, Alaska, aimed at reducing carbon pollution and lowering utility bills. These projects show that, although in its early stages, DHNs can provide sustainable and efficient heating solutions for remote areas [20].

The operation of the DHN in remote communities encompasses special considerations such as piping network design, insulation requirements, burial depth specifications, and the unique challenges posed by low linear heat density and extremely cold ambient temperatures. Thus, an accurate assessment of DHN feasibility in remote regions necessitates a thorough understanding of the DHN detailed dynamic modeling. In this context, the thesis aims to investigate the dynamic modeling of utilizing waste energy from a diesel engine's exhaust to power a DHN in remote communities, considering that existing static and optimization models, like these proposed, for example, in [8], lack the ability to properly represent the piping network characteristics and thermal loads' capacity within the DHN. Furthermore, dynamic modeling allows to study the integration of HPs, considering their ratings and the required number of units to meet thermal demands, along with comprehensive design considerations for all DHN components in remote communities. Therefore, the dynamic studies presented here are a novel contribution to the existing literature, as detailed dynamic operation of DHNs in remote communities has not been addressed previously. It's important to note that the thesis does not address the economic aspects of DHNs in remote communities, which can be found in the existing literature.

#### 1.2.1.3 IEHS Dynamic Modeling

There has been a growing trend towards electrical and thermal systems integration to achieve optimal operation of the combined systems and minimize GHG emissions [21]. Therefore, the presented work also aims to study the integration of DHNs with the EPN

in remote communities, facilitating efficient energy exchange between the two networks by managing HP demand to provide frequency control for the EPN while ensuring the required Quality Of Service (QOS) for DHN customers, which has not been studied in the existing literature for remote MGs. Assessing the QOS in a DHN, particularly under secondary frequency control, requires developing a detailed dynamic model of the DHN to accurately incorporate the characteristic of the DHN, particularly in remote communities where DGUs are redispatched every 15 min [22]. This interval is significant for the DHN, particularly in the presence of HPs.

Dynamic modeling studies of IEHSs including DHNs and EPNs are limited, especially for remote MGs, as previously mentioned. Furthermore, the benefits of DHNs for remote communities, where waste heat from DGUs can be exploited, has not been reported in the context of MGs while considering the DHN dynamics. Thus, several studies have explored diverse strategies aimed at reducing GHG emissions while simultaneously providing ancillary services when integrating DHNs in EPNs based on static DHN models. For example, in [23], a control strategy for a DHN is developed to minimize electric energy consumption from pumping in the Dark Landing Solar Community in Alberta, aiming to reduce GHG emissions associated with fossil fuel-based electricity generation in remote MGs. The authors in [14] introduce a co-generation system using an SMR for district heating and frequency regulation in the presence of variable RESs. Different case studies are discussed in [24], where the potential of DHNs to provide balancing services in the European Union is explored. Reference [25] demonstrates that distributed circulating pumps with variable speed motors are more efficient than central circulating pumps, indicating the possibility of saving electric energy for ancillary reserve power in EPNs. All these references are based on static DHN models suitable for dispatch studies, without accounting for relevant DHN dynamic behavior impacting the EPN in IEHSs.

A dynamic model of an IEHS is crucial for proper system integration, particularly control and energy management. To accurately represent the dynamic response of combined heating and electricity systems, it is necessary to model each major component individually and interconnected, especially for remote communities where the extreme cold temperatures present challenges for the control and operation of DHNs; in fact, existing models oversimplify crucial dynamics. For instance, in [26], an equivalent circuit model for the DHN is proposed without considering relevant dynamics like pipe losses and thermal energy storage in pipe insulators. In [27], the authors introduce an integrated heat and power dispatch model without fully accounting for piping insulation systems or the thermal inertia of consumers. Reference [28] develops a non-iterative equivalent model for the IEHS, focusing solely on the DHN primary circuit and simplifying the representation of the secondary circuit. In [29], the DHN model also neglects the representation of piping

insulation. Moreover, references [26–29] provide the thermal demand as a total aggregated demand, which overlooks the need for disaggregation to understand DHN operations and the impact of thermal fluctuations on the QOS for consumers. Finally, all these references consider a time resolution of hours, which is not sufficient to test the interaction of the DHN and EPN systems to properly understand the relevant dynamics of the IEHS studied in this thesis.

### 1.2.2 BPS Dynamic Analysis and Control with SMRs

#### 1.2.2.1 Nuclear Power Plants for Ancillary Services Provision

A dynamic simulation platform is developed in [30] using Matlab/Simulink to examine the frequency control characteristics of the AP1000 Pressurized Water Reactor (PWR) Nuclear Power Plant (NPP). The paper assesses the frequency response during typical step-load transients that do not require steam dumping or rapid power reduction systems. Dynamic modeling and control issues related to gas turbine NPPs are investigated in [31]. The main objective is to assess the impact of ramp load changes on the stability of advanced NPP facilities, studying load frequency control and temperature control strategies for a load-following NPP based on dynamic models and controller designs. The authors in [32] present an elaborate model of a PWR NPP to assess the transient stability of power systems. The model serves as a valuable reference for examining the dynamic interaction between NPPs and power systems.

As mentioned in [33], NPPs face challenges due to their inflexibility as base-load power sources, making it difficult for them to participate in and profit from peak-shaving services in the electricity market. To overcome this, the paper proposes an electro-thermal coupled model that integrates nuclear power unit characteristics with electric heat storage technology, enabling more effective responses to varying electricity demand and price fluctuations while maximizing profit. However, the primary emphasis is on static modeling for optimal operation rather than the dynamic response of the NPP as an ancillary service provider. On the other hand, the authors in [30], [31], and [32] propose dynamic models for various NPP designs to assess their ability to supply ancillary services to the power system. However, these papers oversimplify or neglect the power grid, which results in an inaccurate representation of BPS dynamics.

#### 1.2.2.2 Dynamic Modeling and Control of SMRs

SMRs are considered the future of nuclear energy, offering clean, reliable power, and potential district heating ancillary services for both urban and remote communities [9], since unlike large nuclear reactors they have the capacity to provide frequency regulation services. Thus, SMRs are recognized for their cost-effectiveness and versatility in various applications. For instance, [10] examines the impact of carbon tax levels on the adoption and placement of SMRs in the United Kingdom; [11] compares the competitiveness of advanced SMRs with conventional nuclear reactors and fossil fuel-based power generation; and [12] presents an optimization model to improve SMR siting and deployment in grids with RESs, identifying large-capacity power stations with independent transmission grids as the preferred sites for SMRs.

Recognizing the aforementioned benefits, OPG, in collaboration with the IESO, plans to deploy North America's first BWSMR at the Darlington nuclear generating station by 2029 [13]. This will require understanding the dynamics of the BWSMR power plant to ensure its stable performance when integrated in a BPS, especially in grids with high penetration of RESs. However, existing research on a Boiling Water Reactor (BWR) power plant dynamics is limited, focusing primarily on reactor stability while neglecting the dynamic interactions between critical components such as the reactor, steam turbine, and steam flow control systems. Additionally, existing works, as shown next, often simplify thermal-hydraulic behavior and overlook the plant's capability to support primary frequency control and co-generation applications. Thus, the thesis addresses these gaps by, for the first time, developing a detailed and comprehensive dynamic model of the BWSMR power plant that integrates all major components, including the reactor, steam turbine, and thermal systems. The proposed model incorporates key thermal-hydraulic dynamics, such as pressure variations and two-phase drift velocity, which are critical for accurately simulating the plant's behavior under dynamic conditions. Furthermore, the study evaluates the primary frequency control performance under both reactor-leading and turbine-leading modes, revealing how each strategy affects the operation of a BWSMR power plant. The presented detailed modeling approach facilitates the reliable integration of BWSMRs into BPS, especially in the context of high RES penetration, and offers a robust foundation for future co-generation studies.

As mentioned, a few research papers propose incomplete models of the BWR power plant dynamics. For instance, a phenomenological nonlinear BWR model to predict limit cycle behavior and identify stable/unstable equilibrium points is presented in [34], which lacks the reactor pressure representation relevant for power plant studies. The model formulates ordinary differential equations for reactor kinetics, heat transfer, and thermal hydraulics, focusing on stability boundaries, but it does not consider the SMR grid inte-

gration. A subsequent quantitative model proposed in [35] includes the reactor pressure dynamics and addresses nonlinearities above the linear stability threshold, emphasizing BWR oscillations over standard operating conditions. In [36], two nonlinear models for the BWR are developed to determine its stability region, including the impact of temperature changes on reactivity. A BWR stability analysis is performed in [37], explaining the physical mechanisms behind BWR power oscillations from a nonlinear feedback perspective. Similarly, in [38], a stability analysis and nonlinear dynamics of natural circulation BWR is performed using a lumped parameter model. All these studies focus solely on the BWR stability and do not address the reactor behavior under various typical operating conditions, as part of a power plant in the context of power grids, which is the focus of the presented research.

A few research works discuss the dynamics of BWRs under normal operation conditions, overlooking critical aspects such as pressure variations and two-phase drift velocity, without adequately describing the reactor dynamics. For example, in [39], the author proposes a model for BWR dynamic behavior considering the fluid dynamics of a natural circulation system under both stable and unstable conditions. However, the short simulation times of 3 to 5 s are inadequate for testing the BWRs, which have slower response times due to their high thermal time constants and safety requirements. Additionally, the authors in [40] present a one-dimensional space-dependent dynamic analysis of BWR systems for forced or natural circulation, providing a relevant schematic diagram of a BWR power plant, but it overlooks crucial components such as the steam turbine and plant control systems as part of a power grid. In [41], a nonlinear model of the BWR derived from physical laws and empirical relations is linearized around an operating point and verified against experimental results. However, the model assumes a constant liquid-to-steam velocity ratio (slip) in the two-phase flow, which inadequately represents the impact of void reactivity on the BWR behavior. None of these references provide a comprehensive study of BWRs in the context of power system dynamics, which are addressed in the thesis.

A detailed dynamic modeling of the BWSMR for power system studies has not yet been reported in the literature. A limited number of research papers introduce oversimplified models for a BWRX-300, which is a tenth generation water-cooled, natural circulation SMR developed by General Electric (GE) Hitachi Nuclear Energy developed in collaboration with OPG for deployment in Ontario's BPS [42]. For example, a BWSMR study is presented in [43], where a BWRX-300 Balance-Of-Plant (BOP) is discussed, but the basic models of the steam turbine, power system, or control systems are not presented. In [44], the reliability of the BWRX-300 SMR's isolation condenser system for emergency cooling and pressure control is assessed, and in [45], a model of the BWRX-300 reactor is developed to simulate normal operation and emergency scenarios. However, both [44] and [45] do not

provide the necessary thermodynamic and thermohydraulic equations of the BWR model needed for power plant integration studies in BPS.

Other studies on SMRs have examined isolated aspects of their operation but fail to provide a unified framework for modeling a complete power plant. For instance, [46] focuses on steam turbine dynamics for conventional nuclear plants but lacks a reactor model, thermal-hydraulic coupling, and power system integration. While it provides detailed turbine expansion and valve control modeling, it does not consider the distinct operational characteristics of SMRs, such as rapid load-following and primary frequency regulation, which are services that conventional nuclear plants are not able to provide. Similarly, [47] presents a dynamic model for an Integrated Pressurized Water Reactor (IPWR) SMR, which differs fundamentally from BWSMRs in design and thermal-hydraulic behavior, with the latter utilizing direct steam expansion, while the former relies on a separate steam generator, which affects the transient response and frequency regulation characteristics. Additionally, [47] examines the SMR behavior in an isolated power grid, not considering its integration in large-scale and its impact on system-wide stability, focusing only on turbine-driven frequency regulation without analyzing reactor-leading frequency regulation services, which are needed for long-term power stability. Thus, neither [46] nor [47] capture the full operational complexity of SMRs in modern power grids.

### 1.2.3 SMR-based Cogeneration Dynamic Modeling and Control

SMRs and their integration with DHNs have gained significant attention due to their potential for decarbonization, grid flexibility, and enhanced load-following capabilities [48]. The growing interest on net-zero energy systems has led to extensive research on SMR deployment, covering aspects ranging from economic feasibility to system integration [49]. In fact, as mentioned previously, the OPG and the IESO are planning to deploy by 2029 North America's first BWSMR at Darlington, Ontario, Canada, to meet growing electricity demand [13]. In this context, the IESO is interested in determining the potential of these SMRs to also supply thermal demand in the region where the reactors are planned to be deployed, and to understand the impact of the DHN on the electrical performance of the facility, which is studied in the thesis.

Various studies investigate the economic feasibility, operational strategies, and potential applications of SMR-based DHNs, aiming to address existing research gaps. For instance, the authors in [50] investigate the role of cogeneration in enhancing the load-following capabilities of SMR-based NPPs, emphasizing that coupling these NPPs with auxiliary systems such as DHN enables efficient utilization of excess power during off-peak periods, improving both operational flexibility and economic viability. Similarly, the authors in [51]

analyze investment pathways for DHN decarbonization, demonstrating that SMR-based DHNs can be more cost-efficient than those relying on HPs. In [52], the authors introduce an SMR-based experimental reactor designed for small DHNs in northern climates, emphasizing its modular design for scalability and inherent safety to supply solely thermal demand.

In the context of SMR-based cogeneration operation, [53] proposes a method to maximize SMR cogeneration utilization for market feasibility, considering thermohydraulic models and economic objectives. Similarly, [54] explores integrating heat-only SMRs with DHNs and organic rankine cycle systems to improve the system's economic performance. The authors in [55] study the potential of SMR cogeneration to enhance MG resilience and reduce carbon emissions, offering a cleaner alternative to diesel generators. Reference [56] presents a coupled system model for nuclear CHP cycles, integrating a Heat eXchanger (HX) with the SMR secondary system, providing valuable insights into their preliminary design and optimization. Finally, [57] proposes a techno-economic optimization and sensitivity analysis of a natural circulation SMR-based DHN primary HX, highlighting key cost drivers, such as the Reactor Pressure Vessel (RPV) and containment vessel costs. References [50–57] focus on economic optimization, investment analysis, and operational feasibility, without considering relevant dynamic and control aspects of the DHN and EPN, which are crucial for fully understanding the feasibility of these cogeneration systems, since stability and transient behavior are important issues that should be analyzed. In this context, limited research in the existing literature focuses on considering the dynamic performance of SMR-based DHNs. For example, the authors in [16] develop an optimal operation model for a hybrid SMR-based cogeneration system integrated with RESs, involving coordinated controls to support load following and frequency regulation, which is then extended in [14] with a dynamic model for an SMR-based hybrid energy system that integrates electricity generation with a DHN. The latter includes a dynamic model of the reactor, with the DHN being represented using a quasi-static approach. However, this modeling approach, although insightful for basic operational understanding, overlooks key dynamics, including piping heat losses, thermal delays, and variations in thermal demand, as well as transient thermal responses and dynamic interactions within the DHN. This limits the model ability to accurately study the system's stability, and its transient thermoelectrical performance under fluctuating load conditions. Furthermore, the absence of an extended broader multi-timescale dynamic analysis restricts the model's ability to address both short-term dynamics (seconds to minutes), critical for transient stability, and long-term behavior (hours to days) necessary for understanding daily load variations.

## 1.3 Objectives

Based on the gaps identified in the literature, the main objectives of this thesis are presented next.

### 1.3.1 IEHS Modeling in MGs

- Develop dynamic models to analyze the feasibility and challenges of the use of waste energy from a diesel engine's exhaust to power a DHN for the provision of thermal heating in remote MGs, considering soil limitations, extreme cold temperatures, and the minimization of heat loss through proper piping insulation, as well as the proper sizing of HPs to meet thermal load requirements that account for weather conditions, the EPN characteristics, and the consumers' thermal needs.

- Design a control system for HP demand response to study the provision of reserve power for the EPN to enhance frequency control in remote MGs.

- Demonstrate the advantages of using DHNs for integration of variable RESs into the EPN of isolated MG to mitigate their adverse dynamic effects, based on a simulated model of a DHN and an actual model of an EPN at the existing KLFN remote community MG, including a comparison between centralized DHNs and decentralized Electric Thermal Storage (ETS) units to supply the community's thermal demand and regulate frequency through HP or ETS demand response strategies.

### 1.3.2 SMR Modeling

- Incorporate key thermal-hydraulic effects such as pressure variations and two-phase drift velocity in the proposed model of a BWSMR power plant, improving accuracy in transient conditions and ensuring better simulation fidelity.

- Propose a new equation to evaluate the impact of reactor pressure variations on the mass flow rate through the steam turbine, improving the understanding of turbine performance under dynamic conditions.

- Evaluate both reactor-leading and turbine-leading control strategies for frequency regulation studies, demonstrating their impact on grid stability and response to frequency deviations.

- Test and validate the BWSMR power plant model in a large-scale power system, using the Ontario BPS to demonstrate its real-world feasibility and impact on system stability.

### 1.3.3 SMR-based DHN Modeling

- Develop a cogeneration power plant integrated model based on a BWSMR, different from a previously proposed model for an IPWR.
- Represent piping heat losses, thermal delays, and variable thermal demand profiles to reflect practical and relevant operating conditions of BWSMR-based DHN systems.
- Integrate both transient electrical and thermal responses of BWSMR-based DHN systems to represent and understand the interdependency among the different components of the cogeneration system.
- Demonstrate the need for Thermal Energy Storage (TES) and HPs to facilitate the effective use of surplus SMR thermal power during low electric demand periods, and thus improve the SMR operation.
- Employ an extended broader multi-timescale dynamic analysis to evaluate system behavior for both short and long time frames, supporting robust control strategies and flexible system management.
- Demonstrate the application of the proposed models and control strategies of a potential BWSMR-based DHN in Darlington, Ontario, Canada, demonstrating their feasibility and effectiveness in real-world applications.

## 1.4 Content

Chapter 1 introduces the core motivations for the presented research, providing a comprehensive literature review of the key issues studied in the thesis, identifying the main gaps addressed in the presented work and the associated main objectives. Chapter 2 provides the necessary background for the thesis, including foundational concepts related to MGs, DHNs, IEHSs, and SMRs, setting the stage for the modeling and control work presented in later chapters.

Chapter 3 discusses the modeling and control of IEHS in remote communities, highlighting the use of DHNs for primary frequency support within MGs through HP demand-side

control, and emphasizing the need for proper dynamic modeling to capture the interaction between thermal and electrical subsystems. The presented dynamic models then are applied, tested, and validated in an existing MG at KLFN in Northern Ontario, showcasing the role of a potential DHN in facilitating RESs integration in an isolated MGs.

Chapter 4 focuses on the development of a comprehensive dynamic model of a BWSMR power plant, addressing key operational dynamics and thermal-electric coupling required for realistic simulation of SMR-based DHNs. The dynamic model of a BWSMR power plant model is then integrated into a widely used power system analysis tool to assess its dynamic performance and impact on Ontario's BPS. The obtained results highlight the operational flexibility and frequency regulation potential of the BWRX-300, demonstrating its feasibility for practical deployment in modern power grids, while discussing the potential challenges of its integration in large-scale power networks.

Chapter 5 presents the application of the developed BWSMR-based IEHS to an urban-scale BPS, exploring an extended broader multi-timescale simulation results and validating the model's feasibility for supporting real-world operation and control. The proposed model and controls are of BWSMR-based DHN are then validated in the context of the integration into the power grid of Ontario, and a potential DHN deployment in the Darlington region. The obtained results highlight the strong potential of SMRs for cogeneration, demonstrating their operational flexibility in a practical application and illustrating a significant reduction in energy consumption compared to heating systems based solely on HPs.

Chapter 6 concludes the thesis by summarizing its key findings and contributions. Potential directions for future research on modeling, control, and optimization of IEHSs are also dicussed.

# Chapter 2

# Background

This chapter provides a concise background overview of the research, focusing on five relevant topics that have been extensively studied, namely, MGs, DHNs, IEHSs, SMRs, and NPP-based cogeneration, briefly discussing their architectures and dynamic modeling and control. This chapter provides a qualitative description of these systems and their models and controls, which are the basis for more detailed and novel models, controls, and studies represented and discussed in Chapters 3, 4, and 5.

## 2.1 Microgrids

MGs facilitate the integration of Distributed Energy Resources (DERs) that include variable and hard-to-predict RESs into distribution networks at both Low Voltages (LVs) and Medium Voltages (MVs) [58]. Essentially, an MG is defined as a distribution network that combines local DERs, i.e., Distributed Generation (DG) sources, energy storage, and controllable loads, to form a self-sufficient EPN. An MG can operate either independently or in conjunction with the main grid. When connected to the grid, frequency and voltage regulation is mainly motivated by the utility grid, with MG DERs basically supplying power to the local loads [59]. In the event of unavailability of the grid in grid-connected mode, the MG should be capable of swiftly disconnecting from the primary grid, seamlessly transitioning into an autonomous system to supply power exclusively to the MG local loads. In this isolated mode, DG units autonomously regulate both the frequency and voltage magnitude, ensuring the reliable provision of active and reactive power to the MG loads.

### 2.1.1 Components and Architecture

As depicted in Figure 2.1, the primary components of an MG encompass loads, DERs, a MV/LV distribution network, a Microgrid Central Controller (MGCC), and communication and control systems [60]. MG loads are typically divided into two categories: Fixed loads which remain constant and flexible loads which are controllable based on economic or operating requirements. DERs include DG units such as DGU, Photovoltaic (PV) generation, Wind Generator (WG), and Energy Storage Systems (ESSs). Dispatchable DERs can be controlled by the MGCC, subject to technical constraints such as capacity limits, ramping limits, minimum on/off time limits, and fuel and emission limits. In contrast, nondispatchable units, primarily renewable sources like PV and WG, are not typically controlled, especially in MGs, given their relatively small size. These units, known for their volatile output, often require reinforcement with ESS to mitigate their variability. The ESS ensures MG generation adequacy, facilitate energy arbitrage, and play a crucial role in MG islanding applications.

The breaker at the Point of Common Coupling (PCC) enables MG islanding by disconnecting the MG from the utility grid. The MGCC determines the MG's interaction with the utility grid, the switching between grid-connected and islanded modes, and the optimal operation of local resources. The communication and control systems are employed to ensure effective and reliable interaction among MG components. The subsequent sections provide a more comprehensive overview of the essential components of the MG.

#### 2.1.1.1 Distributed Generation Resources

Various technologies fall under the DG category suitable for MGs [61]. These technologies encompass a range of options such as DGUs, WG, PV, micro-turbines and fuel cells. Some DG technologies have flexible dynamic response and can provide instantaneous power to the MG such as DGUs, while other DERs such as fuel cells have a limited dynamic response.

#### 2.1.1.2 Energy Storage Systems (ESSs)

ESSs are essential components for the effective operation of MGs, since they are crucial for maintaining the required balance between power generation and demand [62]. These systems have several functions, ensuring proper MG operation despite fluctuations in load and other transient conditions. This is particularly important because DG units, with their lower or zero inertia, may have limited capabilities to respond to such disturbances. Additionally, when there are dynamic variations in RESs, ESSs facilitate the integration

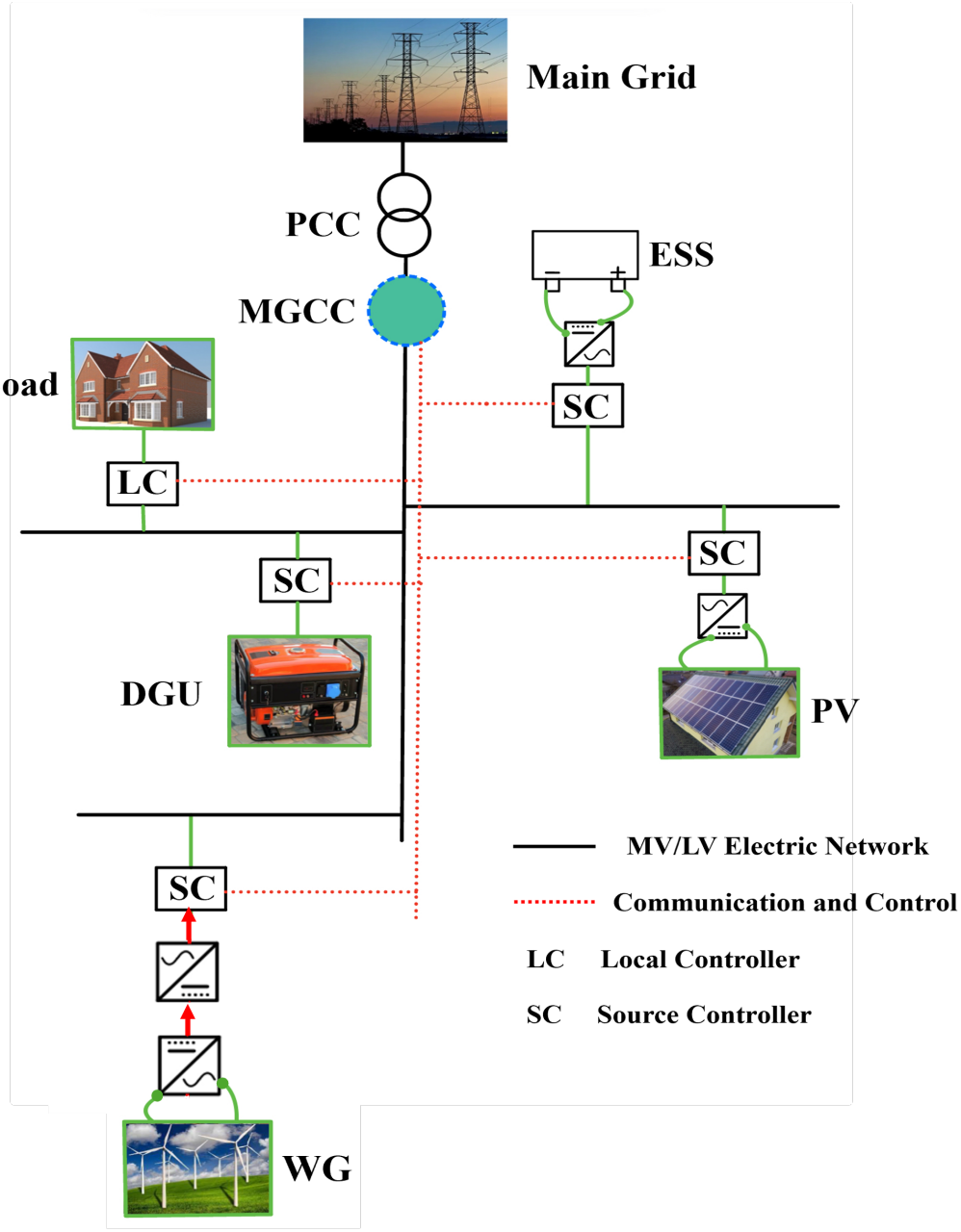



Figure 2.1: MG architecture.

of undispatchable units such as WG and PV. Finally, these systems offer the necessary energy for transitioning between grid-connected and islanded operations of the MG, and vice versa.

Various ESS technologies are available [63], falling into following categories: chemical, including batteries and fuel cells; electrical, encompassing superconducting magnetic energy storage and super or ultra-capacitors; mechanical, such as pumped hydro, flywheels, and compressed air ESSs; and TES based on the thermal inertia of buildings, fluids, or underground. Among these, the most commonly utilized and well-suited storage devices for MGs include batteries, flywheels, fuel cells, and TES.

#### 2.1.1.3 Distribution Grid

Distribution grids can be AC or DC [64], depending on the power electronics interfaces used for connecting DERs to the distribution network. Consequently, the distribution network itself can be categorized into three types: DC lines, 60/50 Hz AC lines, and high-frequency AC lines. This thesis considers only AC grids.

#### 2.1.1.4 Communication Systems

Effective power control and protection in MGs rely significantly on communication systems. An overview of basic communication methods along with their characteristics, and a detailed discussion of their advantages, disadvantages, and protocols can be found in [65]. This thesis does not consider communication system issues, assuming its availability with no significant lags and its focus on frequency regulation issues, based on [66], which demonstrates a limited impact of the communication system delay on MG frequency dynamics.

#### 2.1.1.5 Control

MG control architecture can be centralized or decentralized, as discussed in more detail next. The choice between these depends on the MG size and complexity, the types of DERs used, and the desired level of resilience and optimal operation.

### 2.1.2 Modeling and Control

#### 2.1.2.1 Modeling

The modeling of an MG varies based on its specific components and operating time-frame. For instance, small penetration stability models are presented in [67]. In addition, a state-space model for an islanded MG is developed in [68], encompassing low-frequency and high-frequency dynamics of inverters, network dynamics, and load dynamics. An LV MG with three unbalanced phases is discussed in [69] to analyze an inverter dominated MGs. In this thesis, a detailed MG dynamic model is used for stability and control studies, as discussed at some length in Chapter 3.

#### 2.1.2.2 Control

There are various control techniques and stability considerations in AC MGs as discussed in [70], encompassing aspects such as voltage and frequency control, coordination among DERs for power sharing, MG synchronization, power flow control between multiple MGs, smooth mode switching, loss reduction, economic efficiency, and resiliency. Thus, MG control systems can be either centralized or decentralized [22]. In a fully centralized control system, a dedicated MGCC conducts the necessary computations and decides on control actions for all DERs. This method necessitates extensive communication between the MGCC and the units it oversees. Conversely, in a fully decentralized control system, each unit is operated by its local controller, which receives local and relevant information from at least neighboring controllers, but it lacks a comprehensive view of system-wide variables and the full actions of all controllers.

MG hierarchical centralized control, as shown in Figure 2.2, comprising primary, secondary, and tertiary levels, is employed to fulfill the aforementioned control objectives. The primary control focuses on maintaining voltage and frequency within acceptable limits, ensuring some active and reactive power sharing among DERs, and ensuring some level of plug-and-play operation. The secondary control addresses voltage and frequency deviations via a centralized Energy Management System (EMS), typically being slower than primary control based on optimization and/or machine learning strategies. The tertiary control manages flows between the utility grid and other MGs, enhancing economic operation through adjustment of DERs based on optimization and/or machine learning models and algorithms. This three-level hierarchical control structure plays a crucial role in maintaining stability and efficient operation of isolated and interconnected AC MGs.

The core responsibility of DG units within the MG is to control both real power and reactive power outputs [71]. This control in DERs based on Voltage Source Converters

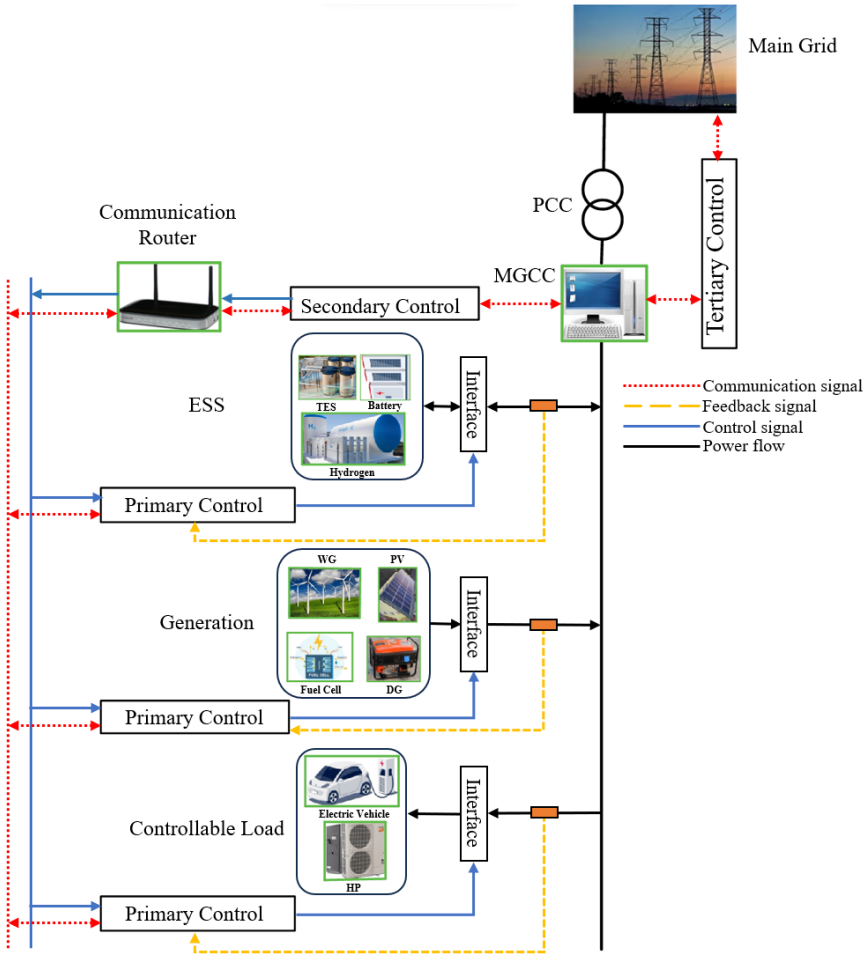



Figure 2.2: Architecture of MG hierarchical control.

(VSCs) can be achieved using either current-based or voltage-based control strategies. The main objective for power flow management through current regulation is to effectively control both real and reactive powers. To achieve this, a real power control loop is implemented to derive the reference current in the synchronous d-axis frame, while a reactive power control loop is used to determine the q-axis current. Subsequently, the synchronous d-q frame current is regulated in a closed-loop hierarchy control mechanism, as elaborated in [72]. On the other hand, power flows can be controlled by regulating the output voltage of DG units [73]. In this framework, the real power flow can be controlled by manipulating the voltage angle at the source, while the control of reactive power flow is accomplished by modulating the voltage magnitudes.

A master-slave control strategy is used in centralized control [74]. It designates one source as the master, with other converters acting as slave units following control directives. This approach relies on high-bandwidth communication, but it has drawbacks such as a single point of failure and dependency on the master. However, it enhances coordination in a multi-layer control strategy, facilitating MG operation. On the other hand, a distributed consensus-based control functions based on a strategy manages information exchange among MG units, offering a distributed and flexible approach to accomplish overall MG control objectives. This includes voltage and frequency regulation, active power sharing, and seamless MG islanding and reconnection to the grid. In this thesis, a centralized control approach is assumed, since this is the most appropriate for isolated MGs [22].

## 2.2 District Heating Network

DHNs have a long history, dating back to the 14th century in Europe, with France's Chaudes-Aigues thermal station initial operation [75]. In the United States, the first DHN was established at the US Naval Academy in 1853, followed by New York's commercial DHN in 1877. Canada deployed its first commercial DHN in 1924 in Winnipeg. District energy involves distributing heating or cooling through underground piping to industrial, commercial, and residential users. The heat can also be used for air conditioning by adding a HP or absorption chiller, offering efficiency, environmental, and economic benefits.

The energy sources for DHNs can range from fossil fuels to renewable options like solar collectors, polygeneration, seasonal heat storage, and biomass systems [76]. Densely populated urban areas, high-density building clusters, industrial complexes, and low-density residential areas have different types of DHNs, each with distinct characteristics and considerations [75].

### 2.2.1 Components and Architecture

DHNs mirror the structure of EPNs, encompassing the following four fundamental architectural components: generation, transmission, distribution, and thermal loads, as shown in Figure 2.3. General descriptions of the diverse elements constituting DHNs are provided next.

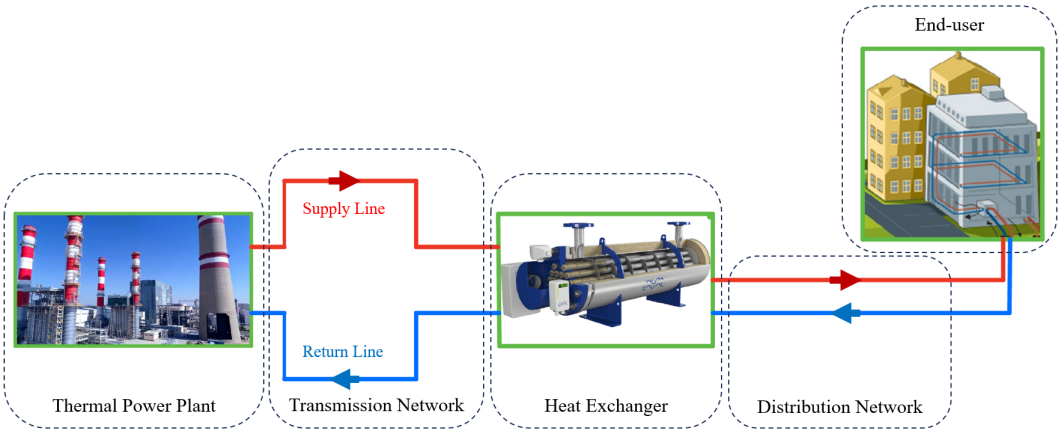



Figure 2.3: DHN architecture.

#### 2.2.1.1 Generation

A crucial feature of DHNs is its versatility in heat sources, allowing the connection of various centralized and decentralized options for reliable and flexible operation, employing basic control strategies [77]. Depending on geographical location and demand, the same DHN can also serve for district cooling in the summer, based on the thermal sources. Conventional heat sources encompass a range of options; including CHP plants that generate both heat and electricity; waste heat from industrial or agricultural processes; geothermal heat from beneath the earth's surface; solar thermal heat in both large and small-scale setups; HPs typically operated with excess electricity, especially in regions with surplus wind energy; and conventional boilers used as a backup during peak load periods. In [77], seven common heat generation technologies are evaluated and ranked based on a "goodness" index that reflects economic, energy, and environmental considerations, as summarized in Table 2.1.

Table 2.1: Evaluation of Heating Systems

| Heating System | Goodness Index | Ranking |
|---|---|---|
| CHP | 0.1732 | 1 |
| Oil-fired Boiler | 0.1261 | 7 |
| Gas-fired Boiler | 0.1491 | 2 |
| Fossil Fuel-fired Boiler | 0.1442 | 4 |
| Solar-energy HP | 0.1273 | 6 |
| Ground-source HP | 0.1355 | 5 |
| Water-source HP | 0.1445 | 3 |

#### 2.2.1.2 Transmission

The transmission network delivers hot water to customers and returns cooled water, or vice versa depending on the season, to the source through underground pipes covering relatively long distances [78]. This thesis focuses on heating DHNs, which can be categorized into the following four generations based on distinct characteristics: first-generation DHNs feature typical supply temperatures exceeding 150 °C; second-generation DHNs with typically supply temperatures surpassing 120 °C; third-generation DHNs supply temperatures ranging from 70 to 120 °C; and fourth-generation DHNs, characterized by typical supply temperatures ranging from 40 to 60 °C.

#### 2.2.1.3 Distribution

A heating DHN provides the primary thermal energy, while the central heating system in a building constitutes the secondary thermal supply [79]. Interconnection between the primary and secondary supplies can be indirect or direct. Indirect connections commonly involve a HX separating primary and secondary heating fluids. Substations facilitate this connection, serving single dwellings or multi-flat buildings. On the other hand, direct connections involve the DHN water directly interacting with the building's central heating system, eliminating heat losses associated with HXs. Direct connections are found in single dwellings to minimize risks, operating at a lower temperature. Common HXs include plate and shell plus tube types, with the latter offering better heat transfer but consuming more

space [78]. Once heat is transferred to the secondary fluid, radiators or underfloor heat emitters are used for space heating.

#### 2.2.1.4 Loads

Thermal demand variations in DHNs arise from both seasonal and daily factors [80]. Seasonal changes are primarily influenced by outdoor temperature fluctuations throughout the year, while daily variations are driven by social patterns and customer behavior. These fluctuations result in increased costs due to the need for peak heat load capacity and the use of expensive peak fuels.

### 2.2.2 Modeling and Control

#### 2.2.2.1 Modeling

Simulation models for DHNs are vital for understanding how DHNs and storage operate, providing a reasonable representation to aid in formulating intelligent control decisions [81]. DHN modeling may require significant computational resources, particularly when simulating extensive DHNs. Detailed modeling of DHNs involves multiple components, including the primary and secondary circuits, thermal loads, distribution pipelines, HXs, and thermal power plants.

In addition to thermal loads, a DHN requires a network of pipes to facilitate the distribution of thermal energy from sources to loads, serving both space heating/cooling and hot water needs [82]. Simulating the transport delay is an essential aspect of the DHN model and can be defined as the time taken for the fluid to flow from the pipe's inlet to its outlet. The pipeline is segmented in the direction of flow, and the total thermal loss from the pipe is the sum of thermal losses from these segments. Transient DHN models offer more precise results for systems with variable flows; however, these models can be computationally demanding.

DHNs can draw thermal power from various sources, each with unique characteristics [83]. For instance, geothermal HPs, ideal for regions with geothermal resources, offer cost-effective heating and cooling but perform best in moderate temperatures. On the other hand, biomass systems provide renewable energy but may have limited availability, while burning urban waste requires proper management to mitigate emissions-related health effects. Utilizing waste heat from industrial processes offsets fuel costs but needs an existing DHN, and solar thermal systems depend on location and demand fluctuations. The choice

of energy source depends on local resources, environmental goals, and efficiency in district energy planning. Finally, the HX needs to be modeled as well, requiring the simulation of the component responsible for transferring thermal energy between two different fluids circulating in the DHN.

#### 2.2.2.2 Control

In DHNs, the generation and delivery of hot water involve a multi-level control system to efficiently provide thermal energy [84]. The first level is a centralized control operating at the heat sources and managing the primary supply temperature and pump speed to meet the overall thermal load variations of the network. The second level is the local control at each heating substation, which adjusts the secondary supply temperature and secondary pump speed to satisfy the variable heating load of consumers. This is achieved by controlling the secondary supply temperature through a HX's control valve on the primary side. The third level is the personal control that operates at each radiator, controlling the radiator's flow rate based on the room temperature difference from the desired value to maintain the room temperature around the desired level. These three control levels work simultaneously to allocate heat to each consumer in the DHN.

## 2.3 Integrated Electricity and Heating System

As discussed in [85], the Paris Agreement mandates achieving net-zero GHG emissions to limit the global average temperature increase to less than 2°C. Subsequently, global efforts have focused on decarbonizing various sectors essential for daily use, encompassing both the electricity and heating sectors. For example, in the heating sector, a range of international measures has been pledged to curb carbon emissions, including support for technologies like CHP, power-to-heat devices utilizing renewable electricity, and the implementation of DHNs. The efficiency advantages of CHP make it a good option for reducing carbon emissions by up to 30%, compared to the separate generation of heat through a gas-fired boiler and an electricity power plant, as discussed in [86].

Because of the promising benefits offered by IEHSs, national legislation encourages the adoption of more sustainable heating and cooling options across all European Union countries, with HPs identified as prime leading candidates [87]. In this context, the DHNs offer pivotal solutions for decarbonizing the heating sector, given their capacity to integrate waste heat and renewable energy [88]. Thus, the DHN market is globally expanding, with China, Russia, and Europe contributing over 90% to global DHN deployment [89].

Moreover, the advantages of DHNs extend to the power sector, where elements of these networks, such as heat pipelines, thermal storage tanks, and costumer buildings, can provide thermal storage for heat converted from low-cost electricity or RESs. This integration provides the EPN with greater temporal flexibility in balancing supply and demand, which enhances the EPN performance with high penetration of RESs. Furthermore, the power-to-heat devices like DHNs HP can also provide ancillary services to EPNs such as virtual inertia and frequency regulation.

### 2.3.1 Components and Architecture

Understanding the architecture of the IEHS is crucial for developing effective models and solutions. Thus, IEHS is comprised of two main subsystems, namely, the EPN and the DHN as shown in Figure 2.4. Power plants within the EPN generate electrical energy through various means such as thermal, hydraulic, nuclear, wind, and solar power. Traditional power units must consider factors like output limits, ramping rates, and reserve capacity [90]. Unlike controllable conventional generators, wind and solar power generation is non-dispatchable due to uncertainties in wind and solar radiation, requiring flexibility to manage these uncertainties. The electrical energy generated by power plants in EPNs is transmitted to users through transmission and distribution networks [91]. On the other hand, DHN consists of heat sources, TESs, pipeline network, HX stations, and thermal loads [92], controlling temperature and flow rate with modern schemes that offer customers control comparable to individual gas boilers but at increased efficiencies.

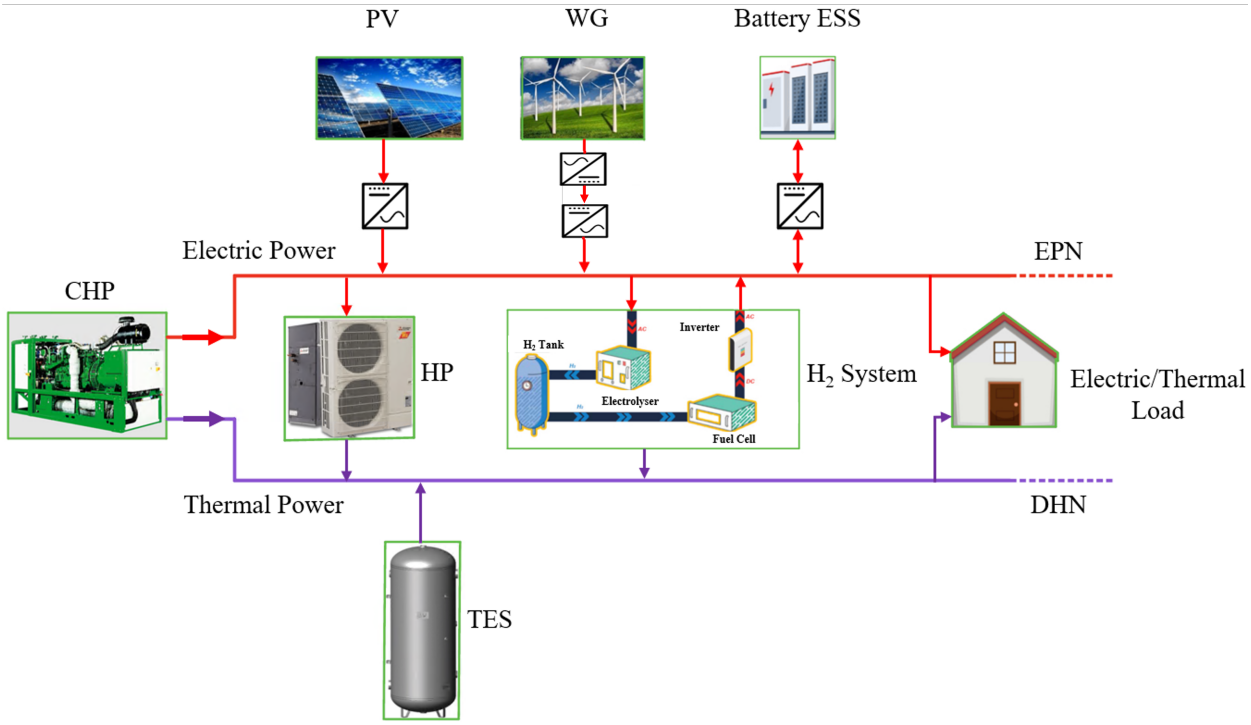



Figure 2.4: IEHS architecture.

HPs and electric boilers are emerging as key tools to enhance the flexibility and sustainability of power systems with high penetration of variable RESs in the context of IEHS [93]. By utilizing low-cost electricity during periods of surplus wind and solar generation, these systems can efficiently substitute more conventional heat sources. The integration of HPs into DHNs is cost-effective, particularly due to the low specific investment and installation costs of large-scale units and thermal storage [94]. Furthermore, the effective deployment of HPs in DHNs relies on optimal placement, connection, and operation within the network. This enables year-round operation and ensures high performance with minimal environmental impact [87].

DHNs, when combined with CHP, are facing challenges due to improved modern building efficiency and individual HP performance, which make DHN losses more significant. Therefore, there are mainly two alternatives to integrate HPs into DHNs, namely, central HPs with HXs, and central HPs with small booster HPs using DHN water as a low-temperature source, with the booster HP approach enables lower DHN temperatures,

enhances central HP efficiency, reduces grid losses, and outperforms individual heating solutions [95].

### 2.3.2 Modeling and Control

#### 2.3.2.1 Modeling

The modeling and analysis of the IEHSs is complex due to the coupling of independent energy systems with distinct characteristics. These systems differ in several aspects [29]. Thus, electric power and thermal power are transmitted at different speeds, with the former moving at the speed of light, while the latter moves at the rate of water flow. On the other hand, varying time delays and thermal losses along different transfer paths hinder the establishment of direct relationships between the control mechanism and controlled states in DHN. Finally, the continuous effect of the control strategy in DHNs on subsequent states is influenced by time delays, making it challenging to quantify the cumulative effects of adjustments, which basically affect the operation of EPNs in IEHSs. Therefore, an explicit model describing the dynamic features in IEHS is crucial for further operational analysis and control design.

As explained in [96], [97], and [98], the DHN model is generally categorized into the following three types: a static model considering only thermal losses; a quasi-dynamic model determining node temperature that considers both thermal losses and transmission delays; and a dynamic model to determine the temperature of each pipe section considering both thermal losses and transmission delays. Among these, quasi-dynamic and dynamic models are more widely used due to their higher accuracy. A quasi-dynamic model computes node temperature with the temperature time series at source nodes, neglecting temperature distribution along the pipe. A dynamic model, on the other hand, discretizes the pipe spatially, computing temperature for each pipe section, with its computation complexity scaling linearly with accuracy. While the quasi-dynamic model reduces computation burden, its error and numerical diffusion increase with time step increments and mass flow changes, making it more suitable for radial DHN with fixed flow rate and direction. In contrast, the dynamic model, while reflects the network's topological structure and thermal transfer properties, is widely applied in practice and is more adequate to properly represent the interactions between the DHN and the EPN in an IEHS.

#### 2.3.2.2 Control

As outlined in [99], the control scheme for the IEHS is developed based on the dynamic characteristics of the IEHS, requiring a heat-power coordinated controller to manage interactions among multiple energy conversion devices. However, the conventional approach of employing tracking controllers for both electrical and thermal sides is considered impractical due to significant differences in control requirements on each side. In this context, the thermal-side control requirement can be relaxed, considering human insensitivity to small temperature variations, while the electrical-side control requirement is highly stringent. The relaxation of the thermal-side control requirement can be practically eliminated once the electric-side controlled variable is adjusted closely to its setpoint.

Each of the two systems in IEHS has its control methodology. For the EPN, droop control is commonly used to achieve primary frequency control and voltage control. For the DHN, thermostatic valves are primarily employed to control the temperature throughout the heating system. Therefore, coordinated control between the two systems is needed for energy exchanges, facilitating the efficient performance of IEHSs.

## 2.4 Small Modular Reactors

SMRs offer a promising solution to meet the world's energy needs to address climate change and environmental issues [49]. Their compact size facilitates easier transportation, making them suitable for remote areas without advanced infrastructure. SMRs also feature innovative design elements, such as integral vessels and natural circulation, not feasible in larger reactors.

An integrated BWSMR can incorporate fully passive safety and coolant circulation systems using a two-phase flow driving head [100]. This leads to a smaller and simpler RPV, eliminating the need for coolant circulation pumps and pressurizers within the reactor vessel.

Compared to BWSMRs, IPWR SMRs differ fundamentally in both design and thermal-hydraulic behavior. As discussed in [101], IPWRs utilize a separate steam generator to transfer heat from the primary loop to the secondary side. This introduces thermal inertia and slower dynamic response, which may limit their effectiveness in fast frequency regulation. In contrast, BWSMRs employ direct steam expansion, where steam generated in the reactor core is routed directly to the turbine [102]. This design offers the following advantages: a simplified system architecture, lower capital and operational costs, faster

dynamic response; and a reduced physical footprint, making BWSMRs particularly attractive for applications in BPSs with high penetration of variable RESs. However, the direct cycle design of BWSMRs also introduces certain challenges. For instance, the turbine and BOP components are exposed to radioactive steam, potentially increasing maintenance complexity, radiological safety concerns, and equipment shielding requirements. Despite these limitations, the BWSMR remains a strong candidate for integration into modern power grids.

### 2.4.1 Natural Circulation BWSMR

Figure 2.5 depicts a simplified schematic of a natural circulation BWSMR. The core contains the nuclear fuel rods where fission reactions produce heat, converting surrounding water into steam [103]. The control rods in the core manage the reaction rate by absorbing neutrons, and their insertion is controlled using Fine Motion Control Rod Drives (FMCRDs). The chimney, installed above the core, enhances the natural circulation of the water-steam mixture by providing an extended path for steam to rise and separate from the water, thereby increasing the natural circulation flow rate. The steam separators and steam dryer at the top ensure dry steam is sent to the turbines. The downcomer, located outside the chimney, directs the cooler water from the steam separators back down to the bottom of the reactor vessel, facilitating the natural circulation process.

The RPV encloses the core, steam separators and dryer, providing containment for the nuclear reaction and heat transfer process. Steam generated in the reactor is directed to the turbine via the steam outlet, where it generates electricity. Cooled water from the turbine condenser returns to the reactor vessel through the feedwater inlet after being reheated. This setup ensures a continuous supply of water into the RPV via feedwater pumps.

### 2.4.2 BWSMR Steam Turbine and Heat Extraction

Figure 2.6 illustrates a typical steam turbine system for a BWSMR, including configurations for both electricity generation and heat extraction. The RPV generates relatively high-pressure, high-temperature steam using the heat from a nuclear reactor [46]. This steam first flows to the Main Steam Inlet (MSI) valve, which regulates the flow of steam into the High Pressure Turbine (HPT), where it expands and converts thermal energy into mechanical energy, spinning the turbine rotor to drive the generator.

After passing through the HPT, the steam enters a moisture separator that removes water droplets, enhancing efficiency and protecting turbine blades. The dry steam is then

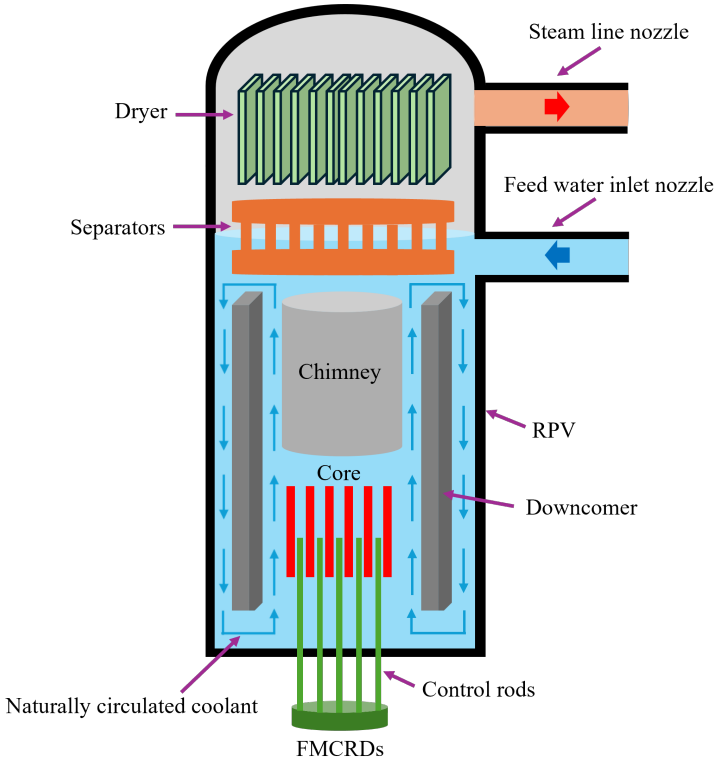



Figure 2.5: Schematic of natural circulation BWR.

reheated and directed into the Low Pressure Turbine (LPT) for further expansion and energy conversion. The exhaust steam from the LPT is routed to the condenser, where it is condensed under vacuum conditions to improve cycle efficiency.

Before reaching the LPT, a controlled fraction of steam can be extracted to supply heat to a DHN and to charge the TES system, as proposed here. The Extracted Steam (ES) transfers heat through HXs, and the condensate is returned to the feedwater system, enhancing the overall thermal efficiency of the BWSMR cycle. The remainder of the steam is condensed and recirculated via feedwater pumps, passing through feedwater heaters that use ES from various turbine stages. The Bypass (BP) valve plays a key role in regulating RPV pressure and temperature by diverting steam directly to the condenser when necessary.

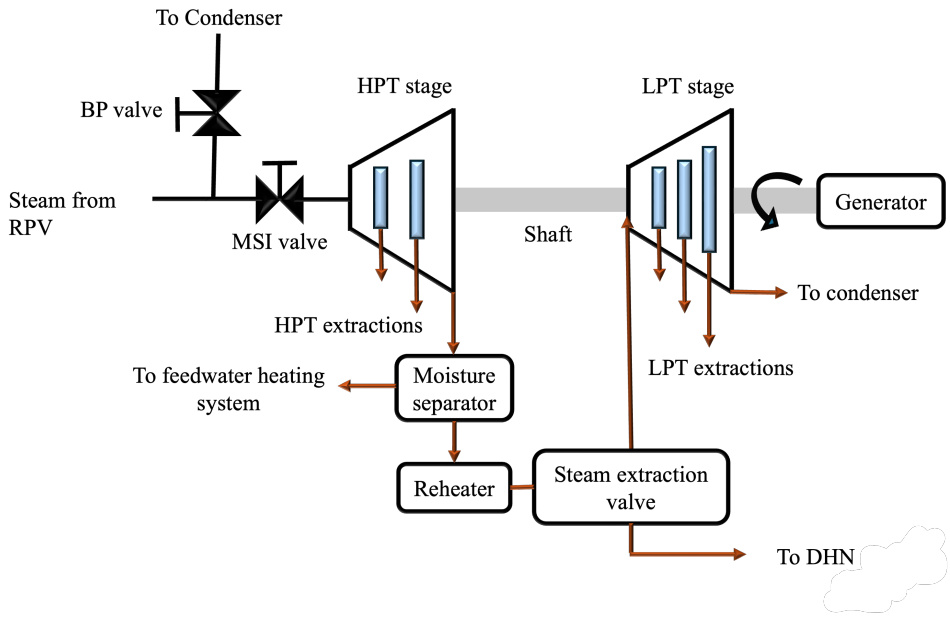



Figure 2.6: Schematic of a BWSMR steam cycle with steam extraction for DHN and TES.

### 2.4.3 Control Strategies in SMRs

Effective control strategies are essential for the safe and efficient operation of SMRs, ensuring stable power output, reactivity regulation, and thermal management. As discussed in [104], control systems in light water reactor-based SMRs typically manage power and reactivity through control rod positioning and coolant temperature regulation, leveraging negative reactivity feedback to maintain operational stability. These systems often utilize a three-channel control configuration, with one channel measuring the coolant temperature, another generating the reference signal, and a third one adjusting for power mismatch; the combined signal governs the movement of the control rods. In the case of liquid metal-cooled reactor-based SMRs, core control involves multiple subsystems, including reactivity regulation via control rod movement, coolant flow and temperature control, and real-time feedback loops. Several control methods have been applied to SMRs, including Proportional-Integral (PI) controllers, which correct error based on proportional and integral terms; model predictive control, which forecasts future states and optimizes control decisions accordingly; fuzzy logic controllers, which are robust against uncertainties and nonlinearities; and neural network-based controllers, which adaptively learn from historical data to optimize system performance. These approaches are necessary to respond to load changes, system transients, and emergency conditions while maintaining the safety and

reliability of SMRs.

## 2.5 NPP-based Cogeneration Systems

NPPs have traditionally been deployed to supply the base-load of electricity demand [50]. Instead of relying solely on control rod insertion or similar methods to reduce nuclear generation, a more efficient strategy is load following by cogeneration, where surplus thermal energy is redirected to auxiliary systems rather than curtailed. Thus, NPPs have been used to supply both electricity and heat for industrial or residential applications [105]. This approach involves identifying necessary modifications to existing turbine systems and determining optimal conditions for heat generation and distribution.

A central aspect of the NPP cogeneration concept is diverting a portion of the steam from the turbines for heating use in various applications such as seawater desalination, as nuclear desalination plants offer high efficiency and economic advantages [106]. Moreover, NPPs can supply not only carbon-free electricity but also significant amounts of carbon-free heat for district heating and cooling systems [107]. Although this potential has been demonstrated in several countries, it remains largely underutilized. As another application, NPPs can be integrated into flexible energy systems by combining them with liquid air energy storage to provide load-following electricity without changing the nuclear output [108]. Finally, as RES penetration increases, conventional plants must provide greater flexibility to balance fluctuating output. In this context, integrating TES with NPPs offers a promising solution to enhance their flexibility and efficiency [109].

## 2.6 Summary

Chapter 2 presented a comprehensive background qualitative review of the key systems studied in this thesis. The chapter began with a discussion of MGs, highlighting their architecture, components, dynamic modeling, and hierarchical control strategies, particularly in the context of DG and islanded operation. It then explored DHNs, describing their historical evolution, components, energy sources, and control hierarchies, with a focus on modeling approaches that capture relevant thermal losses and delays. Following this, IEHSs were introduced as a promising solution for achieving energy sector decarbonization, supported by coordinated control between electrical and thermal subsystems.

The chapter concluded with an overview of SMRs, especially BWSMRs, discussing their natural circulation design and control, turbine operation, and cogeneration potential, including modeling of steam extraction. Finally, cogeneration systems based on NPPs for DHNs and other applications were briefly discussed. These foundational concepts and modeling principles set the stage for the detailed dynamic modeling and control studies presented in Chapters 3 through 5.

# Chapter 3

# Dynamic Model of Integrated Electricity and District Heating for Remote Communities

DHNs offer efficient and centralized thermal energy solutions for remote communities, especially those relying on diesel-based electricity generation. This chapter addresses gaps in the existing literature by developing dynamic models that integrate DHNs within EPNs, enabling a detailed analysis of their benefits and challenges in isolated MGs. The models highlight the potential of DHNs to utilize waste energy in these MGs, supporting energy exchanges between electricity and heating systems, and providing ancillary services for systems with high RESs penetration. Key modeling considerations include soil limitations, extreme cold conditions, and piping insulation in northern communities. The chapter also presents methods for sizing HPs based on actual thermal loads and proposes demand-side control strategies to enhance frequency regulation. Model validation is conducted through a case study of the KLFN MG in Northern Ontario, demonstrating the role of DHNs in improving energy efficiency and renewable integration in remote settings.

## Nomenclature

### Parameters

| | |
|---|---|
| $A$ | Normalized house area [$m^2$] |

| | |
|---|---|
| $A_{HX}$ | HX surface area [$m^2$] |
| $A_p$ | Pipeline control volume surface area [$m^2$] |
| $C_{ins1}$ | First layer insulator heat capacity [J/°C] |
| $C_{ins2}$ | Second layer insulator heat capacity [J/°C] |
| $C_{rdh}$ | Radiator thermal capacity [J/°C] |
| $C_{st}$ | Carbon steel heat capacity [J/°C] |
| $C_w$ | Water heat capacity inside pipeline [J/°C] |
| $h$ | Convective heat transfer coefficient between feed water and pipe wall [$W/m^2 \cdot °C$] |
| $k$ | Thermostatic Radiator Valve (TRV) regulation constant |
| $k_{DR1,2,3}$ | ETS demand response adjustment constants |
| $k_{ins1}$ | First insulator thermal conductivity [W/m·°C] |
| $k_{ins2}$ | Second insulator thermal conductivity [W/m·°C] |
| $k_s$ | Soil thermal conductivity [W/m·°C] |
| $k_{st}$ | Carbon steel thermal conductivity [W/m·°C] |
| $k_w$ | Water thermal conductivity [W/m·°C] |
| $L_p$ | Pipeline control volume length [m] |
| $r_1$ | Pipeline inner radius [m] |
| $r_2$ | Carbon steel layer radius [m] |
| $r_3$ | First insulator layer radius [m] |
| $r_4$ | Second insulator layer radius [m] |
| $R_{rdh}$ | Radiator hot side resistance [°C/W] |
| $R_{rdr}$ | Radiator cold side resistance [°C/W] |

| | |
|---|---|
| $S_H$ | House number of floors |
| $Z$ | Pipeline depth [m] |
| $\overline{P}_{DR}$ | ETS peak power at a given time [W] |
| $\tau_{HP}$ | Reference HP induction motor torque [N·m] |

**Variables**

| | |
|---|---|
| $COP$ | HP coefficient of performance [p.u.] |
| $C_r$ | Fluids heat capacity rate ratio in HX [p.u.] |
| $\Delta f$ | Frequency deviation [Hz] |
| $\dot{m}_w$ | Water mass flow rate [kg/s] |
| $f$ | Frequency [Hz] |
| $f_o$ | Reference frequency [Hz] |
| $f_v$ | TRV control function [kg/s] |
| $K_i$ | Integral controller gain |
| $K_p$ | Proportional controller gain |
| $NTU$ | Number of transfer units for HX [p.u.] |
| $P_{EHth}$ | Thermal power of an electric heater unit [W] |
| $P_{EHe}$ | Electric power of an electric heater unit [W] |
| $P_{HPe}$ | HP electrical power [W] |
| $P_{HPth}$ | HP thermal power [W] |
| $P_{Hth}$ | House thermal power [W] |
| $Q$ | Transferred power between HX fluids [W] |
| $Q_{rd}$ | Radiator thermal power [W] |

| | |
|---|---|
| $Q_{w,st}$ | Pipeline heat loss transferred from water to carbon steel layer [W] |
| $\tau_{HP}$ | Reference HP induction motor torque [N·m] |
| $T_a$ | Ambient temperature [°C] |
| $T_{mix}$ | Mixer resultant temperature [°C] |
| $T_{HPin}$ | HP inlet temperature [°C] |
| $T_{HPout}$ | HP outlet temperature [°C] |
| $T_{HXcin}$ | Cold fluid inlet temperature of the HX [°C] |
| $T_{HXhin}$ | Hot fluid inlet temperature of the HX [°C] |
| $T_{ins1}$ | Temperature of first layer insulator [°C] |
| $T_{ins2}$ | Temperature of second layer insulator [°C] |
| $T_{ph}$ | Pipeline hot temperature [°C] |
| $T_{rdh}$ | Radiator hot side temperature [°C] |
| $T_{rdr}$ | Radiator return water temperature [°C] |
| $T_{st}$ | Temperature of carbon steel layer [°C] |
| $T_{wh}$ | Hot water temperature inside pipelines [°C] |
| $T_S$ | Space temperature [°C] |
| $\varepsilon$ | Effectiveness of HX |
| $\omega_{HPo}$ | Reference speed of HP induction motor [rad/s] |
| $\psi$ | HP second-law efficiency [p.u.] |
| $\mathbb{1}$ | Vector of ones |

## 3.1 DHN Model

An IEHS requires the integration of multiple components to meet the electricity and heating demands of a community. This section discusses the essential elements of a DHN in a remote community IEHS, considering for the first time relevant thermal system dynamics, and demonstrates and discusses its application to the KLFN community.

### 3.1.1 Household Model

The Smart Residential Load Simulator (SRLS) tool has been used here for studying IEHS in smart grids [110]. The package contains detailed models of appliances, Heating, Ventilation, and Air Conditioning (HVAC) systems, and thermal components in homes. In this chapter, this tool is utilized to model the individual household thermal dynamics, which is a fundamental component of a DHN. In this context, replacing the heating source from individual furnaces with a DHN heat supply in a household requires detailed modeling of a radiator and its control, as detailed in [111]. Additionally, the representation of temperatures resulting from mixing multiple mass flow rates at different temperatures within a household is needed [112].

Based on [113], a typical Canadian household consists of four main spaces[1] with varying dimensions and thermodynamic properties. In the context of a DHN, each space is presumed to have different radiator capacity corresponding to its heating area, with hot water being distributed among the radiators, starting from the inlet pipeline at the house's entrance and mixed at the outlet pipeline. Consequently, the household model for DHN studies comprises individual models for each space, along with a mixer model that calculates the resultant temperature after combining the mass flow rates and corresponding temperatures of the four spaces. The thermal dynamics of such a household can be modeled using proper models and simulation tools, as described in detail next.

#### 3.1.1.1 Single Space Model

The dynamic thermal model of a single space in the SRLS is described in some detail in [110], based on an electric circuit model that represents the thermal dynamics of the area. In this model, the radiator can be readily integrated by adding the following equations [111]:

[1]Spaces refer to generalized areas used for thermal modeling purposes, which may represent entire rooms or combined zones and are not strictly associated with physical room boundaries.

$$\frac{dT_{rdh}}{dt} = \frac{T_S - T_{rdh}}{C_{rdh}R_{rdh}} + \frac{Q_{rd}}{C_{rdh}} \tag{3.1}$$

$$Q_{rd} = c_w \dot{m}_w (T_{ph} - T_{rdh}) \tag{3.2}$$

$$\frac{dT_{rdr}}{dt} = \frac{T_{rdh} - T_{rdr}}{C_{rdh}R_{rdr}} \tag{3.3}$$

where all variables and parameters in these and other equations are defined in the Nomenclature section of this chapter, where separate listings are provided to simplify the presentation due to the large number of terms involved. It is assumed that $T_{rdh}$ and $T_{rdr}$ are approximately the same, which allows the radiator's virtual resistance $R_{vr} = \frac{1}{c_w \dot{m}w}$ in (3.2) to be included in the space's electric circuit model.

To simulate TRV operation and control hot water flow rate, the following function can be utilized:

$$f_v = \frac{\dot{m}_{max}}{1 + e^{-k(T_{So} - T_S)}} \tag{3.4}$$

In this study, only conductive thermal resistances are considered, assuming a uniform space temperature.

#### 3.1.1.2 House and Mixer Models

The household thermal dynamic model consists of individual models for each of the four spaces, assuming that the return mixed temperature can be described as follows [112]:

$$T_{mix} = \frac{\sum \dot{m}_w T_{rdr}}{\sum \dot{m}_w} \tag{3.5}$$

The household model takes into account the internally generated thermal power, as well the solar irradiation considering all surrounding directions (south, north, east, west, and roof), based on the equations described in [110], which discusses in some detail the thermal heat generated from solar irradiation on the household used in the present work. It assumes that heat from solar radiation passing through windows and impacting external walls is stored in the room's internal thermal mass and external walls' thermal mass, respectively. This model requires the following specific input data: beam irradiance (W/m$^2$), diffuse

irradiance ($W/m^2$) for a specific day of interest throughout the year, and the latitude of the location under study. The model has been implemented in the SRLS tool [113], which is a Matlab-Simulink-GUIDE tool that facilitates the study of energy management systems in smart grids.

### 3.1.2 Pipeline Heat Loss

The household dynamic thermal model is a fundamental component of the DHN's secondary circuit. This model is integrated into the DHN, which also includes pipelines to form a heat distribution network with both hot- and cold-water flows to deliver thermal power from the heat sources to individual consumers. Accurate modeling of the pipelines, including considerations for insulation and pipe material, is crucial to capture the dynamics of stored energy within the pipes. Proper modeling of pipelines is essential to represent thermal losses and temperature variations accurately, with the diameters of these pipelines playing a significant role. These pipelines can be efficiently designed using Geographic Information Systems (GIS) and thermal network design tools, which allow estimating mass flow rates, heat loss, and temperature drops within the heat distribution network, ensuring efficient thermal power delivery to households.

The following equations govern the pipeline model [114]:

$$C_w(\frac{dT_{wh}}{dt}) = (T_{ph} - T_{wh})c_w\dot{m}_w + Q_{w,st} \tag{3.6}$$

$$C_{st}(\frac{dT_{st}}{dt}) = \frac{T_{ins1} - T_{st}}{\frac{ln(r_2/r_1)}{2\pi k_{st}L_p}} - Q_{w,st} \tag{3.7}$$

$$C_{ins1}(\frac{dT_{ins1}}{dt}) = \frac{T_{ins2} - T_{ins1}}{\frac{ln(r_3/r_2)}{2\pi k_{ins1}L_p}} - \frac{T_{ins1} - T_{st}}{\frac{ln(r_2/r_1)}{2\pi k_{st}L_p}} \tag{3.8}$$

$$C_{ins2}(\frac{dT_{ins2}}{dt}) = \frac{T_a - T_{ins2}}{\frac{ln(r_4/r_3)}{2\pi k_{ins2}L_p} + \frac{ln(2Z/r_4)}{2\pi k_s L_p}} - \frac{T_{ins2} - T_{ins1}}{\frac{ln(r_3/r_2)}{2\pi k_{ins1}L_p}} \tag{3.9}$$

$$Q_{w,st} = \begin{cases} hA_p(T_{st} - T_{wh}) & \text{if } \dot{m}_w > 0 \\ 8\pi k_w L_p(T_{st} - T_{wh}) & \text{if } \dot{m}_w = 0 \end{cases} \tag{3.10}$$

$$R_1 = \frac{ln(r_2/r_1)}{2\pi k_{st}L_p} \tag{3.11}$$

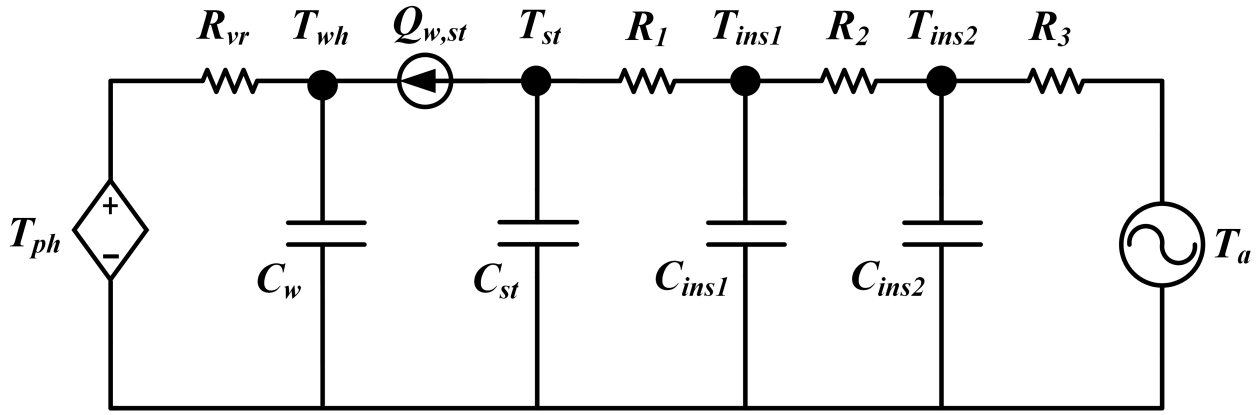



Figure 3.1: Electric equivalent circuit of the pipeline control volume.

$$R_2 = \frac{ln(r_3/r_2)}{2\pi k_{ins1} L_p} \tag{3.12}$$

$$R_3 = \frac{ln(r_4/r_3)}{2\pi k_{ins2} L_p} + \frac{ln(2Z/r_4)}{2\pi k_s L_p} \tag{3.13}$$

These equations describe the behavior and dynamics of the pipeline system using the electric-circuit analogy, with Figure 3.1 illustrating an electric circuit model of a specific pipeline control volume.

The underlying principles and equations governing heat transfer and temperature dynamics apply to both the hot and cold sides of the system. Therefore, the aforementioned equations can be utilized to model and analyze the behavior of the entire pipeline network, regardless of whether it pertains to hot or cold water.

### 3.1.3 Heat Exchanger

The HX is a vital component in DHNs that transfers heat between fluids of different temperatures. It facilitates efficient heat transfer from the primary circuit, where heat is generated, to the secondary distribution circuit for heating purposes. Different types of HXs are used in DHNs [115]. Here, the design aspects of the Counter Flow Heat eXchanger (CFHX) are considered for a given generated thermal power capacity, accounting for the Exhaust Gas (EG) peak thermal power. Thus, the CFHX can be effectively modeled using the effective number of transfer units (effective-NTU) method, which involves the following equations [116]:

$$Q = \varepsilon \underline{C}(T_{HXhin} - T_{HXcin}) \tag{3.14}$$

$$\varepsilon = \begin{cases} \frac{1-e^{(-NTU(1-C_r))}}{1-C_r e^{(-NTU(1-C_r))}} & \text{if } C_r = \underline{C} \,/\, \overline{C} < 1 \\ \frac{NTU}{1+NTU} & \text{if } C_r = 1 \end{cases} \tag{3.15}$$

$$NTU = \frac{U_{HX} A_{HX}}{\underline{C}} \tag{3.16}$$

### 3.1.4 Thermal Power Plant

A thermal heat source serves as the primary energy source for the DHN. Common examples include CHP plants, biomass boilers, and geothermal energy. In this chapter, the focus is on utilizing waste heat from the EG of DGUs in remote communities as the primary heat source. However, during peak thermal demand, the power generated from the EG recovery system may be insufficient to meet the consumers' temperature requirements. Hence, HPs are employed to compensate for the thermal power shortage. The integration of the EG recovery system and a single HP, which is likely sufficient in a remote community, given their relatively small footprint, forms the thermal power plant for the DHN. The main thermal power model comprises three components: an EG mass flow rate $\dot{m}_{gas}$ and temperature $T_{gas}$ model, a HX model, and a mass flow rate control model. Each of these components, which are discussed next, can be characterized by detailed average models, including the HP model as an integral part of the DHN thermal plant.

#### 3.1.4.1 Diesel Exhaust Gas

The thermodynamic properties of the EG can be accurately modeled by utilizing the tabular data provided by the manufacturer for DGUs of different power ratings. Thus, using curve fitting techniques, the EG mass flow rate and temperature can be expressed as functions of the generator electric loading condition $P_{gen}$ as follows:

$$\dot{m}_{gas} = -2{P_{gen}}^2 + 3.836P_{gen} + 3.925 \tag{3.17}$$

$$T_{gas} = -21.6{P_{gen}}^2 + 139.9P_{gen} + 412.1 \tag{3.18}$$

The density of the EG is typically assumed to be 1.33 kg/m3 based on experimental studies in [117], while the specific heat capacity of the EG is assumed to be 1.005 KJ/Kg°C [118]. In order to regulate the mass flow rate of the EG, a proportional controller can be employed.

#### 3.1.4.2 Heat Pump

To compensate for any shortage in the generated thermal power, an electricity-driven HP is necessary. The average model of the HP can be described using the following equations, based on [119], [120] and [121], starting with the HP Coefficient Of Performance (COP) based on the Carnot cycle:

$$COP_{max} = \frac{T_{hot}}{T_{hot} - T_{cold}} \tag{3.19}$$

$$COP = \psi \cdot \frac{T_{hot}}{T_{hot} - T_{cold}} \tag{3.20}$$

$$T_{hot} = \frac{T_{HPin} + T_{HPout}}{2} \tag{3.21}$$

$$T_{cold} = T_a \tag{3.22}$$

$$COP = \psi \cdot \frac{\frac{T_{HPin}+T_{HPout}}{2}}{\frac{T_{HPin}+T_{HPout}}{2} - T_a} \tag{3.23}$$

However, as per the Carnot theorem, all temperatures in the $COP$ equation should be absolute temperatures in K, which can be converted to °C as follows:

$$COP = \psi \cdot \frac{(T_{HPin} + T_{HPout})/2 + 273.15}{(T_{HPin} + T_{HPout})/2 - T_a} \tag{3.24}$$

where $COP$ is a dimensionless quantity. Additionally, the heat gained by the water through the HP $P_{HPth}$ increases its temperature by $\Delta T$ as follows:

$$COP = \frac{P_{HPth}}{P_{HPe}} \tag{3.25}$$

$$\Delta T = \frac{P_{HPth}}{c_w \dot{m}_w} \tag{3.26}$$

$$T_{HPout} = T_{HPin} + \Delta T \tag{3.27}$$

$$T_{HPout} = T_{HPin} + \psi \frac{P_{HPe} \cdot 0.5(T_{HPout} + T_{HPin}) + 273.15}{c_w \dot{m}_w \cdot 0.5(T_{HPout} + T_{HPin}) - T_a} \tag{3.28}$$

The HP is strategically connected in series with the return piping, near the main thermal plant. Its primary function is to compensate for the limited thermal power provided by the EG recovery system by increasing the temperature of the return water. The HP is driven by a variable speed Induction Motor (IM), which is controlled using direct torque control technology. To regulate the thermal power generated by the HP, a temperature hysteresis control is employed, which turns the HP on or off to prevent the undesired evaporation of water during light thermal loading conditions. However, for ancillary services, the frequency droop control of the IM driving the HP is used here to directly control its speed, demonstrating through dynamic studies that thermal comfort is not affected by temporary HP thermal power reductions.

### 3.1.5 KLFN Community Example

This subsection presents the methodology employed to estimate the total thermal demand in the KLFN community, and discusses the feasibility and challenges of deploying a DHN to properly supply the community's thermal needs, based on the relevant DHN models and controls presented in the previous sections.

#### 3.1.5.1 Thermal Demand Estimation

By using the household's thermal model provided in [110] for a typical North American house, the thermal demand of the community homes and buildings can be estimated based on the specific area considered. A normalization technique can then be used to estimate the thermal load for each residential house in the KLFN community, where there are 215 residential homes. There are also 10 additional community and commercial buildings, which include the school, police station, band office, nursing center, and church, with each of these structures being modeled independently as a separate consumer group using the same household thermal dynamic model discussed in Section 3.1.1, and based on their respective areas, heights, and usage patterns. A water treatment plant and sewage plant, where heating is only provided to the control rooms, are also part of the community buildings. A large grocery store and a hotel form the commercial demand.

The thermal power demand of a building can be estimated using the following equation [122]:

$$P_{Hth} = AS_H\overline{P}_{Hth} \tag{3.29}$$

Based on the SRLS, a thermal peak power of around 16.4 kW is necessary to fulfill the heating requirements of a 196 $m^2$ area. This calculation takes into account a minimum ambient temperature range of -38°C over a 24-hour time interval in January, according to [123], with a maximum indoor setpoint temperature of 25°C. The residential houses in the KLFN community are categorized as either single-detached, semi-detached, or row houses, as per [124]. These house structures adhere to the standard Canadian house design [110]. The normalized area $A$ for each house can be obtained using Google Earth to determine the areas of the 215 houses and the other 10 community and commercial buildings, which allows to calculate the thermal demand of the DHN.

The design of the piping routing plays a critical role in the establishment of a radial DHN. In this study, the THERMOS program has been utilized to generate the optimal routing, determine the appropriate pipe diameters, and calculate the actual length of the pipelines specific to the particular case being studied [125]. To estimate the maximum thermal power demand in the KLFN community for the purpose of pipe sizing and network routing, the following steps are used:

1. Run the SRLS for a standard Canadian household, considering the worst expected weather conditions, neglecting solar thermal power and internally generated thermal power.

2. Assign the maximum required thermal demand for an individual household and apply the area normalization procedure to obtain the required thermal demand for each of the 215 houses, as well as community and commercial buildings.

3. Utilize THERMOS to estimate the piping routing requirements.

#### 3.1.5.2 Thermal Demand Grouping

Simulating all residential houses in a potential DHN is time-consuming and computationally demanding. To reduce simulation time, the model assumes groupings of nearby thermal loads, treating them as a single load. This methodology significantly reduces simulation time while maintaining accuracy, based on pipe length limitations and the DHN characteristics. Thus, the grouping of houses is limited to a distance of 150 m along the radial DHN, ignoring the temperature drop within this distance. No grouping is considered for pipeline lengths less than 50 m to minimize the number of groups. Furthermore, due to the faster response of the mass flow rate to internal or external variations compared to the radiator return temperature, the thermal power of a building can be assumed to be directly proportional to the mass flow rate.

#### 3.1.5.3 Piping Routing Design

The pipeline system under consideration consists of a double-way routing and comprises several layers, as depicted in Figure 3.2. These layers include the following: a Carbon steel layer, which is the first layer of the pipeline and serves as the structural component; a Polyurethane insulation layer, which is composed of Polyurethane insulation material with a very low thermal conductivity to minimize heat transfer and reduce heat loss from the pipeline; and a Polyisocyanurate insulation layer, which also presents low thermal conductivity. All these layers are buried underground at a depth denoted by Z to protect the pipeline and insulation layers from external environmental conditions and further minimize heat loss. Table 3.1 presents the key thermal properties and parameters of the materials used in the pipeline insulating system.

The following issues need to be considered in the design of the DHN piping network for the KLFN community:

- The linear heat density in the community is significantly lower compared to most typical DHNs. This results in a high ratio between piping heat loss and thermal demand.

Table 3.1: Piping Network Design Parameters

| Parameter | Value |
|---|---|
| Carbon steel density | 7843 kg/m$^3$ |
| Carbon steel specific heat capacity | 434 J/Kg°C |
| Carbon steel thermal conductivity | 45 W/m°C |
| First-insulator density | 30 kg/m$^3$ |
| First-insulator specific heat capacity | 1500 J/Kg°C |
| First-insulator thermal conductivity | 0.02 W/m°C |
| Second-insulator density | 32 kg/m$^3$ |
| Second-insulator specific heat capacity | 1400 J/Kg°C |
| Second-insulator thermal conductivity | 0.02 W/m°C |
| Soil thermal conductivity | 0.38 W/m°C |
| Water thermal conductivity | 0.64 W/m°C |
| Pipeline burying depth | 0.6 m |

- The soil properties in KLFN impose limitations on burying depth and the feasibility of excavation, since the considered area is predominantly covered by up to 4 m of glacial boulder till, overlaid by 20-30 m of fine sand and clay [126]. These soil conditions complicate the civil engineering works, thus increasing deployment costs.
- The community experiences harsh weather conditions, with temperatures dropping as low as -38°C during the Winter season. These extreme low temperatures further increase heat loss in the pipes.
- The main thermal plant is located approximately 1.65 km away from the starting point of the thermal demand. This results in increased heat losses and affects the QOS .

To minimize the excessive piping heat loss in the KLFN community, the following assumptions have been made:

- Due to the composition of the soil, increasing the burying depth is not feasible. Thus, the maximum burying depth considered is 0.6 m, as per recommended standards [127].

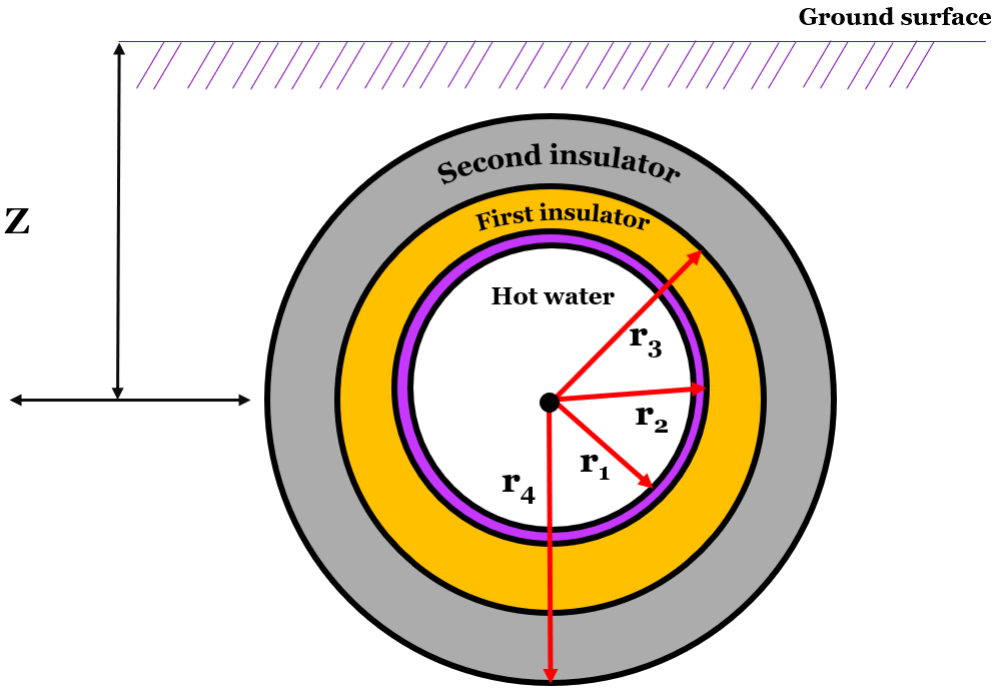



Figure 3.2: Cross-sectional design of a DHN pipeline.

- Modern insulation materials with low thermal conductivity, such as Polyurethane or Polyisocyanurate, are used to increase pipeline radial thermal resistance and reduce heat loss transfer.

- To minimize soil thermal conductivity, artificial soil such as mixed sandy loam can be used [128]. Although this approach may have a high initial cost, it is necessary to reduce the excessive piping heat loss. Moreover, by utilizing EG from DGUs, the CHP system efficiency can be improved, potentially offsetting initial costs over time. This cleaner heating source decreases the KLFN community's reliance on oil, reducing high carbon emissions and pollution, and enhances the EPN reliability by taking advantage of the DHN's thermal inertia. These benefits may justify the high initial cost of the IEHS in remote communities. However, it important to emphasize that this thesis does not assess the economic feasibility of DHN deployment; instead, the focus is on analyzing the dynamic operation and interaction between the EPN and DHN in remote community settings.

These considerations yield the diametrical ratios presented in Table 3.2 for different layers

Table 3.2: Pipeline Layers' Diametrical Ratios for Figure 3.2 in KLFN

| $r_2/r_1$ | $r_3/r_2$ | $r_4/r_3$ | $r_4/r_1$ |
|---|---|---|---|
| 1.1 | 1.364 | 1.333 | 2 |

Table 3.3: EG Recovery System Data for Different DGU Loadings

| DGU loading (%) | 100 | 75 | 50 | 25 |
|---|---|---|---|---|
| EG temperature (°C) | 524.0 | 524.0 | 457.5 | 452.1 |
| EG flow (kg/s) | 5.742 | 5.742 | 5.278 | 4.784 |
| Heat rejection (kW) | 1202 | 1202 | 1038 | 933 |

of carbon steel and insulation materials relative to the original inner pipe diameter, ensuring efficient heat transfer and minimizing heat loss.

#### 3.1.5.4 Waste Heat Recovery System

The assumed waste heat recovery system employs an HX to extract thermal power from the EG of KLFN community DGUs through water heating. The energy collected by the recovery system is modeled using tabular data from Caterpillar generators [129], with Table 3.3 illustrating the EG recovery system data for different DGU loadings. This data varies with DGU electrical loading conditions. The EG recovery system's energy consumption is minimal, primarily involving the operation of a control valve that regulates the EG mass flow rate, and thus its energy consumption is negligible compared to the energy collected, resulting in a rather large efficient factor.

#### 3.1.5.5 Simulation Results

This subsection presents some relevant results for the designed DHN of the KLFN community, with the dynamic components of the KLFN's DHN being modeled with equations (3.1)-(3.28) in Matlab/Simulink, with a fixed discrete solver and a time step of 0.278 ms. This time step was chosen because Matlab/Simulink simulation must be run in seconds and not hours, which are the time constants of the DHN model; hence, one can convert the DHN time-based signals from seconds to hours as follows: $0.278\,\text{ms} \times 3{,}600 = 1\,\text{s} \equiv 1\,\text{h}$. The setpoint temperatures range from 18°C to 25°C, at different times depending on the

Table 3.4: KLFN Thermostat Temperature Setpoints

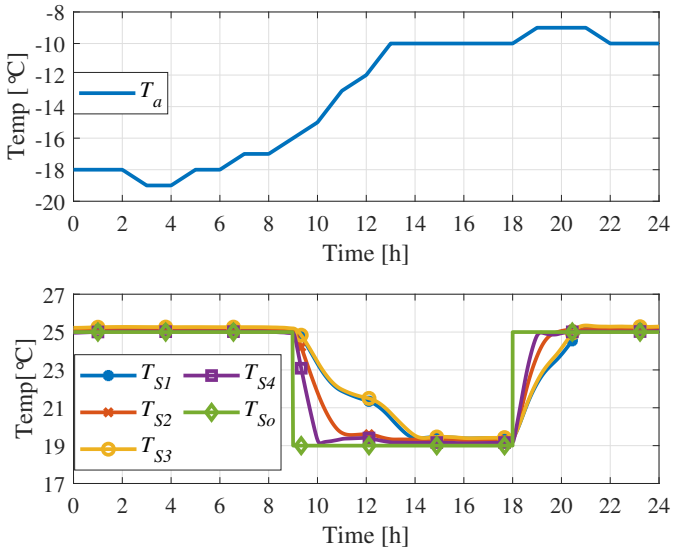
| Building | Time Intervals | | Setpoint |
|---|---|---|---|
| | From | To | |
| Residential | 9AM | 5PM | 18°C |
| | 6PM | 8AM | 25°C |
| Commercial | 6AM | 10PM | 25°C |
| | 11PM | 5AM | 18°C |
| Community | 8AM | 5PM | 25°C |
| | 6PM | 7AM | 18°C |

building topology. Table 3.4 illustrates the thermostat setpoints used for different KLFN community structures.

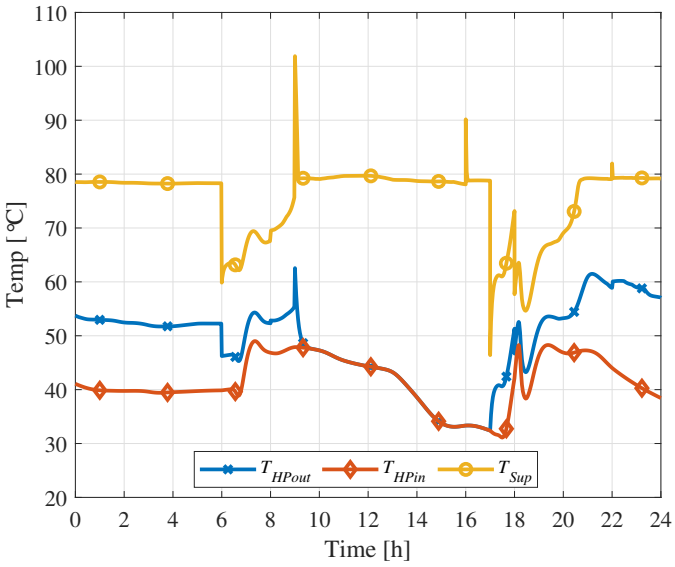
The presented results correspond to January 2, 2020, for 24 h and considering solar irradiance data from [123]. Figure 3.3a illustrates the variation in temperature setpoints for a consumer group situated at the distant end of the DHN, which has the largest temperature drop in the system. Note that when the temperature setpoint is low, the space temperatures do not decrease rapidly due to the existing solar thermal power and the thermal inertia of the spaces. The temperature response illustrates the temperature of each space within the four areas considered for a household. Observe that the modeled TRVs effectively track the temperature setpoints under the given ambient temperature conditions, ensuring satisfactory temperature regulation within the different spaces.

Figure 3.3b depicts the regulated supply temperature $T_{Sup}$ and water temperatures $T_{HPin}$ and $T_{HPout}$ of the HP. Since this device assists in preheating the return water when the thermal demand exceeds the capability of the EG heat recovery system, to ensure satisfactory QOS and accurate tracking of the temperature setpoint, the outlet temperature of the HP increases when it is active.

The required on/off HP operation is performed once every several hours, taking into account the high mechanical inertia of the IM driving the HP. Figure 3.4 illustrates the dynamics of thermal power demand, EG recovered power, piping heat loss, and HP-generated power. Note that the heat demand increases with increasing temperature setpoint and decreases with decreasing setpoint. Similarly, the generated thermal power is proportional to the thermal demand, but it does not necessarily balance the heat demand instanta-




(a)




(b)

Figure 3.3: (a) Ambient temperature and temperature response of the thermal group located at the far end of the DHN, and (b) temperature response of the thermal power plant and the HP.

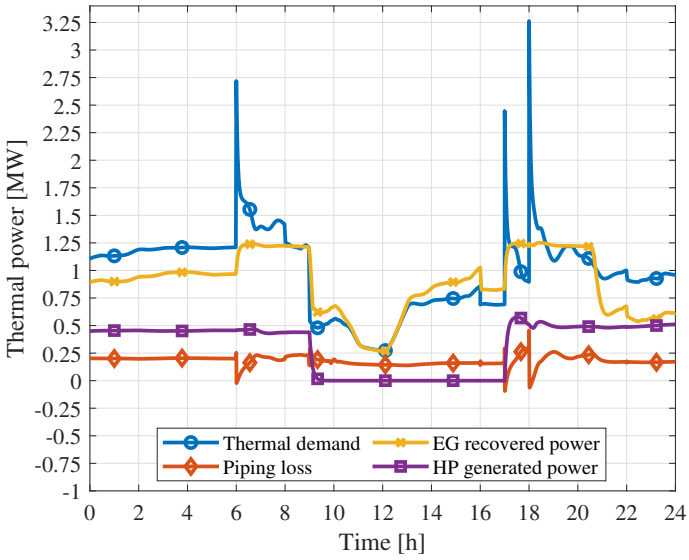



Figure 3.4: Thermal power demand, EG recovered power, piping heat loss, and HP generated power.

neously, as expected. Observe that the piping thermal losses under steady-state conditions do not exceed 20% of the thermal demand due to the use of low thermal conductivity insulators within the system, which is necessary in remote communities for the considered pipelines [130].

The fluctuations in the supply temperature in Figure 3.3b and the thermal demand in Figure 3.4 are due to the dynamic behavior of the DHN customers. For instance, at 9 h in Figure 3.3b, a decrease in setpoint temperatures by DHN consumers causes radiator valves to lower the hot water mass flow rate, significantly reducing the total thermal demand. This change is rapid, as radiator valves react within seconds, and requires a reduction in generated power, as depicted in Figure 3.4 at 9 h. Due to the time lag in the EG valve response, there is a temporary excess in thermal energy storage, which heats the supply water and increases its temperature. The same principle applies when thermal demand increases, leading to supply temperature fluctuations due to the time lag in adjusting the generated power. This lag in the EG valve controller is imposed to prevent the hot-water supply from boiling, which could cause pressure problems in the DHN piping system.

The heat balance between the thermal demand plus piping losses and the EG recovered power plus HP generated power is shown in Figure 3.5, showing that there are periods when the heat supply is either less than or greater than the heat load demand, with this deviation being managed through the thermal inertia of the DHN. For example, at 6 h in

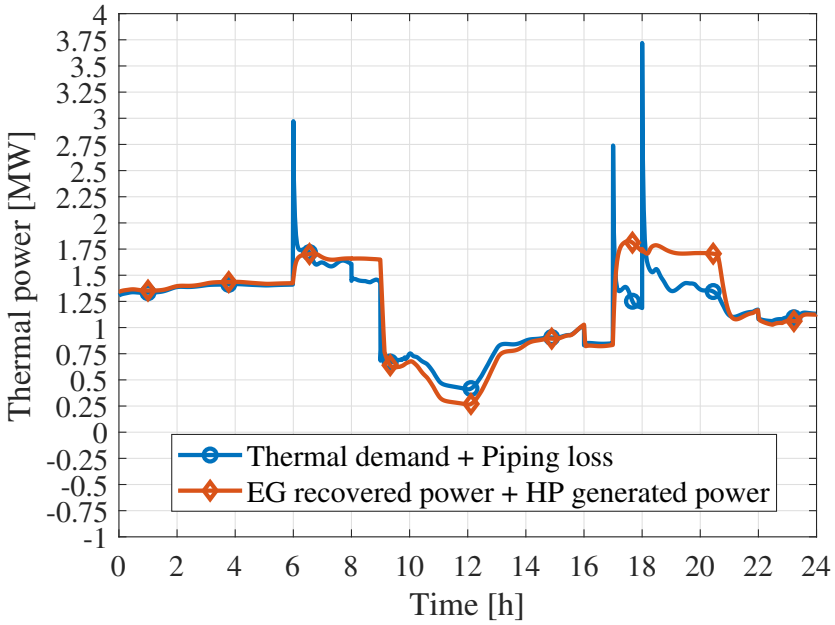



Figure 3.5: Heat balance between the thermal supply and demand of the KLFN DHN.

Figure 3.4, the thermal demand exceeds the supply, with the deficit being compensated by drawing thermal power from the DHN stored thermal energy, resulting in a decrease in the supply temperature as shown in Figure 3.3b. Conversely, at 9 h, when the supply exceeds the demand, the excess energy is stored, increasing the supply temperature. The slight time lag between the net stored energy and the supply temperature variation observed is compensated by the DHN thermal inertia acting as a buffer, smoothing out discrepancies between supply and demand, maintaining stability in supply temperature, and ensuring continuous and reliable heat delivery. To control thermal heat generation, both the EG recovery system and the HP are controlled to avoid undesirable spikes. This is achieved through an exhaust gas valve control for the EG recovery system and the direct torque load control of the HP, as previously discussed.

The aforementioned results demonstrate the feasibility of deploying a DHN in an actual remote community in the North. It is shown for the first time through detailed dynamic studies that the community thermal needs can be properly supplied by a DHN that takes advantage of the waste heat of DGUs in the community's EPN. These results further strengthening the case for such DHN deployment in remote communities, which have been demonstrated feasible through economic analyses based on static DHNs model. However, it is also shown that to accomplish this, there are challenges that need to be addressed with respect to DHN proper design and deployment, which may have a significant impact

on the potential deployment of DHNs in these communities, as it has been suspected but it is now demonstrated in this chapter through detailed dynamic modeling and studies.

It is important to highlight that a verification of the KLFN DHN model is conducted by confirming that the dynamic simulation results align with expected thermal behavior under varying operating conditions. For instance, the observed temperature responses depicted in Figure 3.3 across various building types are as expected following thermostat schedules and exhibiting moderated fluctuations due to thermal inertia and solar gains. As shown in Figures 3.3–3.5, the model outputs, including temperature profiles, thermal power contributions from various sources and losses, and the overall thermal power balance, consistently reflect expected trends. Thus, the simulated heat supply tracks demand with reasonable accuracy, and transient mismatches are buffered by the DHN's thermal storage capacity. Variations in supply temperature also correspond to changes in thermal demand, validating the modeled radiator valve dynamics and the time-delayed control of heat generation. Furthermore, piping losses remained within expected limits (below 20%), confirming the effectiveness of the applied insulation. Although direct validation with real-world measurements is not possible because the proposed DHN has not yet been implemented in the KLFN community, the model results are consistent and aligned with physical expectations.

## 3.2 EPN Model

This section describes briefly the traditional dynamic models considered for EPNs in remote MGs, and focuses on discussing the results of applying them to study the IEHS for the KLFN community. It also demonstrates the use of demand response control in the DHN HP for EPN frequency regulation to facilitate the integration of RES in remote MGs.

### 3.2.1 Isolated Microgrid Dynamic Model

#### 3.2.1.1 Diesel Generator

Synchronous DGUs are widely used in remote MGs as dispatchable grid-forming resources to support the system frequency. In this work, the Simscape Electrical library is utilized for accurate DGU dynamic modeling, including all required controls [131]. The synchronous machine model simulates the behavior of an alternator and can be adjusted to fit the specific parameters of MG generators. Cascading blocks are used to represent the governor droop

for frequency control. The automatic voltage regulator model ensures that the terminal voltage is maintained at the specified nominal voltage levels.

#### 3.2.1.2 Wind Generators

The WGs modeled here are based on full VSC interfaces. The VSC model utilized for the WGs, along with its controls, is described in detail in [132].

#### 3.2.1.3 PV Panels

The PV array block considered here contains PV modules arranged in parallel and series strings, with a "perturb and observe" control that adjusts the panel's voltage and current to track the maximum power point. This control algorithm optimizes power generation output by adapting to changing conditions as explained in detail in [133].

#### 3.2.1.4 Electric Loads

A constant impedance Z, current I, and power P load model is considered in the presented studies, which properly reflects the voltage sensitivity of MG loads [132].

#### 3.2.1.5 Heat Pump Ancillary Services

The DHN has a longer time response compared to the EPN due to its significant thermal inertia. This unique characteristic allows the DHN to play an important role in regulating the frequency of the EPN. Thus, for primary frequency control, the electrical demand of the HP can be adjusted for a specific duration, allowing to provide frequency regulation, while maintaining the desired DHN QOS. This is accomplished here using a frequency droop control to manage the speed of the three-phase variable speed IM that controls the thermal power generated by the HP, which can be modeled with the following equations that account for the compressor load torque applied to the HP's IM shaft:

$$\omega_{HPo} = P_{HPo} + k_{HP}\Delta f \tag{3.30}$$

$$\Delta f = f - f_o \tag{3.31}$$

Table 3.5: HP IM Drive Parameters

| **Parameter** | **Value** |
|---|---|
| $P_{HPo}$ | 250 kW |
| $k_c$ | 0.04354 kW·s$^3$ |
| $d\omega_{HP}/dt$ | 125.664 rad/s$^2$ |
| $k_{HP}$ | 25 p.u. |
| $k_p$ | 10 p.u. |
| $k_i$ | 100 p.u./s |

$$\tau_{HP} = k_c \omega_{HPo}^2 \tag{3.32}$$

Droop control allows the HP IM to improve the performance of the EPN frequency response compared to solely applying droop control to the DGU units. Table 3.5 depicts the main parameters used to represent the HP IM drive model, including the maximum rate of change of the angular velocity $d\omega_{HP}/dt$.

To fully leverage the high thermal inertia of the DHN, it is proposed here to implement a secondary frequency control strategy to rapidly mitigate steady-state frequency deviations within seconds, without the need to wait for approximately 15 min for DGU redispatch, which is the usual dispatch rate of MG energy management system [22]. Thus, secondary frequency control is implemented here on the HP's IM drives utilizing an anti-wind PI controller. This controller is employed to adapt the HP shaft power reference, based on the following equation:

$$P_{HPo} = K_p \, \Delta f(t) + K_i \int \Delta f(t) dt \tag{3.33}$$

Note that the values of $k_p$, $k_i$, and $k_{HP}$ in Table 3.5 are expressed in per unit based on a power base of 250 kW, a frequency base of 60 Hz, and a speed base of 188.496 rad/s for the compressor's four-pole IM.

The HP demand response used here for frequency regulation purposes has a negative impact on the HP thermal power, which affects the performance of the DHN. In this context, it is important to study the temperature changes in the community to evaluate the impact of the HP thermal power reduction on the DHN dynamics, considering the

typical 15 min dispatch of the EG heat source, which is within the dynamic time constants of the DHN. This issue cannot properly captured in existing studies based on DHN static models.

### 3.2.2 KLFN Community Example

#### 3.2.2.1 EPN Description

Each dynamic component of the KLFN 's EPN system is modeled using Simscape in Matlab/Simulink, with a fixed discrete solver and a time step of 0.1 ms. The simulations are based on measured data from existing electrical sources and loads, collected at the KLFN community during 2014 and 2015 to study the deployment of additional RES for the EPN [134]. Thus, there are three 1500 kW, 1000 kW, and 600 kW DGU units. As per the utility's dispatch rules, only one unit operates at a time. Additionally, there is a 10 kW roof-top PV panel and 4 wind turbines totaling 60 kW (three 10 kW single phase converter-interfaced units and one 30 kW direct-connected unit), which are modeled here as a single VSC-interfaced unit, to represent WG systems currently being deployed in isolated MGs. A 250 kW PV array is also considered to study the impact of RES power fluctuations on the performance of the EPN, as discussed in [135].

Figure 3.6 shows the PV power fluctuations assumed from the modeled 250 kW PV panel, based on scaled real measured data for the existing 10 kW PV panel over a 100 s time window. To test the IEHS performance for a significant EPN contingency, it is assumed that a rapid loss of PV generation at about 50 s due to sudden cloudy conditions, followed by its tripping due to a grid contingency.

The demand of the commercial and community buildings are represented using measured data collected for the various existing facilities, and the total residential demand is calculated by subtracting the demands of the commercial and community buildings from the measured total generation, realistically assuming minimal losses in the MG feeders. A 24.7% unbalance condition is considered, as commonly observed during Winter months in the KLFN MG [134]. During the simulation for January 2, 2020, considered in the DHN studies, the electrical load is assumed initially to be 523.6 kW, with the demand gradually increasing and peaking roughly at 900 kW, excluding the HP power demand. The 1000 kW DGU unit is assumed to be supplying the electrical load needs.

Table 3.6 presents the nominal power of various generation sources in the community. Additionally, Table 3.7 presents the power ratings for different types of loads considered in the simulation. These loads are modeled as 60% constant Z, 30% I current, and 10% constant P.

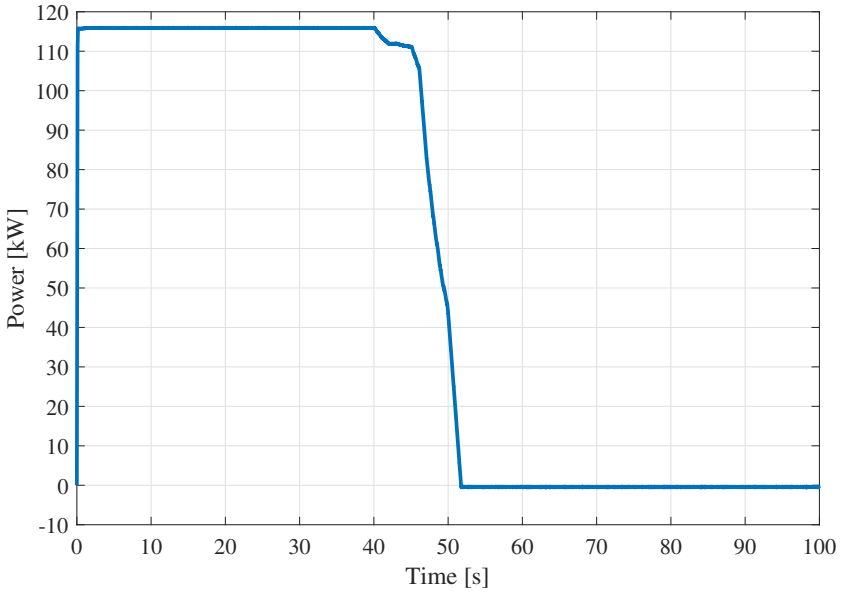



Figure 3.6: Power fluctuation of PV panels, with a sudden trip at about 50 s.

Figure 3.7 shows the KLFN's IEHS structure, depicting the KLFN potential DHN described in Section 3.1.5, illustrating 55 thermal load groups corresponding to 215 residential houses along with the 10 community and commercial buildings. This figure shows the interconnections between the EPN and the DHN.

In the KLFN IEHS, both the DGU and the HP IM present frequency droop controls with opposite slopes, as shown in Figure 3.8. The compressor load torque in the IM drive is modeled with (3.32).

#### 3.2.2.2 Simulation Results

The frequency response for KLFN EPN is illustrated in Figure 3.9 for the 100 s studied window for four distinct case studies:

- Case 1 represents the EPN operating independently without the DHN, solely supplying the base electrical load of 688 kW.
- Case 2 examines the IEHS without HP demand management.
- Case 3 studies the IEHS with HP droop control.

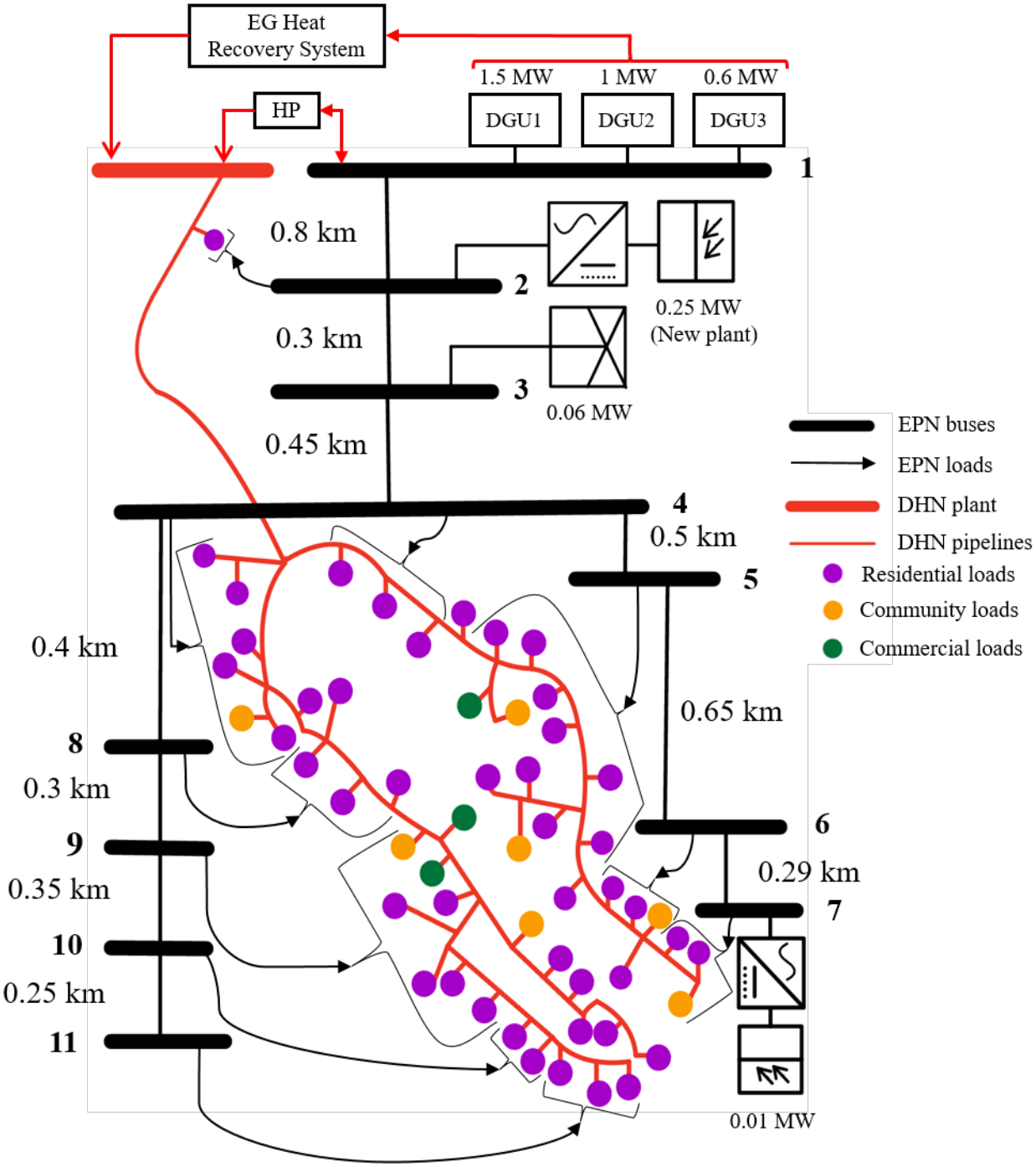



Figure 3.7: KLFN Community IEHS.

Table 3.6: KLFN Generator Ratings

| **Generator Type** | **Rating** |
|---|---|
| DGU1 | 1500 kW |
| DGU2 | 1000 kW |
| DGU3 | 600 kW |
| WG | 60 kW |
| Exist. PV | 10 kW |
| Added PV | 250 kW |

Table 3.7: KLFN Load Types and Powers

| **Load Type** | **Min.** | **Max.** |
|---|---|---|
| Police Station | 8.07 kW | 13.6 kW |
| School | 11.03 kW | 18.6 kW |
| Sewage Plant | 3.56 kW | 6 kW |
| Water Treatment Plant | 19.4 kW | 32.7 kW |
| Nursing Station | 12.1 kW | 20.4 kW |
| Grocery Store | 37.55 kW | 63.3 kW |
| Residential | 431.84 kW | 760.8 kW |

- Case 4 correspond to the IEHS with HP secondary frequency control capability.

Observe in Figure 3.9 that the electrical load stays close to 688 kW (excluding HP power consumption for Case 1), since the voltage at the load buses does not change significantly, consistent with [135]. Note the initial frequency variations due to the system components' startup, notably the DGU, the WG, and the HP's IM, followed by a steady frequency for roughly 40 s, given the fixed PV output power during this period. Subsequently, there is a change in solar irradiance probably due to cloud movement followed by a rapid reduction and then loss of PV generation at about 50 s, resulting in the frequency dropping to 59.84 Hz for Cases 1 and 2. During this period, only the DGU droop control is responsible for regulating the frequency in these two cases, while the demand from the HP motor remains

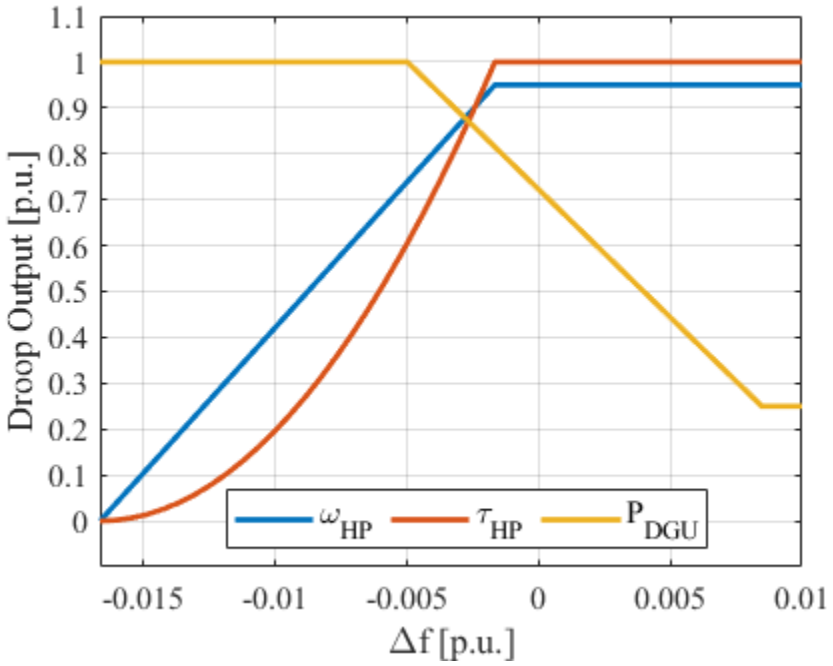



Figure 3.8: Droop control for DGU and HP IM.

constant. In contrast, with the HP droop control, Case 3 shows a faster frequency response and reduced frequency deviation compared to Cases 1 and 2, with the frequency stabilizing at 59.89 Hz. The best frequency response is achieved in Case 4 by implementing secondary frequency control, which restores the frequency to 60 Hz within 15 s, without the need for DGU redispatch.

Figure 3.10 presents the power output from the DGU for Case 4, which remain fixed at 825 kW to supply the base EPN and DHN HP loads, as per the required dispatch rules at KLFN [135]. Note that the power and shaft speed of the HP change with the frequency due to the HP secondary frequency control.

The variations in electric power generation due to the change and loss of PV generation significantly influences the thermal power supplied to the DHN, primarily due to the reduction in HP shaft power interacting with the EPN frequency variations, as depicted in Figure 3.11. Following the loss of PV generation, a 15 min monitoring period of HP and DGU powers is used to assess the worst-case scenario before a subsequent DGU redispatching, reasonably assuming constant thermal power demand. In contrast, the base electric load undergoes a ramp variation from 688 kW to 753 kW, based on measured

data for the KLFN community. Despite these EPN generation and load fluctuations, DGU power remains relatively constant at 825 kW, while HP shaft power notably decreases from 242 kW to 87 kW to compensate for both the PV generation variations and the increase in the base load during the 15 min interval to mitigate EPN steady-state frequency deviations. At the same time, HP thermal generation decreases from 490 kW to 200 kW, indicating a significant loss in thermal power generation that impacts the DHN supplied thermal power. Additionally, Figure 3.11 illustrates HP 's COP variations, highlighting its nonlinear variation, which directly depends on HP thermal and electrical power values.

As shown in Figure 3.10, the electrical system is being simulated with seconds resolution, whereas the thermal system is simulated with min resolution, as shown in Figure 3.11. This is possible due to the IEHS electrical and heating systems having different time constants, since for example, the thermal inertia of the HP is much higher than its mechanical inertia, thus allowing the computationally efficient co-simulation of the two systems with different time scales, using fractions of a second for the electrical system and fractions of a minute for the thermal system, without significant simulation errors. The use of the shorter electrical system time intervals to simulate both systems would require extensive computation time, without significant changes in the results.

It is important to highlight that in the 15 min interval shown in Figure 3.11, the load varies gradually, as per actual measurements at the KLFN community [135], while the DGU power remains basically fixed, since this is only re-dispatched every 15 min through the existing EMS. The figure shows that the DGU governor's impact on the generator power output is small, since the HP regulates the frequency in this case, as illustrated in Figure 3.10.

To examine the impact of HP thermal power reduction due to droop and secondary frequency controls, Figure 3.12 depicts the DHN temperature dynamics. Observe that due to the high thermal inertia of the DHN, noticeable change on building temperatures would require a considerable amount of time, as depicted in Figure 3.12. This figure illustrates the various building spaces and setpoint temperatures for the consumer group situated at the distant end of the DHN for the studied 15 min timeframe. Thus, the minimal heating requirements are met without disrupting consumer QOS, assuming no heat load service interruptions, with only a 0.15°C temperature drop in 15 min after the HP thermal power reduction. This indicates that it would take several hours for DHN customers to notice any significant impact from the reduced thermal power generation in the HP. Furthermore, after 15 min, these slight temperature changes would be corrected with the DGU re-dispatch that allows resuming the HP normal operation.

When the EG thermal power generated is sufficient to supply the KLFN thermal demand, the HP would not be needed and hence would be turned off. Consequently, sec-

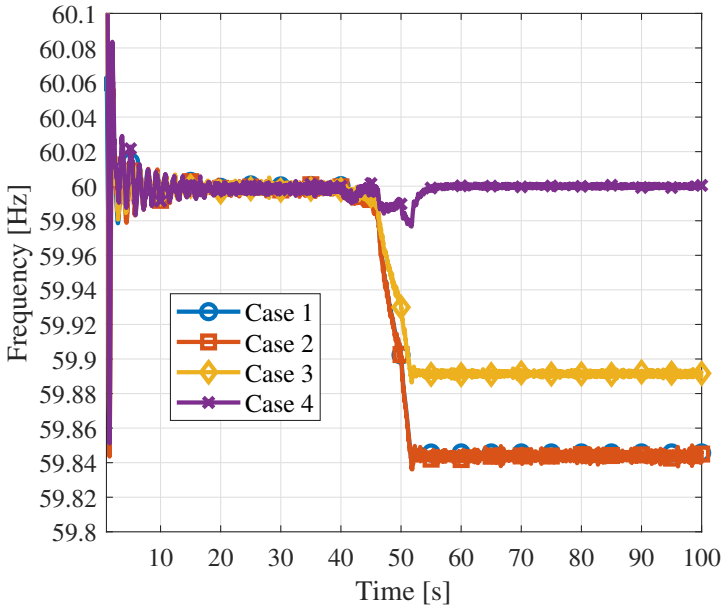



Figure 3.9: Comparison of frequency response with and without DHN and HP droop control.

ondary frequency control cannot be provided using the HP, with the DGU having to deliver this regulation service during the usual 15 min DGU redispatch intervals, as it is now the case in existing remote EPNs, which would be costlier compared to utilizing the DHN thermal inertia for this purpose.

#### 3.2.2.3 Electric Thermal Storage Heating

To further highlight the effectiveness of the potential DHN in the KLFN community, this section discusses the case where all thermal demand in KLFN community is met by individual ETS units currently deployed in some remote communities, comparing the EPN performance with respect to the IEHS results.

To estimate the electric power demand required to fulfill the thermal demand of the community with ETS units, the SRLS tool was used. Thus, Figure 3.13 illustrates the building heating control for the ETS units used in the SRLS to represent the thermal dynamics of a household. The model takes into account external ambient temperature and the thermal power generated by the ETS units to maintain the household space temperatures at a specified setpoint by adjusting the discharge resistance $R_{disch}$, which reflects the variable speed of the ETS unit's heat distribution fan. In this case, it is assumed that all

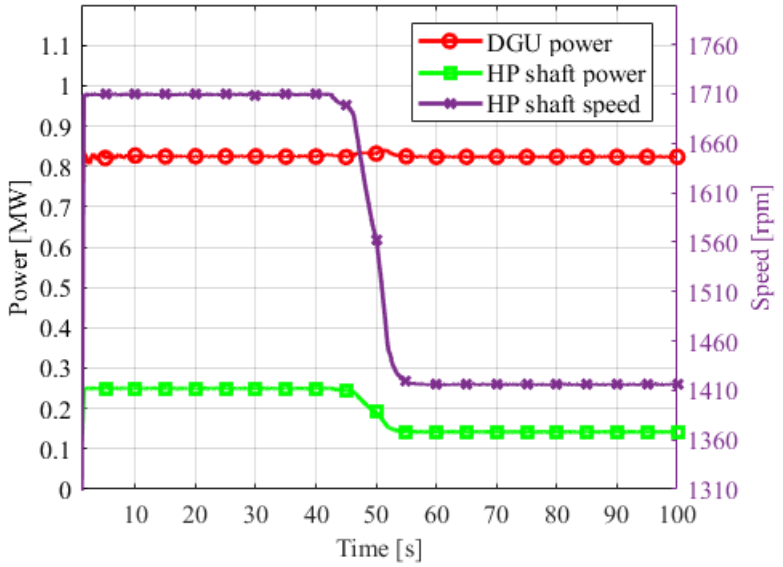



Figure 3.10: Generator power, HP shaft power, and shaft speed with frequency changes.

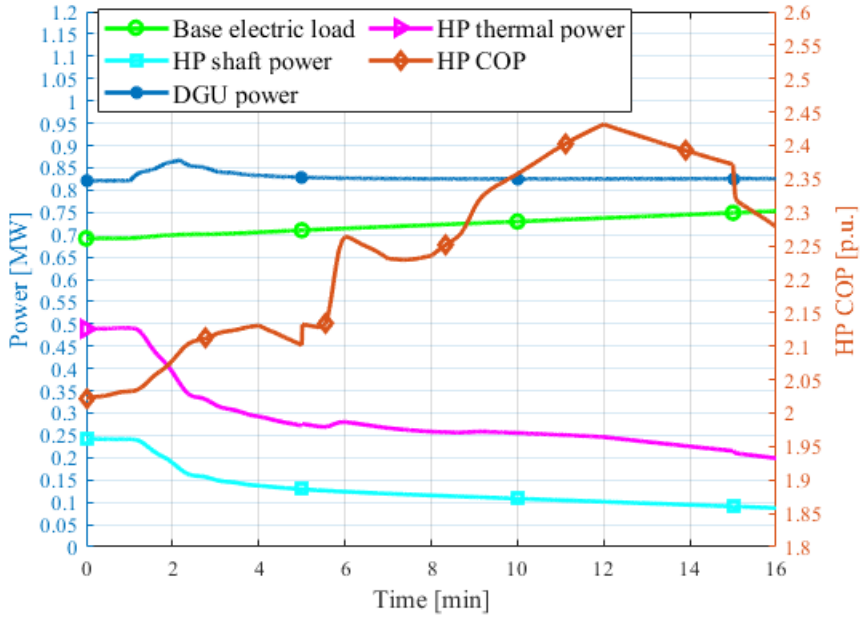



Figure 3.11: Generator power, HP shaft and thermal powers, base electric load, and HP's COP.

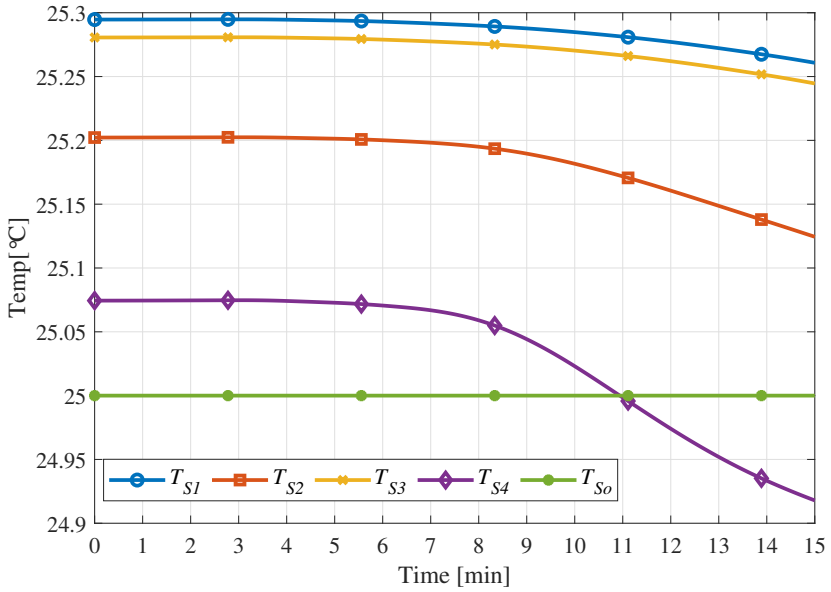



Figure 3.12: Temperature response of the thermal group located at the far end of the DHN after HP thermal power reduction imposed by the secondary frequency control.

ETS units utilized in KLFN community have an overall efficiency of 95%. Further details of the dynamic modeling and control of the ETS unit are available in [136], [137], and [138].

To ensure an equitable comparison between IEHS with DHN and with ETS units for ancillary services provision, demand management is also applied to the ETS units, based on the approach outlined in [139], which is implemented here using the following equations:

$$f_{DR} = \frac{1}{1 + e^{k_{DR1}(\Delta f + k_{DR2})}} - \frac{1}{2} \tag{3.34}$$

$$\frac{dP_{DR1}}{dt} = k_{DR3} f_{DR} \overline{P}_{DR} - P_{DR1} \tag{3.35}$$

$$P_{DR2} = \min\left(\mid \mathbf{P_{DR}} - P_{DR1} \mathbb{1} \mid\right) \tag{3.36}$$

where the control function $f_{DR}$, based on sigmoid function due to its smooth, non-linear, saturating behavior, and ease of adjustment, effectively generates the desired demand response $P_{DR1}$ based on the frequency deviation $\Delta f$, with constants $k_{DR1}$, $k_{DR2}$, $k_{DR3}$, and $\overline{P}_{DR}$ defined in the Nomenclature. $P_{DR1}$ is then compared with $\mathbf{P_{DR}}$, which signifies the vector encompassing all the potential on/off combinations of ETS power consumption

Table 3.8: ETS Demand Response Control Parameters

| **Parameter** | **Value** |
|---|---|
| $k_{DR1}$ | $-600$ p.u. |
| $k_{DR2}$ | $-0.02$ p.u. |
| $k_{DR3}$ | 100 p.u. |

of 55 groups in the KLFN community. The value closest to $P_{DR1}$ among the elements of $\mathbf{P_{DR}}$ defines the ETS load combination selected to generate the actual actuating demand response $P_{DR2}$. Table 3.8 presents the parameter values used in (3.34)-(3.36) to model the demand response control of the ETS units, which determine their response for primary frequency control.

Figure 3.14 depicts the thermal demand of the community with a DHN vis-à-vis the ETS units. Note the need for a minimum 1.8 MW power capacity to fulfill the required heat demand using only ETS units. Considering a peak electrical load of 0.9 MW for the studied day results in a total demand of 2.7 MW for both electrical and thermal loads. Hence, two DGUs would need to be dispatched, which is not the usual dispatch strategy in remote Ontario communities [140].

Two additional case studies are added here to the previously discussed four case studies:

- Case 5 correspond to the EPN and ETS heating units without ETS demand response control.
- Case 6 incorporates the EPN and ETS heating units with ETS demand response control.

For these cases, the total electrical load of the EPN is 2,488 kW, being supplied by the DGUs DGU1 and DGU2, which corresponds to 688 kW of base electric load, as in the EPN+DHN simulations, and 1,800 kW of demand from the ETS units. The two generators have droop control, sharing the power changes proportionally to their capacity.

Under the same variations in PV generation power discussed in Figure 3.6, Figure 3.15 depicts the frequency responses for the IEHS and the EPN equipped with ETS units, for the same 100 s time window utilized before. Observe that in ETS Cases 5 and 6, the frequency deviation is lower compared to the droop control Cases 1, 2, and 3. This can be attributed to the presence of two generators, which effectively distribute PV fluctuations. Note that distributed ETS demand response enhances the primary frequency control of the

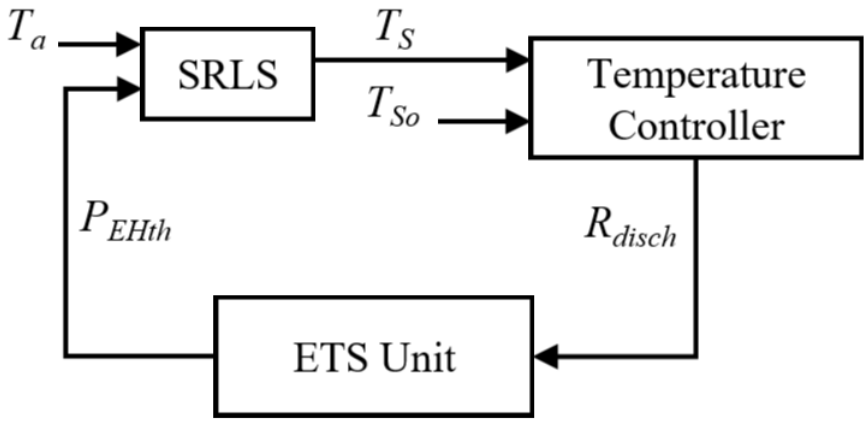



Figure 3.13: Schematic of building heating with ETS unit.

EPN compared to the centralized HP-based control. However, this requires a more complex distributed approach, with more significant control and communication requirements than the centralized HP-based frequency regulation technique. Furthermore, the proposed ETS frequency regulation control presents significant uncertainties associated with the individual ETS power availability. Finally, the proposed HP demand response for frequency regulation facilitates the implementation of a secondary frequency control.

From the presented results, the advantage of using a DHN versus ETS units to supply the community thermal loads is clear. Thus, first, emissions would significantly increase with the ETS units, as more DGUs would need to be dispatched, and the DGU exhaust thermal power not being utilized. Second, the DHN would allow a better integration of variable RES through the ready utilization of its significant thermal storage capacity via HP frequency droop control. Finally, the IEHS featuring HP droop control and secondary frequency control would be preferable over the use of ETS units due to a simpler communication network and control requirements, plus smoother and less uncertain HP speed control compared to ETS demand response switching.

#### 3.2.2.4 HP and ETS Frequency Control Comparison

This section compares the performance of the demand response centralized control of ETS units and the centralized HP droop control for primary frequency control in the KLFN EPN. To accomplish this, a step increase in base load from 686 kW to 825 kW at 50 s is studied here, with the power output from the RESs remaining constant. Figure 3.16a shows that both controllers react by adjusting their demand to maintain adequate primary

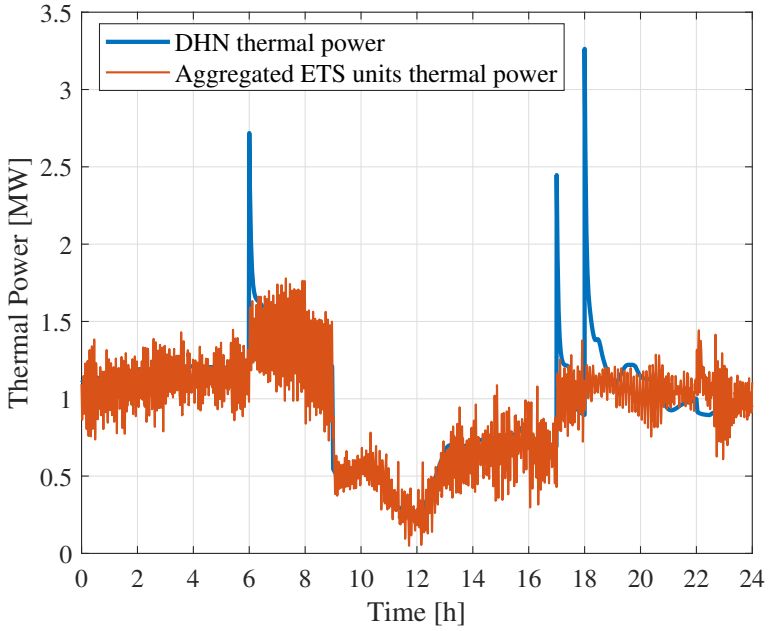



Figure 3.14: Comparison between DHN and ETS units for thermal demand provision.

frequency control, with the ETS units' demand decreasing from 1792 kW to 1745 kW and the HP shaft power decreasing from 250 kW to 213 kW. However, Figure 3.16b demonstrates that the ETS demand response control is faster than the centralized HP droop control. This is due to the overall mechanical inertia of the HP and its droop control, which allow the IM speed change to regulate the frequency with a maximum rate of speed change of $\pm$1200 RPM/s to realize a smooth speed control, which causes latency in the HP shaft power's response, thus affecting frequency control. On the other hand, the centralized ETS control utilizes multiple ETS units across the community, resulting in a faster control response through the on/off operation of designated ETS units. As shown in Figure 3.16b, the time difference between both controllers before reaching a stable frequency is roughly 2 s, illustrating the faster ETS demand response for primary frequency control.

#### 3.2.2.5 IEHS Frequency Control For Overlapping RES and Load Fluctuations

To further evaluate the capability of the DHN for providing effective secondary frequency control in remote MGs, the KLFN IEHS is tested under an overlapping RES dips and a sudden load increase. Thus, as depicted in Figure 3.17, the PV power variations are the same as those shown in Figure 3.6, but now an additional sudden loss of 31 kW of WG power is assumed to take place at 60 s. Furthermore, a load step from 688 kW to 730

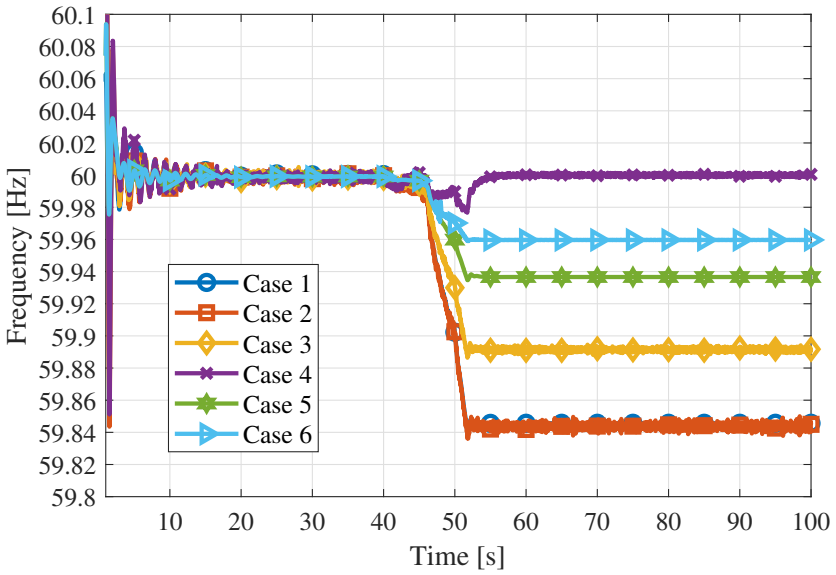



Figure 3.15: Comparison of frequency response between IEHS and EPN with ETS units.

kW at 80 s is introduced. As expected, observe that the HP power decreases its power to help maintain a stable frequency at 60 Hz through its primary and secondary frequency controls. Since during this period, the DGU is not yet re-dispatched, its power remains fixed, with small variations due to its governor actions. This demonstrates the effectiveness of the proposed DHN controls for maintaining frequency stability in the EPN.

It is important to highlight that the KLFN EPN model dynamic response under various operating conditions is consistent with its expected behavior. For example, the simulation results shown in Figures 3.9, 3.10, and 3.15 illustrate realistic frequency dynamics, load-sharing behavior, and generator responses under load fluctuations and renewable generation variability, respectively. The modeled also system accurately reflects frequency deviations and recovery following changes in PV output and load steps, consistent with established EPN dynamics. Thus, generator droop control, HP response, and secondary frequency regulation are all properly reflected, with minimal overshoot and settling times aligning with expectations for MGs with similar inertia and control settings. Furthermore, dynamic measurements for the existing KLFN EPN community, as discussed previously in Section 3.2.2.1, have been used to inform and validate key modeling assumptions, particularly base load trends and generation dispatch practices, reinforcing the reliability of the EPN simulation outcomes.

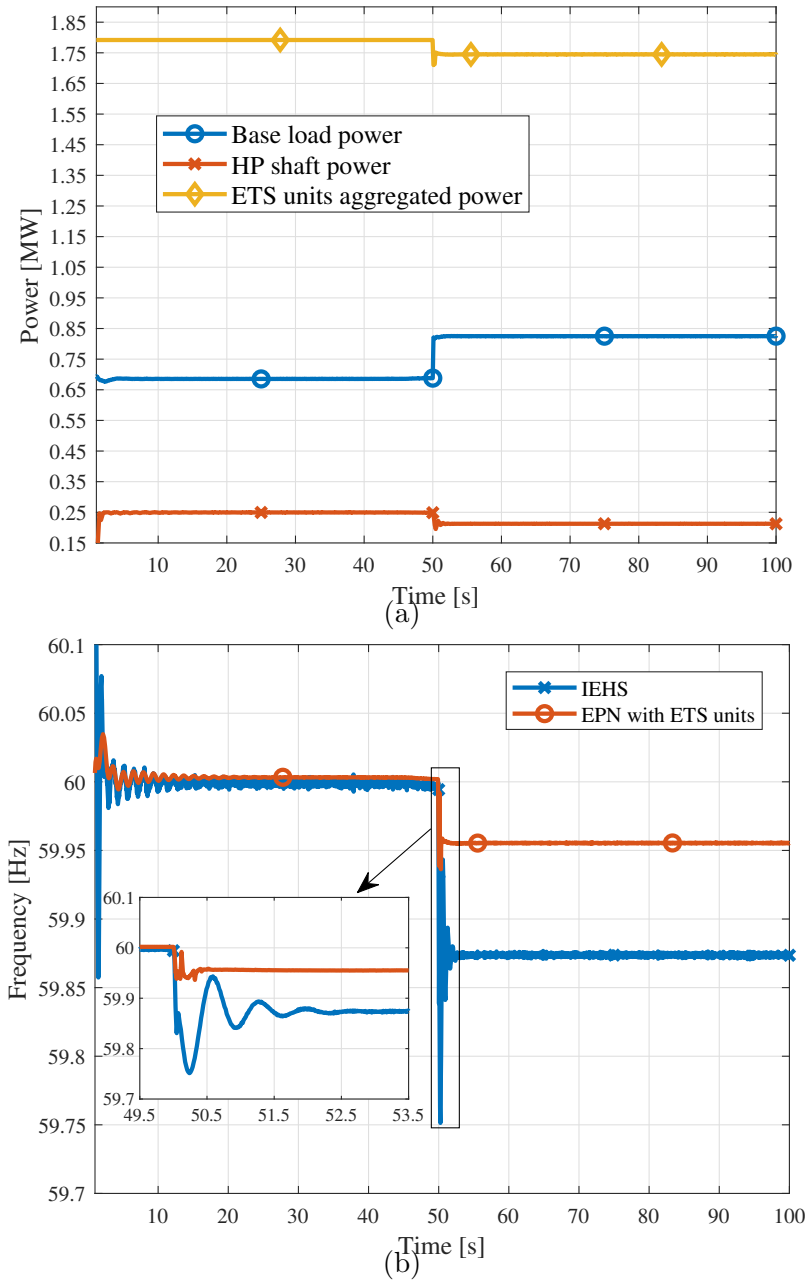



Figure 3.16: Comparison of primary frequency control response between IEHS and EPN with ETS units for a step load increase: (a) electrical power and (b) frequency.

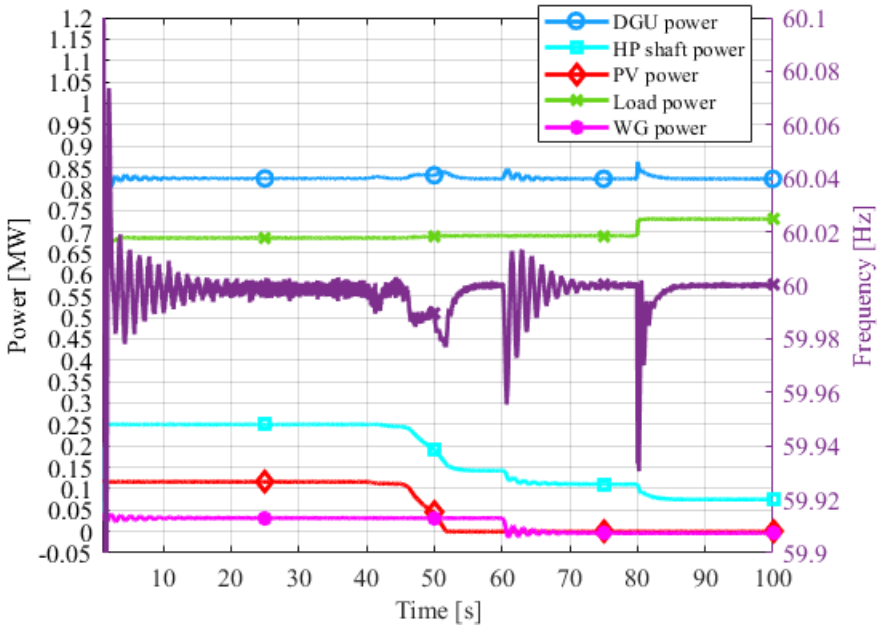



Figure 3.17: IEHS secondary frequency control under overlapping RES and load fluctuations.

## 3.3 Summary

Detailed dynamic modeling and control of IEHSs in isolated MGs were developed and validated, with a focus on remote communities. The design and modeling of a DHN to provide space heating in these communities was discussed in detail, based on the utilization of waste heat energy from DGU exhaust systems. In this context, the developed dynamic model allowed to analyze the specific insulation needs of the piping for a DHN distribution network in remote areas due to their low linear heat density, which would not be possible using existing static models.

The dynamic IEHS model of the DHN and EPN including HPs was also presented, including a proposed primary and secondary frequency control, offering power reserves for frequency regulation in isolated MGs for the proper integration of variable RES, taking advantage of the significant thermal energy storage of DHNs. Finally, the feasibility and advantages of using an DHN+EPN IEHS to supply both thermal and electric demand for remote communities was demonstrated through dynamic studies, and by comparing the integrated system with an ETS-based approach. The results show the successful utilization of DHN for meeting thermal requirements and regulating EPN frequency in isolated MGs

with significant penetration of RES. The presented study, which was published in [141], could be expanded to explore the feasibility of supplying domestic hot water to consumers in remote communities through the DHN.

# Chapter 4

# Dynamic Modeling and Practical Application of Boiling Water Small Modular Reactor Power Plants

This chapter presents a comprehensive dynamic model of a BWSMR power plant, incorporating all essential components including the reactor, steam turbine, and steam flow control system to evaluate its practical applications in modern BPSs. Unlike previous studies that primarily focus on individual elements, this work proposes the first full-system model featuring direct steam expansion, capturing key thermal-hydraulic dynamics of the reactor such as pressure variations and two-phase drift velocity, thereby improving simulation fidelity.

The developed model also includes a detailed representation of the thermal systems to support the co-generation studies discussed in the next chapter, particularly for DHNs. Furthermore, the primary frequency control capabilities of the 10th generation BWRX-300 BWSMR, currently being developed in Ontario, Canada, are evaluated under both reactor leading and turbine leading control strategies. The latter is shown to provide superior performance, especially in scenarios with increasing levels of RESs penetration. Finally, the model is integrated into a widely used power system analysis tool to assess its dynamic behavior and overall impact on Ontario's BPS.

# Nomenclature

### Parameters

| | |
|---|---|
| $A_c$ | Core cross-sectional area [$m^2$] |
| $A_s$ | Core heat transfer surface area [$m^2$] |
| $C_f$ | Mass heat capacity [kJ/°C] |
| $c_p$ | Specific heat capacity [kJ/kg·°C] |
| $c_w$ | Water specific heat capacity [kJ/kg·°C] |
| $H_b$ | Heat transfer coefficient, boiling region [W/$m^2$·°C] |
| $H_{nb}$ | Heat transfer coefficient, core non-boiling region [W/$m^2$·°C] |
| $K$ | Linear fitting slope of HPT [p.u] |
| $K_{droop}$ | Droop control coefficient [p.u] |
| $P_{Gref}$ | Reference power [MW] |
| $T_{set}$ | Setpoint temperature [°C] |
| $\Delta T_b$ | Temperature difference, core boiling region [°C] |
| $\alpha_f$ | Fuel temperature feedback reactivity coefficient [p.u] |
| $\alpha_v$ | Void feedback reactivity coefficient [p.u] |
| $\beta$ | Delayed neutron fraction [p.u] |
| $\beta_{sp}$ | Moisture separated from HPT outlet [p.u] |
| $\delta$ | Fraction of fission energy deposited promptly in reactor coolant [p.u] |
| $f_{ref}$ | Reference frequency [Hz] |
| $g$ | Acceleration due to gravity [$m/s^2$] |
| $k_{HPT}$ | HPT input-output pressure ratio [p.u] |

| | |
|---|---|
| $k_i$ | PI controller integral gain |
| $k_p$ | PI controller proportional gain |
| $k_{pe}$ | Polytropic expansion factor [p.u] |
| $l$ | Neutron generation time [s] |
| $\lambda_i$ | Decay constant of the $i$-th group of delayed neutrons [$s^{-1}$] |
| $\sigma$ | Surface tension [N/m] |
| $\tau_{HPT}$ | HPT time constant [s] |
| $\tau_{sp}$ | Moisture separator time constant [s] |
| $\eta_{HP}$ | High pressure turbine efficiency [p.u] |
| $\eta_{LP}$ | Low pressure turbine efficiency [p.u] |
| $\dot{m}_{nom}$ | Nominal coolant mass flow rate [kg/s] |
| $\dot{m}_{set}$ | BP valve setpoint mass flow rate [kg/s] |

**Variables**

| | |
|---|---|
| $C_i$ | Concentration of the $i$-th group of delayed neutrons [p.u] |
| $P_{in}$ | HPT inlet pressure [MPa] |
| $P_{out}$ | HPT outlet pressure [MPa] |
| $P_{sat}$ | Saturation pressure [MPa] |
| $Q$ | Thermal power [MW] |
| $SG$ | Specific gravity [p.u] |
| $T_0$ | Coolant inlet temperature [°C] |
| $T_f$ | Fuel temperature [°C] |
| $T_{fw}$ | Feedwater temperature [°C] |

| | |
|---|---|
| $T_{in}$ | HPT inlet temperature [°C] |
| $T_m$ | Metal temperature, non-boiling region [°C] |
| $T_{out}$ | HPT outlet temperature [°C] |
| $T_{sat}$ | Saturation temperature [°C] |
| $W_{HPT}$ | HPT mechanical power [MW] |
| $W_{LPT}$ | LPT mechanical power [MW] |
| $\Delta P$ | Pressure drop [MPa] |
| $\Delta \dot{m}_{MSI}$ | Change in MSI valve mass flow rate [kg/s] |
| $\dot{m}_{BP}$ | BP valve mass flow rate [kg/s] |
| $\dot{m}_{LPT}$ | LPT inlet mass flow rate [kg/s] |
| $\dot{m}_{MSI}$ | MSI valve mass flow rate [kg/s] |
| $\dot{m}_c$ | Coolant mass flow rate [kg/s] |
| $\dot{m}_{ex1,ex2,...}$ | LPT extracted mass flow rates [kg/s] |
| $\dot{m}_{in}$ | HPT inlet mass flow rate [kg/s] |
| $\dot{m}_{sp}$ | Moisture separator mass flow rate [kg/s] |
| $\dot{m}_{st}$ | Steam mass flow rate [kg/s] |
| $f$ | Frequency [Hz] |
| $h_{LPT}$ | Specific enthalpy of LPT inlet steam [kJ/kg] |
| $h_{ex1,ex2,...}$ | Specific enthalpies of LPT extractions [kJ/kg] |
| $m_f$ | Mass of liquid [kg] |
| $m_g$ | Mass of vapor [kg] |
| $q''$ | Heat flux [MW/m$^2$] |
| $u$ | Specific internal energy [kJ/kg] |

| | |
|---|---|
| $u_f$ | Specific internal energy of liquid [kJ/kg] |
| $u_g$ | Specific internal energy of vapor [kJ/kg] |
| $u_{fg}$ | Latent heat of vaporization [kJ/kg] |
| $u_{gj}$ | Two-phase drift velocity [m/s] |
| $v_d$ | Void fraction [p.u] |
| $v_f$ | Specific volume of liquid [$m^3$/kg] |
| $v_g$ | Specific volume of vapor [$m^3$/kg] |
| $x$ | Steam quality [p.u] |
| $\phi$ | Average neutron flux [p.u] |
| $\rho$ | Net core reactivity [p.u] |
| $\rho_{ex}$ | External reactivity [p.u] |
| $\rho_f$ | Density of liquid [kg/$m^3$] |
| $\rho_g$ | Density of vapor [kg/$m^3$] |

## 4.1 BWSMR Modeling

The dynamic modeling of the BWSMR power plant involves developing detailed models for various critical and relevant components. This section presents the modeling justification and process for the essential components which are necessary to properly represent the BWSMR dynamics for proper grid control and stability studies. Thus, the proposed model of the BWSMR power plant should include the following components, as per the justification provided next:

1. Nuclear reactor core system: Fuel rods, coolant, neutron kinetics and thermal feedback reactivity (Doppler and void), and control rod dynamics.

2. Direct loop for a natural circulation BWSMR: RPV, riser and downcomer sections, and core hydraulic structure.

3. Steam turbine system: HPTs and LPTs, turbine control valves, BP valves, moisture separator, steam extraction ports, reheater, and droop-based governor system.

4. Generator and electrical interface: synchronous generator, excitation system, automatic voltage regulator, breaker and transformer, and load-following interface with the electric grid.

The reason for modeling these components, as opposed to representing all reactor and associated plant elements, is to capture the dominant physical and control dynamics of a BWSMR power plant operating under usual grid-connected or standalone conditions, such as load-following operation, grid fault conditions, and voltage and frequency regulation. Thus, several other components that are part of SMR power plants have not been modeled based on their limited influence on the dynamic behavior of interest. Specifically, safety and auxiliary systems, such as the emergency core cooling system, automatic depressurization system, residual heat removal, containment isolation mechanisms, and fire suppression systems, have not been modeled, these systems are primarily activated under abnormal condition such as a sudden loss of cooling, and hence remain inactive during usual operating conditions, which is the focus of this study. Similarly, environmental interface systems, such as suppression pools and water chemistry management, have been omitted, as their effects are negligible on the core thermal-hydraulic and electrical response under the usual plant operating conditions. Supervisory and operator-level platforms, including human–machine interfaces, alarm and protection coordination systems, and cybersecurity frameworks, have also been excluded, since these are designed for monitoring and interface purposes rather than influencing the plant's dynamics. The aforementioned modeling strategy is consistent with validated methodologies in the literature. Notably, the authors in [142] developed a dynamic model of a combined-cycle power plant for simulating frequency excursions, where several plant subsystems are intentionally excluded, such as the feedwater system, condenser, attemperators, water chemistry, and all supervisory-level controls. This was justified based on the negligible impact of these systems on the dynamic response of interest. For instance, the feedwater system responds rapidly to operational changes, minimally influencing the overall dynamic behavior of the plant. Thus, explicit modeling of feedwater flow and control is unnecessary for studies focused on frequency response or load-following conditions. For these reasons, a fixed RPV water level is assumed here, as it is well-regulated during usual operation and has negligible impact on steam and power dynamics in this study. Therefore, by modeling the essential thermal-hydraulic and generator-side components that govern the power plant's dynamic interaction with the grid,

and intentionally omitting systems that do not affect dynamic performance under normal conditions, the proposed BWSMR power plant model is considered both comprehensive and appropriate for simulating load-following, grid faults, voltage and frequency regulation, and other typical operating conditions relevant to power plant control and stability studies.

It is important to highlight that, given the focus of the proposed models on typical grid-interactive scenarios, as previously discussed, the proposed models do not capture the activation of safety systems such as the Isolation Condenser System (ICS), which are designed to operate only during emergencies [45]. Thus transients, while potentially significant in emerging situations, have no impact under normal grid dynamics. For such studies, high-fidelity thermal-hydraulic tools like RELAP5 or TRACE, which simulate the behavior of nuclear reactor systems during transient and accident conditions, would be needed, which is beyond the scope of this thesis. On the other hand, the exclusion of auxiliary systems, such as feedwater pumps, condensers, and heaters, can be justified, under the assumption that these have fast local control, and thus do not influence system-level dynamics. Therefore, the proposed BWSMR model can be assumed to be robust for frequency regulation, load-following, and BPS integration studies, which is the focus of this thesis.

### 4.1.1 Point Kinetic Equations

The dynamic behavior of the reactor core is captured using the point kinetic equations, as described in [39]. These equations detail the changes in neutron flux density $\phi$ over time and are represented as follows:

$$\frac{d\phi}{dt} = \frac{\rho}{l} - \frac{\beta}{l}\phi + \sum_i \lambda_i C_i \tag{4.1}$$

$$\frac{dC_i}{dt} = \frac{\beta_i}{l}\phi - \lambda_i C_i, \quad i = 1, 2, \ldots, 6 \tag{4.2}$$

where all parameters and variables in these and the following equations are defined in the Nomenclature section of this chapter. The reactivity $\rho$ is influenced by external reactivity changes, fuel temperature, and mixture's void fraction as follows:

$$\rho = \rho_{ex} + \alpha_f(T_f - T_{fo}) + \alpha_v(v_d - v_{do}) \tag{4.3}$$

### 4.1.2 Thermodynamic Equations

The neutron flux density is assumed to be linearly proportional to the thermal power $Q$ produced by the reactor core. This thermal power is transferred from the fuel rods to the light water coolant. The thermodynamic heat transfer from the fuel core to the coolant can be described by [39]:

$$Q = A_s H_b (T_f - T_{sat}) + \delta\phi \tag{4.4}$$

And the temperature changes in the fuel and coolant can be modeled using the following differential equations:

$$\frac{dT_f}{dt} = \frac{(1-\delta)\phi}{C_f} - \frac{A_s H_b (T_f - T_{sat})}{C_f} \tag{4.5}$$

$$\frac{dT_m}{dt} = \frac{(1-\delta)\phi}{C_f} - \frac{A_s H_{nb}}{C_f}\left(T_m - \frac{T_0 + T_{sat}}{2}\right) \tag{4.6}$$

Equations (4.1)–(4.6) are sufficient to model the dynamic behavior of the RPV of a BWR, as they capture the key thermal and neutronic interactions, including fuel heat transfer, subcooled and region dynamics [39]. One simplification considered here is that the coolant temperature is assumed constant and equal to $T_{sat}$ along the axial direction of each fuel channel, neglecting spatial variation along the vertical core length. This assumption is acceptable and consistent with the existing literature, such as [143], where $T_{sat}$ is taken as uniform.

### 4.1.3 Mixture Void Formation

As the thermal power transfers to the coolant, the water heats up and converts to steam, creating voids. The void fraction, indicating the proportion of steam to water, is estimated using the following empirical formulas from [144] and [145]:

$$\dot{m}_c = \dot{m}_{nom} Q^{1/3} \tag{4.7}$$

$$x = \frac{Q}{\dot{m}_c u_{fg}} \tag{4.8}$$

Where the drift velocity $u_{gj}$ and the void fraction $v_d$ are calculated as follows:

$$u_{gj} = 1.53 \left( \frac{g\sigma(\rho_f - \rho_g)}{\rho_f^2} \right)^{1/4} \tag{4.9}$$

$$v_d = \frac{1}{1.2 \left(1 + \left(\frac{1-x}{x}\right)\left(\frac{\rho_g}{\rho_f}\right)\right) + u_{gj}\left(\frac{\rho_g A_c}{x\dot{m}_c}\right)} \tag{4.10}$$

The drift-flux void fraction model in (4.10) employed in this work is consistent with established formulations widely used to represent the general framework of drift-flux modeling [145]. Furthermore, the void fraction is explicitly linked to the steam quality $x$, which itself depends on the thermal power input and the total mass flow rate through the core, as described by (4.7) and (4.8). This relationship captures the buoyancy-driven flow in the natural circulation loop comprising the riser and downcomer sections.

### 4.1.4 Thermohydraulic Equations

The pressure inside the RPV varies based on the thermodynamic properties of the saturated steam, the generated thermal power, and the feedwater mass flow and temperature. The thermodynamics of BWSMR steam generation are described by the following differential equations [146]:

$$\frac{dP_{sat}}{dt} = \frac{Q - \dot{m}_{st}(u_g - c_w T_{fw})}{K_s} \tag{4.11}$$

$$K_s = m_f \frac{du_f}{dP_{sat}} + m_g \frac{du_g}{dP_{sat}} - \frac{m_g u_{fg}}{v_g - v_f} \frac{dv_g}{dP_{sat}} \tag{4.12}$$

The variables in equation (4.12) are dependent on the thermodynamic properties of saturated water and steam, which can be estimated using curve-fitting methods based on data from saturated water/steam tables [147].

The thermohydraulic equations in [146] represent a secondary fluid lump model derived using mass and volume balances, along with an energy balance that links the steam generation rate $\dot{m}_{st}$ to the heat transfer input and feedwater subcooling. This leads to the thermohydraulic formulation in (4.12), which captures the core dynamics of saturated

steam generation under varying thermal loads. While based on classical PWR secondary-side models [146], the approach is adapted here for the direct-cycle BWR configuration, where steam is generated in the core and sent directly to the turbine. The model thus reflects the single-loop structure of BWRs, where pressure, steam quality, and heat transfer are tightly coupled in the RPV.

## 4.2 Steam Turbine

This section provides a brief description of a widely-used steam turbine dynamic modeling from a perspective of power system dynamic studies [148]. The steam turbine for a BWSMR may consist of several components, namely, the HPT, moisture separator, reheater, LPT, and various extraction levels, as discussed next, which allow to properly model the power plant in frequency regulation and cogeneration studies.

### 4.2.1 High Pressure Turbine

The relationship between the mass flow rate and the pressure drop across the HPT, including the effect of inlet temperature, can be defined as follows:

$$\dot{m}_{in} = \frac{K}{\sqrt{T_{in}}}\sqrt{P_{in}^2 - P_{out}^2} \tag{4.13}$$

The transfer function for the HPT input-output pressure, considering the HPT time delay, is given by:

$$\frac{P_{out}}{P_{in}} = \frac{k_{HPT}}{\tau_{HPT}s + 1} \tag{4.14}$$

Assuming that the expansion in the HPT is adiabatic and isentropic, the output temperature can be calculated using the ideal gas law for pressure–temperature as follows:

$$\frac{T_{out}}{T_{in}} = \left(\frac{P_{out}}{P_{in}}\right)^{\frac{k_{pe}-1}{k_{pe}}} \tag{4.15}$$

And the generated mechanical power equation for adiabatic expansion through the HPT is given by:

$$W_{HPT} = \eta_{HPT} c_p \dot{m}_{in} (T_{in} - T_{out}) \tag{4.16}$$

### 4.2.2 Moisture Separator

A small fraction of steam wetness is removed from the HPT outlet before entering the LPT to reduce blade corrosion. The moisture separator's outlet flow can be expressed as follows:

$$\tau_{sp} \frac{\dot{m}_{sp}}{dt} = (1 - \beta_{sp}) \dot{m}_{in} - \dot{m}_{sp} \tag{4.17}$$

The reheater dynamics are neglected in this case and modeled as a constant proportional factor due to their minimal impact.

### 4.2.3 Low Pressure Turbine

The LPTs have a more complex structure compared to the HPT, with multiple extraction stages. Thus, the steam pressure decreases progressively across these stages, affecting turbine performance and power output. It is crucial to use nonlinear functions to evaluate specific enthalpy and entropy throughout the different extraction levels of the LPT, considering temperature $T$ and pressure $P$ as independent variables as follows:

$$F(P, T) = F_f(P_{sat}(T)) + R(T) \times (P - P_{sat}) \tag{4.18}$$

$$F(P, T) = F_g(P) + R(P, T) \times (T - T_{sat}) \tag{4.19}$$

where $F$ denotes a thermodynamic property of the working fluid, such as specific enthalpy or entropy, and $R$ represents a function capturing $F$'s sensitivity to pressure or temperature changes, as defined in [147].

The mechanical power generated by the LPT and the overall mechanical power can be calculated as follows:

$$\begin{aligned} W_{LPT} = \eta_{LPT} [&\dot{m}_{LPT}(h_{LPT} - h_{ex1}) \\ &+ (\dot{m}_{LPT} - \dot{m}_{ex1})(h_{ex1} - h_{ex2}) + \ldots] \end{aligned} \tag{4.20}$$

$$P_{mech} = W_{HPT} + W_{LPT} \tag{4.21}$$

## 4.3 Steam Flow Control

In this study, the MSI valve flow is regulated to achieve primary frequency regulation and facilitate BWSMR primary frequency control using two operation modes. In the reactor-leading mode, only the MSI valve is controlled while the BP valve remains closed. The FMCRDs adjust the thermal power to match load changes, causing fluctuations in fuel temperature, coolant pressure, and temperature. In the turbine-leading mode, both BP and MSI valves regulate steam flow while maintaining fixed reactor thermal power. The control rod position remains unchanged, extending the lifespan of BWSMR internal components.

In the reactor-leading mode, a PI controller is used here to regulate the steam outlet temperature by adjusting the reactor's external reactivity as follows:

$$\rho_{ex} = k_p \left(T_{set} - T_{sat}\right) + k_i \int \left(T_{set} - T_{sat}\right) dt \tag{4.22}$$

In the turbine-leading mode, MSI valve operation with droop control is proposed for frequency regulation. This approach is further enhanced by accounting for the impact of steam pressure on the MSI valve mass flow variation, as follows:

$$\dot{m}_{MSI} = P_{Gref} - \frac{f - f_{ref}}{k_{droop}} + \Delta\dot{m}_{MSI}(P_{sat}) \tag{4.23}$$

where $\Delta\dot{m}_{MSI}$ varies with the output pressure from the RPV $P_{sat}$. By incorporating steam pressure effects, the proposed model more accurately captures transient steam flow variations, improving frequency control stability.

The flow rate through the MSI valve can be determined by its opening degree $K_v$ as follows [149]:

$$P_{sat} = P_{in} + \frac{\mathrm{SG}(1296000\dot{m}_{MSI}^2)}{K_v^2 \rho_g^2} \tag{4.24}$$

Additionally, the BP valve operation can be described as follows:

$$\tau_{BP}\frac{d\dot{m}_{BP}}{dt} = (\dot{m}_{set} - \dot{m}_{MSI}) - \dot{m}_{BP} \tag{4.25}$$

Equations (4.22)-(4.25) model steam flow dynamics in both reactor-loading and turbine-loading modes, assuming MSI valve control with a specified ramp rate for both modes.

The aforementioned modeling framework provides a comprehensive representation of the BWSMR power plant, capturing critical thermal and mechanical dynamics. It establishes a coordinated system that reflects the interaction between the reactor, steam turbine, and control components in a BWSMR power plant, which are necessary to properly model the power plant in frequency regulation studies, and thus understand one of the main advantages of SMRs compared to conventional NPPs. Furthermore, the proposed model will allow to analyze the use of SMRs in cogeneration studies presented in Chapter 5.

The next section applies these models to the 10th-generation BWRX-300, providing data to test the proposed dynamic models.

## 4.4 Results and Discussion

In this section, the BWRX-300 parameters are introduced first, since this is the reactor being deployed in Ontario, Canada, by OPG. Two main case studies are then discussed to evaluate the performance of the BWRX-300 power plant when connected to power systems. Thus, the first case study assesses the primary frequency control capabilities of the BWRX-300 using its two operational modes through Matlab/Simulink simulations [131]. This scenario involves a ramp load fluctuations, with matched rates for both load and generation to maintain power system stability. The second case study examines the response of the BWSMR power plant, planned for deployment at Darlington, to a three-phase fault within the Ontario BPS using DSATools [150], which is used by the IESO for power grid studies, and compares its performance to the existing NPP, implementing a detailed User-Defined Model of the BWSMR in this software tool, based on the relevant equations and controls described in Sections 4.1, 4.2, and 4.3.

### 4.4.1 BWRX-300 Example

Figure 4.1 illustrates the BWRX-300 power plant connected to a dynamic PQ load via a short transmission line. The dynamic model includes a synchronous machine, governor droop for frequency control, and excitation control to maintain terminal voltage.

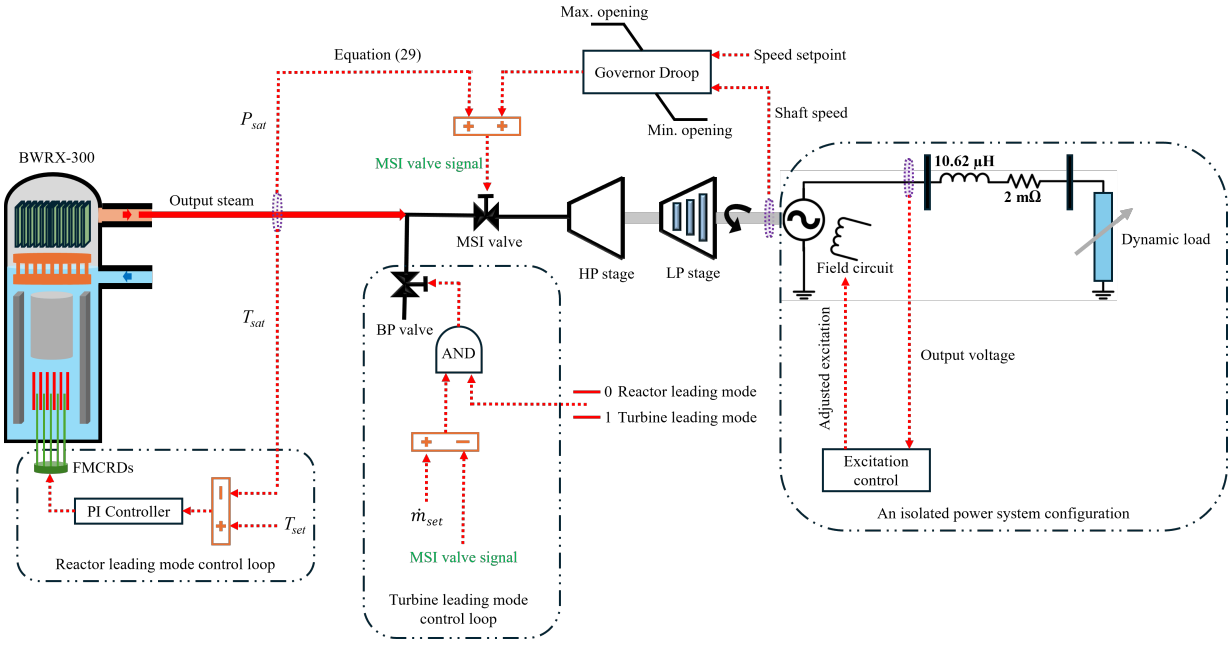



Figure 4.1: Schematic of BWRX-300 power plant.

#### 4.4.1.1 BWRX-300 Modeling

Table 4.1 lists the essential parameters of the BWRX-300 used to model the kinetic equations (4.1)-(4.3) [47]. Table 4.2 provides the main dimensions and rated operation conditions of the BWRX-300 from [45], which are utilized to compute the heat transfer coefficients required for the thermodynamic modeling in equations (4.4)-(4.6) as follows:

$$q'' = \frac{Q}{A_s} \tag{4.26}$$

$$H_{nb} = \frac{q''}{\Delta T_{nb}} \tag{4.27}$$

$$H_b = \frac{q''}{\Delta T_b} \tag{4.28}$$

The result of these calculations is shown in Table 4.3.

Table 4.1: Parameters for Modeling Kinetic Equations [47]

| Parameter | Value |
|---|---|
| $l$ | $2 \times 10^{-5}$s |
| $\lambda$ | $0.1\text{s}^{-1}$ |
| $\beta$ | 0.007 |
| $\overline{\rho_{ex}}$ | 0.007 |
| $\underline{\rho_{ex}}$ | $-0.007$ |
| $\alpha_v$ | $-0.005$ |
| $\alpha_f$ | $-2 \times 10^{-5}°\text{C}^{-1}$ |
| $T_{fo}$ | 900°C |
| $vdo$ | 0 |

#### 4.4.1.2 Steam Turbine Parameters

Table 4.4 lists key parameters for modeling the HPT and LPTs, including specific heat capacity, polytropic expansion factor, efficiencies, slope of the linear fitting, and nominal mass flow rate as per [148]. These parameters are crucial for evaluating turbine performance under different operating conditions.

#### 4.4.1.3 Effect of RPV Pressure on MSI Valve Operation

The steam flow through the MSI valve is influenced by reactor pressure. The mean matrix approach can be utilized to characterize the changes in mass flow rate $\Delta\dot{m}_{MSI}$ under varying pressures, averaging key parameters in (4.24), such as flow coefficient, pressure drop, and steam density to simplify the relationship between steam flow and reactor pressure. This novel approach yields the following simplified equation, replacing (4.24):

$$\begin{aligned}\Delta\dot{m}(P_{sat}) = {} & 0.025385P_{sat}^4 - 0.76221P_{sat}^3 \\ & + 8.5136P_{sat}^2 - 41.702P_{sat} + 75.181\end{aligned} \tag{4.29}$$

Table 4.2: BWRX-300 Dimensions and Rated Conditions [45]

| Parameter | Value |
|---|---|
| **Reactor Dimensions** | |
| RPV height | 26.0 m |
| RPV inner diameter | 4.0 m |
| Reactor core diameter | 3.4 m |
| Reactor core height | 3.8 m |
| Fuel bundles amount | 240 |
| Full-length fuel rods in each bundle | 78 |
| Fuel rod diameter | 11 mm |
| Total surface area, $A_s$ | 2458.28 $m^2$ |
| Reactor core volume | 19 $m^3$ |
| **Steady-State Parameters** | |
| Total reactor core thermal power | 870 MW |
| Nominal vessel pressure | 7.2 MPa |
| Nominal fuel temperature | 919.45 °C |
| Core inlet/outlet coolant temperature | 270/288 °C |
| Mass flow rate of the coolant | 512 kg/s |

#### 4.4.1.4 Operational Boundary Constraints of the BWRX-300 Model

The dynamic model of the BWRX-300 power plant incorporates essential operational boundary constraints to ensure accuracy and reliability during transient analyses. These constraints reflect both the physical and regulatory limits of the reactor and its associated systems, maintaining realistic operating conditions, as previously mentioned.

Safety limits for the BWRX-300 specify that overpressure is controlled within 1.1 times the design pressure of 10.3 MPa, setting the maximum allowable pressure at 11.33 MPa [151]. Regulatory standards limit the maximum fuel element cladding temperature to 1204.4°C [42]. The reactor can adjust its power from 100% to 50% at a ramp rate of 0.5%

Table 4.3: Heat Transfer Coefficients at Rated Conditions

| **Parameter** | **Value** |
|---|---|
| $q''$ | 0.354 MW/m$^2$ |
| $T_{sat}$ | 288 °C |
| $\Delta T_{nb}$ | 640.45 °C |
| $\Delta T_b$ | 631.45 °C |
| $H_{nb}$ | 0.55 kW/m$^2$ °C |
| $H_b$ | 0.56 kW/m$^2$ °C |
| $C_f$ | 21.295 MJ/°C |

Table 4.4: HPT and LPT Parameters [148]

| **Parameter** | **Value** |
|---|---|
| $c_p$ | 1.9035 kJ/kg°C |
| $k_{pe}$ | 1.1148 |
| $\eta_{HPT}$ | 89.31% |
| $\eta_{LPT}$ | 82% |
| $K$ | 1194.3 |
| $\dot{m}_{st}$ | 512 kg/s |

per minute, with the ability to return to full power at the same rate on a daily basis [102]. Furthermore, the model incorporates a coolant inlet temperature of 270°C and a steam temperature at the turbine inlet of 288°C to mitigate thermal stress. The steam mass flow rate varies from 256 kg/s at 50% power to approximately 550 kg/s under controlled uprate conditions. The feedwater flow rate follows a similar range to ensure effective heat removal.

### 4.4.2 BWRX-300 Primary Frequency Control

As illustrated in Figure 4.2, the initial power drawn from the BWRX-300 power plant for the dynamic load is 190 MW, which increases to 290 MW with a ramp rate of 80%/min

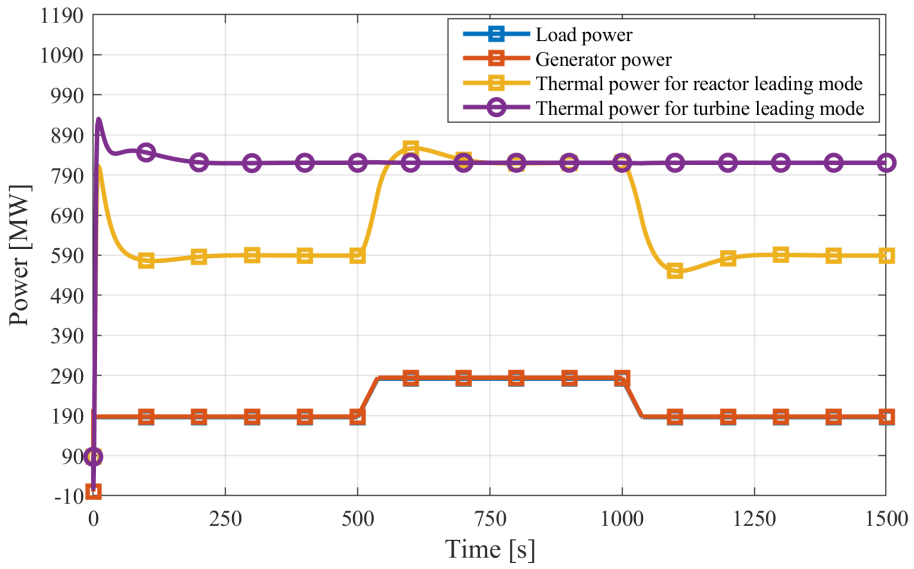



Figure 4.2: Thermal and electrical power output of the simulated 300 MW BWRX-300 power plant under varying load conditions.

at 500 s, returning to 190 MW at 1000 s. Note that the generation adapts to load changes in both operating modes. Observe also that the reactor thermal power variation changes between 590 MW and 820 MW in the reactor-leading mode, while in the turbine-leading mode, a fixed reactor thermal power is maintained, with the BP valve acting as a buffer to minimize disturbances.

Figure 4.3 depicts the frequency or turbine speed for both modes. Note that the turbine speed stabilizes after the initial fluctuations, with the turbine-leading mode showing superior performance due to the BP valve's fast response, compared to the external reactivity control, which is influenced by the RPV's high thermal inertia. Observe as well that the frequency drops from 60 Hz to 59.36 Hz and then returns to 60 Hz.

Figure 4.4 highlights the reactor fuel temperature response. Note that in the reactor-leading mode, fuel temperature fluctuates between 710°C and 890°C due to thermal power changes. However, it remains stable at 890°C in the turbine-leading mode, where reactor power is regulated with a fixed value. Figure 4.5 shows the saturated steam pressure and temperature responses inside the RPV. During load increases, reactor pressure decreases due to increased steam demand, and increases when the load decreases, stabilizing at 7.2 MPa and 288°C for pressure and temperature, respectively. The turbine-leading mode exhibits minimal disturbances in steam output pressure and temperature, as the BP valve adjusts quickly to maintain stability.

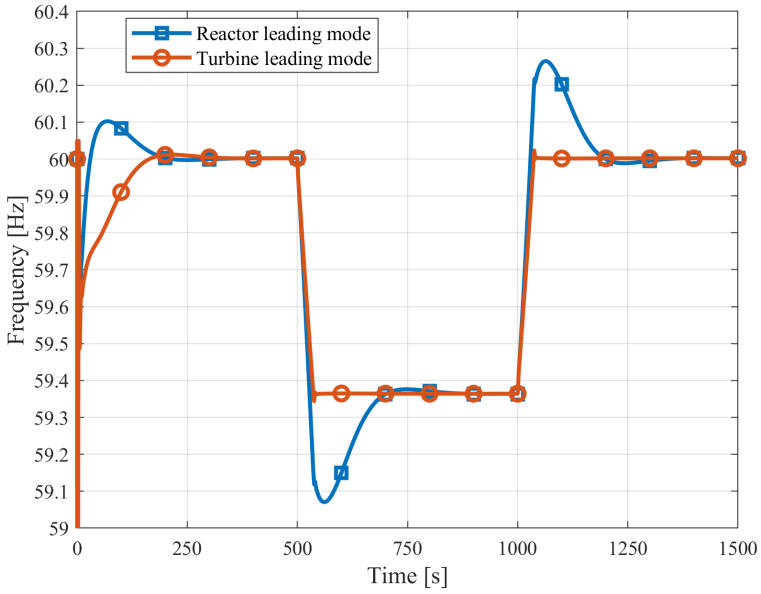



Figure 4.3: Frequency response under varying load conditions.

Figure 4.6 shows the control rod reactivity, fuel temperature feedback reactivity, void fraction, and the resultant reactivity. Note that these variables fluctuate in the reactor-leading mode but remain constant in the turbine-leading mode.

Figure 4.7 presents the input and output temperatures of the HPT, including the reheat temperature of the steam output from the HPT. Observe that these temperatures vary due to changes in the turbine's mechanical power, adapting to load changes and behaving similarly under both operation modes. Figure 4.8 shows the steam flow rates through the MSI valve, the PB valve, and the RPV inlet, which are adjusted according to load changes. Note that the MSI valve regulates steam flow in both operation modes, while in the turbine-leading mode, the BP valve provides additional regulation, remaining closed in the reactor-leading mode. Observe also that in the reactor-leading mode, the MSI valve's steam flow matches the RPV flow, while in the turbine-leading mode, the RPV mass flow stays relatively constant.

Based on the results obtained, it is evident that the BWSMR is capable of providing satisfactory primary frequency regulation, particularly when utilizing turbine-leading control strategies, which is not the case with existing NPP technologies. Hence, this technology can be used in modern power grids with increasing penetration of variable RESs, aiming to phase out $CO_2$-emitting generation plants and facilitate the transition to a net-zero energy

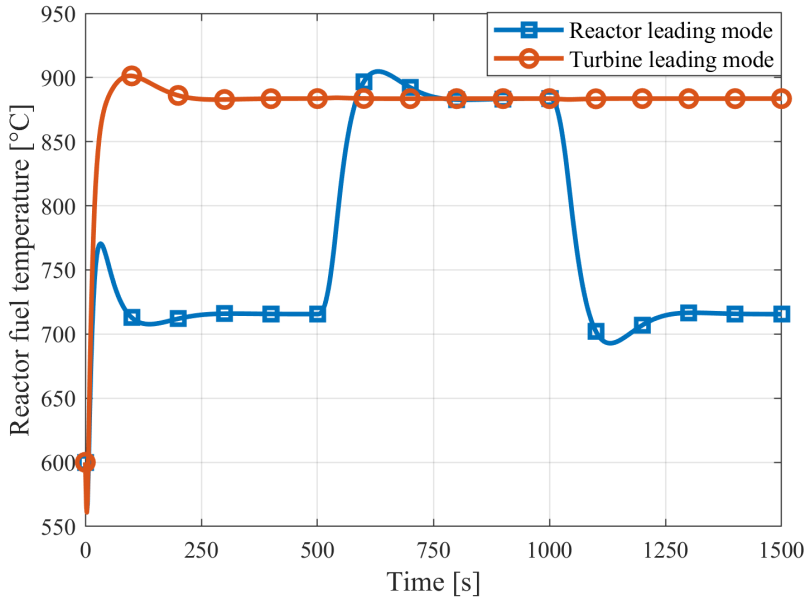



Figure 4.4: Fuel temperature response under varying load conditions.

system.

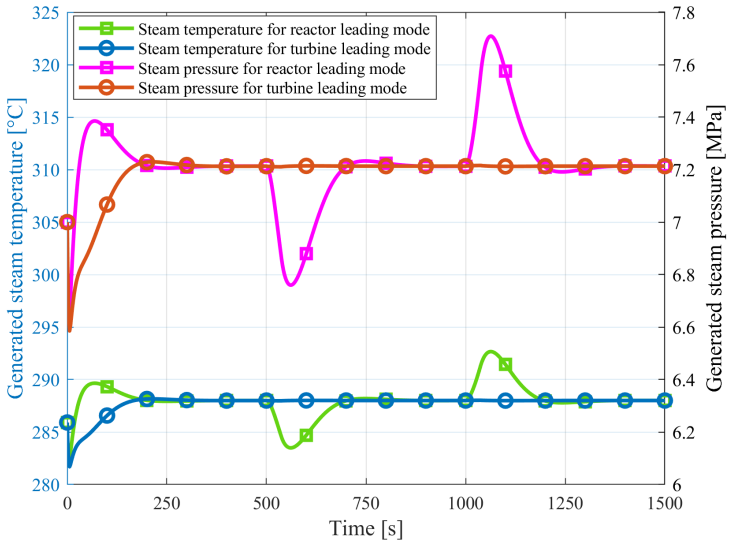



Figure 4.5: Generated steam pressure and temperature response under varying load conditions.

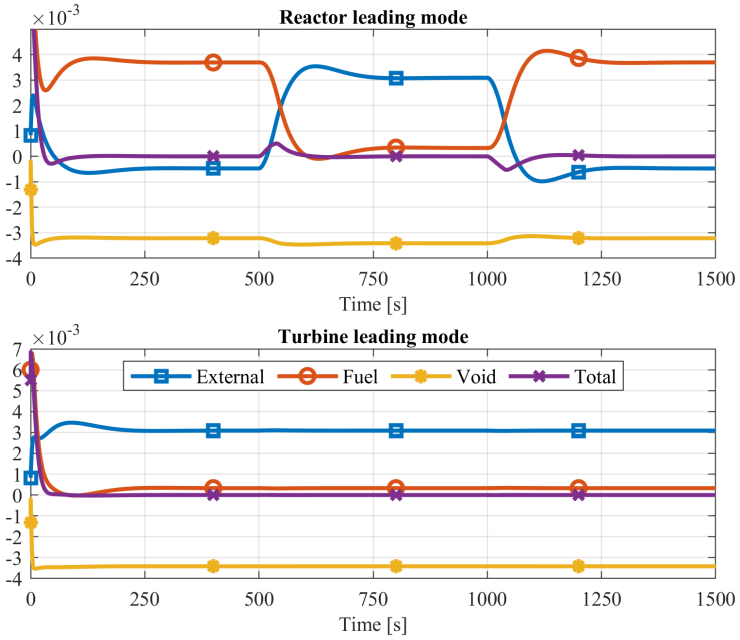



Figure 4.6: Reactivity response under varying load conditions.

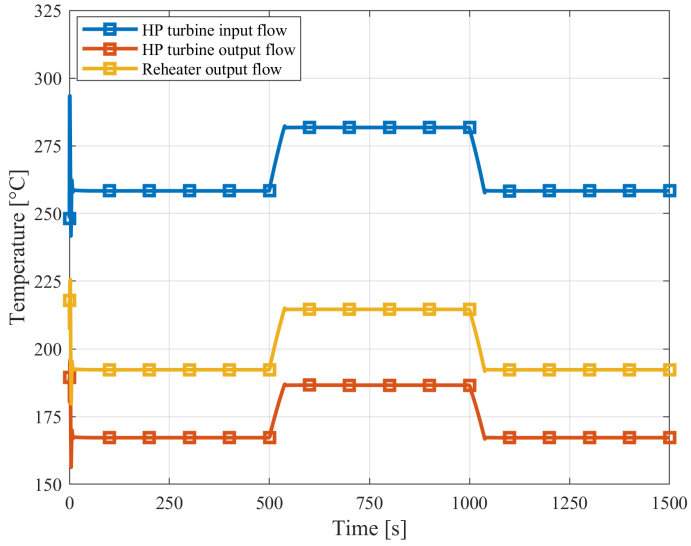



Figure 4.7: HPT and reheater temperature response under varying load conditions.

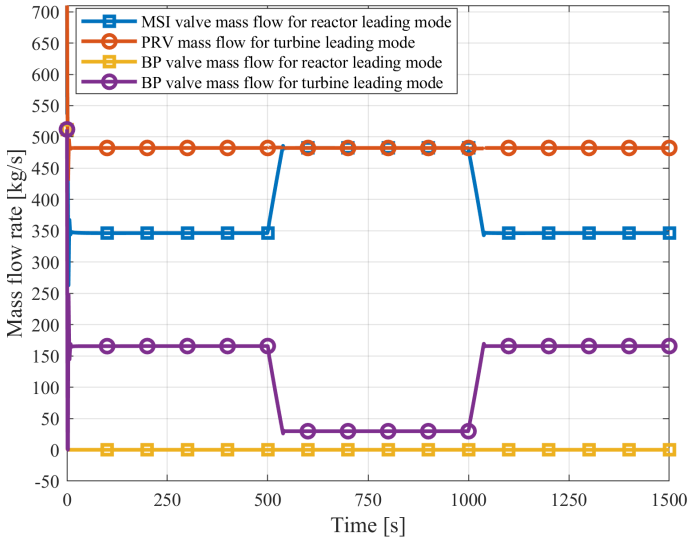



Figure 4.8: The mass flow rates of the MSI valve, the BP valve, and the RPV inlet mass flow rate under varying load conditions.

### 4.4.3 SMR Versus Existing NPP Units

The Ontario BPS model consists of 4,275 AC buses and 533 generators, and is connected to 59 other areas, including other provinces in Canada like Quebec and Manitoba, as well as relevant equivalents from neighboring jurisdictions in the United States, such as Minnesota, Michigan, and New York. The Darlington NPP, part of this system, includes four generator units, each with a capacity of 935 MW. In this study, only units 3 and 4 are assumed to be operational, with unit 4 replaced by three BWRX-300 units. These three units exhibit similar behavior, and thus only the response of one unit is discussed next.

A three-phase fault is applied at the midpoint of a 500 kV transmission line connecting unit 3 to a nearby transmission bus, as per a typical dynamic contingency study performed by the IESO, with the turbine-leading mode utilized to control the steam flow in the BWSMR units. The frequency response, shown in Figure 4.9, assumes a fault occurring at 20 s, followed by the removal of the faulted transmission line and the tripping of unit 3 after 0.07 s. Note that the frequency of the BWSMR units, equipped with droop governor control, exhibits higher oscillations compared to Unit 4 of the existing NPP, which operates without droop governor control, due to the lower inertia of the BWSMR units. Observe as well that the frequency stabilizes at 59.99 Hz at around 25 s, indicating the expected robust recovery, since Ontario's BPS relies on external areas to compensate for the generation loss during the short-term disturbance caused by the fault.

The inertia constant of the BWSMR unit within the BPS can be estimated based on the frequency response depicted in Figure 4.9 and by using the following swing equation [152]:

$$\frac{2H}{f_o}\frac{df}{dt} = \Delta P \tag{4.30}$$

where $H$ is the inertia constant in s, $f_o$ is the nominal frequency of 60 Hz, $\frac{df}{dt}$ is the Rate Of Change Of Frequency (ROCOF), and $\Delta P$ is the power imbalance in per unit.

Thus, as shown in Figure 4.9, the frequency response after the fault indicates a deviation of 0.55 Hz for the BWSMR and 0.15 Hz for the existing NPP unit, both occurring within a time window of approximately 0.06 s. Given the power imbalance of 1 p.u. following the fault, from (4.30) the existing NPP system shows a significantly higher inertia constant of 12 s than the BWSMR system, which shows an inertia of 3.27 s. This explains the larger oscillations observed for the BWSMR units in Figure 4.9, compared to the smoother frequency response of the NPP system.

The voltage response, shown in Figure 4.10, drops sharply from 1 p.u. to 0.34 p.u. during the fault, and returns to 1 p.u. at 25 s in the simulation. Note that the power

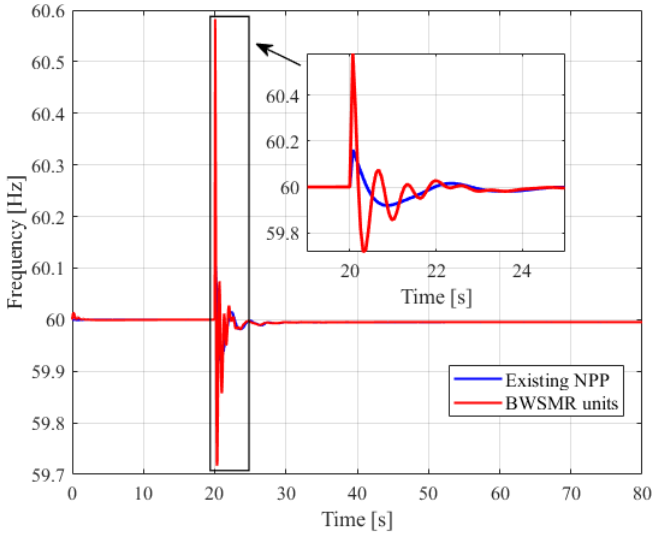



Figure 4.9: Frequency response of BWSMR and existing NPP units during a three-phase fault contingency near the Darlington plant.

response, illustrated in Figure 4.11, shows more power oscillations of the BWSMR units compared with Unit 4 of the existing NPP. Finally, Figure 4.12 illustrates the mechanical power of the BWSMR units, showing very minimal change, due to the small variations in grid frequency, as expected from the robust BPS interconnections.

In the light of the aforementioned discussion, the application of the proposed BWSMR power plant dynamic model to the Ontario's BPS shows that, despite the higher frequency oscillations expected due to the BWSMR units' lower inertia, that are within the mandated dynamic limits of frequency regulation in Ontario [153], there is no significant impact on the stability of the BPS. This highlights the important role of the large system inertia in the North American Eastern Interconnection power grid, ensuring stability without compromising grid reliability, in spite of the lower inertia of the expected compact SMRs compared to large NPPs.

It is important to highlight that the simulation results of the proposed BWSMR power plant dynamic model align with the expected physical behavior under both standalone and integrated system conditions. Specifically, the reactor and turbine responses under varying load scenarios, as shown in Figures 4.2–4.8, follow expected trends in thermal power, steam flow, and frequency regulation, which are consistent with SMR design principles and the inertia of the coupled turbine-generator set. Also, the two control strategies, i.e., reactor-leading and turbine-leading, demonstrate the anticipated performance differences,

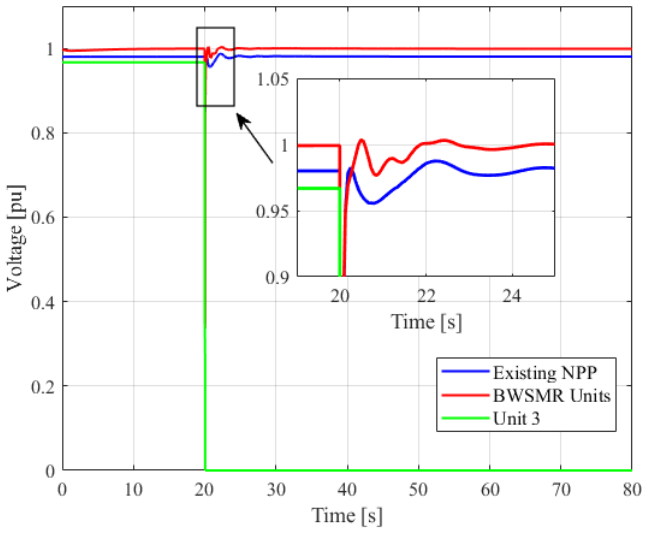



Figure 4.10: Voltage response of BWSMR and existing NPP units during a three-phase fault contingency near the Darlington plant.

particularly in frequency and fuel temperature dynamics. Furthermore, the integration into the Ontario BPS and the application of standard contingency events, i.e., three-phase fault, produce expected frequency and voltage responses, as shown in Figures 4.9–4.12. These include transient frequency standard deviations, voltage dips, and mechanical power changes comparable to those observed in dynamic studies. Finally, note that the BPS model used to study the integration of BWRX-300 power plant with Ontario's power grid is based on the real IESO base case, which is typically employed for system stability assessments in Ontario, as discussed in Section 4.4.3. While the BWRX-300 model has not been validated against real-world operational data due to the reactor's ongoing development, the alignment of the simulation outputs with expected grid behavior, basically validates the proposed models and controls.

## 4.5 Summary

This chapter addressed and justified the development of a comprehensive dynamic model for BWSMR power plants that includes crucial components such as the reactor, steam turbine, power system, and steam flow controls. The primary goal of this work, which was submitted for publication in [154], is to provide an adequate physics-based model of the

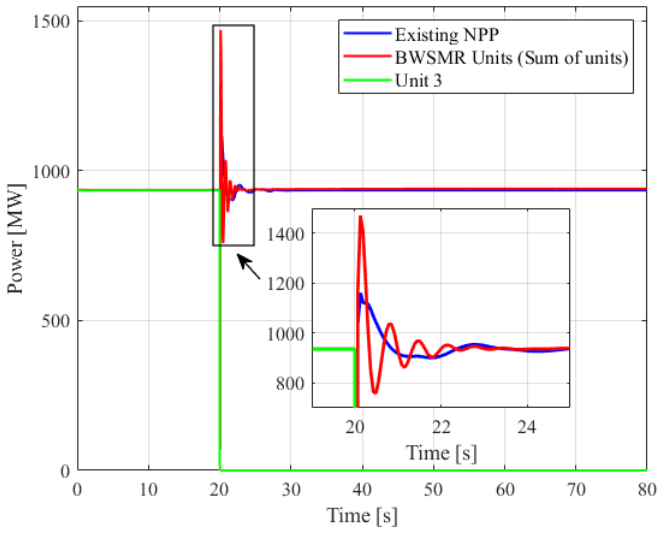



Figure 4.11: Power response of BWSMR and existing NPP units during a three-phase fault contingency.

BWSMR operation under typical conditions for power grid dynamic studies, incorporating essential dynamics such as pressure variations and two-phase drift velocity, which improve simulation fidelity and reliability.

The proposed dynamic models were tested and validated through simulations of a simple generator-load system as well as Ontario's BPS, comparing two operational modes for primary frequency control, namely, reactor-leading and turbine-leading. The results demonstrated the superior performance of the turbine-leading mode in primary frequency regulation, confirming that the BWSMR power plant can effectively manage load fluctuations through dynamic adjustments in steam flow and pressure control. These findings validate the BWSMR's primary frequency control capabilities and suitability for integration into existing power systems. The practical application of the proposed BWSMR power plant dynamic model in Ontario's BPS demonstrated that with all the advantages of SMRs, it is essential that grid operators consider the lower inertia challenge when replacing conventional reactors with new SMR technologies.

It is important to highlight the fact that the thermal model of BWSMR power plants proposed allows to study the BWSMR's capability to provide both electricity and heating in integrated energy systems. Thus, the model facilitates the potential for steam extraction between the HPTs and LPTs at adequate temperatures and pressures, which will be explored in Chapter 5 for applications such as district heating and integration with

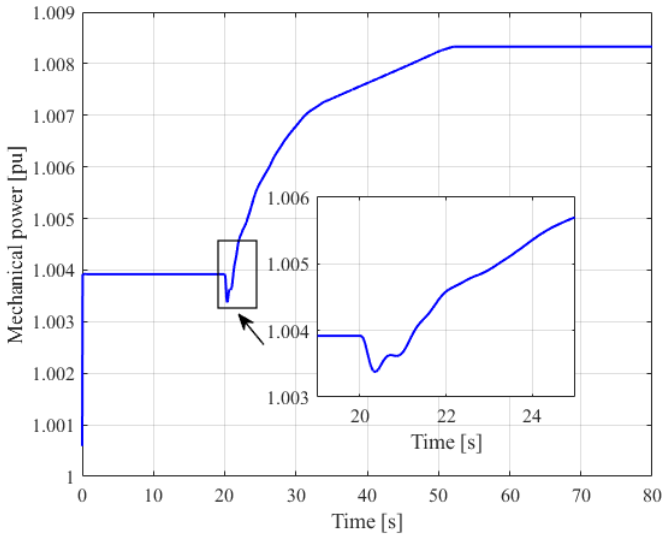



Figure 4.12: Turbine mechanical power for the BWSMR units during a three-phase fault contingency.

thermal energy storage systems. Additionally, the model accounts for the impact of steam extraction on mechanical power output, ensuring an accurate assessment of power plant performance under co-generation scenarios.

# Chapter 5

# Modeling and Control of a Boiling Water Small Modular Reactor Cogeneration System for District Heating Applications

Building on Chapter 4, this chapter proposes a novel approach for modeling and controlling an SMR-based cogeneration power plant designed to support DHNs, contributing to energy system decarbonization and enhancing BPSs flexibility. While previous work in the existing literature has explored certain aspects of integrated SMR-based cogeneration systems, existing studies lack a comprehensive representation of critical elements such as piping heat losses, thermal delays, variable DHN thermal demand, and the integration of an extended broader multi-timescale dynamic behavior.

To address these gaps, this chapter presents a set of dynamic models and control strategies for SMR-based cogeneration systems, featuring detailed thermoelectric modeling. The proposed framework captures both short- and long-term system responses, enabling robust analysis of transient behavior and steady-state performance under varying operating conditions. The proposed cogeneration system is validated using the tenth-generation BWRX-300 SMR, with a case study focused on its potential integration into Ontario's BPS and deployment within a DHN in the Darlington region. Since the comprehensive models of the BWSMR power plant were discussed in Chapter 4, this chapter focuses solely on modeling the additional components required for the BWSMR-based cogeneration analysis.

# Nomenclature

## Parameters

| | |
|---|---|
| $c_w$ | Specific heat capacity of water [J/kg·°C] |
| $c_{st}$ | Specific heat capacity of steam [J/kg·°C] |
| $\delta$ | Electrical power margin threshold |
| $\delta_e$ | Reduction percentage in electrical power |
| $\eta_{HPT}$ | Efficiency of the high-pressure turbine |
| $\eta_{LPT}$ | Efficiency of the low-pressure turbine |
| $\gamma$ | Steam ramp control coefficient |
| $\varepsilon_1$ | Effectiveness of steam-to-TES heat exchanger |
| $\varepsilon_2$ | Effectiveness of TES-to-water heat exchanger |
| $\alpha_e$ | Steam extraction coefficient for DHN |
| $\Delta t$ | Simulation time step [s] |

## Variables

| | |
|---|---|
| $W_{HPT}$ | Thermal power from the high-pressure turbine [W] |
| $W_{LPT}$ | Thermal power from the low-pressure turbine [W] |
| $P_{mech}$ | Total mechanical turbine power [W] |
| $P_{el}$ | Electrical power output [W] |
| $P_{el,\mathbf{max}}$ | Maximum electric power output [W] |
| $P_{HPe}$ | Total power input to central heat pumps [W] |
| $P_{HP1}, P_{HP2}, \ldots, P_{HPn}$ | Power inputs of individual central heat pumps [W] |

| | |
|---|---|
| $T_{in}, T_{out}$ | Inlet and outlet steam temperatures [°C] |
| $T_{st}$ | Steam temperature entering TES [°C] |
| $T_{\mathbf{TES}}$ | TES tank temperature [°C] |
| $T_{TESnew}, T_{TESold}$ | New and previous TES temperature states [°C] |
| $T_{ret}$ | Return water temperature [°C] |
| $\dot{m}_{in}$ | Inlet mass flow rate to HPT [kg/s] |
| $\dot{m}_{LPT}$ | Steam mass flow rate to LPT [kg/s] |
| $\dot{m}_{ex1}$ | First extraction steam flow rate [kg/s] |
| $\dot{m}_{DHN}$ | Steam flow rate to DHN [kg/s] |
| $\dot{m}_{HX1}, \dot{m}_{HX2}$ | Steam flow rates to heat exchangers [kg/s] |
| $\dot{m}_{waste}$ | Unused steam mass flow rate [kg/s] |
| $\dot{m}_{st2}$ | Steam flow rate to TES [kg/s] |
| $\dot{m}_{w}$ | Water flow rate from TES [kg/s] |
| $\dot{m}_{HPT-LPT}$ | Steam flow rate from HPT to LPT [kg/s] |
| $h_{LPT}, h_{ex1}, h_{ex2}$ | Specific enthalpies at turbine and extraction points [J/kg] |
| $m_{\mathbf{TES}}$ | TES water mass [kg] |
| $\frac{dE_{\mathbf{TES}}}{dt}$ | Rate of energy change in TES [W] |
| $\frac{d\dot{m}_{DHN}}{dt}$ | Time derivative of steam flow to DHN [kg/s$^2$] |
| $\frac{d\dot{m}_{MSI}}{dt}$ | Time derivative of MSI flow [kg/s$^2$] |
| $TES_{\mathbf{mode}}$ | TES operating mode (Charge/Discharge) |
| $\Delta T_{sup}$ | DHN supply temperature deviation [°C] |

## 5.1 Dynamic Modeling of a Cogeneration System

The proper modeling of the proposed BWSMR cogeneration plant requires dynamic models for the reactor, ES, HX, DHN, TES, and HP. Given that the dynamic models of the reactor, HX, DHN, and HP have been proposed and validated in Chapters 3 and 4, this chapter focuses on proposing proper dynamic models for the remaining essential components, as discussed in detail next, based on basic component models available in the technical literature. Thus, a main contribution of the present work is the development of a full integrated BWSMR-DHN dynamic model.

### 5.1.1 Steam Extraction

Figure 5.1 shows the proposed steam extraction-based DHN integrating TES and central HPs for continuous heat supply. The ES between the HPT and LPT is directed through a control valve to HX1, where it heats the DHN return water. Any excess steam is diverted via another control valve to HX2 for TES charging. When steam extraction is unavailable, a control valve allows TES discharge through HX3 to maintain the heat of the DHN's return water. If TES energy is insufficient, another control valve regulates the activation of central HPs to supply the required heat, ensuring a continuous and stable heat supply.

Steam extractions reduce the available mass flow for expansion in the turbines, directly impacting the mechanical power generated by the LPT, while the HPT remains unaffected. The following equations model how steam extraction affects the mechanical power output of each turbine stage and the total turbine output [148]:

$$W_{HPT} = \eta_{HPT}\, c_{st}\, \dot{m}_{in}\, (T_{in} - T_{out}) \tag{5.1}$$

$$\begin{aligned} W_{LPT} = \eta_{LPT}\, [&(\dot{m}_{LPT} - \dot{m}_{DHN})(h_{LPT} - h_{ex1}) \\ &+ (\dot{m}_{LPT} - \dot{m}_{DHN} - \dot{m}_{ex1})\, (h_{ex1} - h_{ex2}) + \ldots] \end{aligned} \tag{5.2}$$

$$P_{mech} = W_{HPT} + W_{LPT} \tag{5.3}$$

where all variables and parameters in these and other equations are defined in the Nomenclature section.

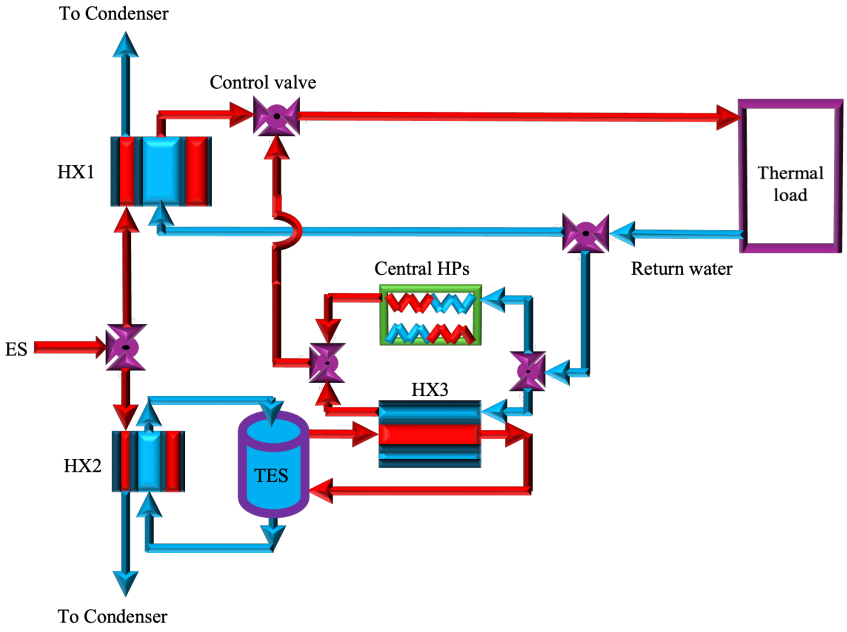



Figure 5.1: Schematic representation of the proposed steam extraction-based DHN model.

### 5.1.2 Thermal Energy Storage

The TES system is modeled using energy balance principle to represent both charging and discharging processes. The heat is transferred from the ES to the hot water tank storage during charging, and from the storage to the DHN water during discharging. The temperature of the TES is updated based on the net heat energy gained or lost, considering parameters such as mass flow rates, specific heat capacity, and storage volume. The overall energy balance for the TES can be expressed as follows [14]:

$$\frac{dE_{\text{TES}}}{dt} = \varepsilon_1 \, \dot{m}_{st2} \, c_{st} \, (T_{st} - T_{\text{TES}}) - \varepsilon_2 \, \dot{m}_w \, c_w \, (T_{\text{TES}} - T_{ret}) \tag{5.4}$$

And the temperature of the thermal energy storage can be updated as follows:

$$T_{\text{TESnew}} = T_{\text{TESold}} + \frac{\Delta t}{m_{\text{TES}} \, c_w} \left[ \frac{dE_{\text{TES}}}{dt} \right] \tag{5.5}$$

### 5.1.3 Controls

#### 5.1.3.1 Reactor Control

The reactor control system maintains stable thermal power output while responding to load variations. The external reactivity is regulated to control the reactor's thermal output using a PI controller based on the deviation between the setpoint and steam saturation temperatures as per (4.22).

#### 5.1.3.2 Governor Control

The governor control system manages steam flow through the MSI and BP valves to achieve primary frequency regulation and maintain system stability. The MSI valve operates under droop control as per (4.23) and (4.25).

#### 5.1.3.3 Steam Extraction Control

A controlled fraction of steam is proposed here to be extracted between the HPT and LPT stages of the steam turbine to supply a DHN. As shown in Figure 5.1, the ES passes through a control valve and is directed to HX1 and HX2, where it transfers heat to the DHN return water and store thermal energy into the TES, respectively, with the mass flow rate of ES to the DHN being controlled here as follows:

$$\dot{m}_{DHN} = \begin{cases} \alpha_e \, \dot{m}_{HPT-LPT} & \text{if } P_{el} \leq (1 - \delta_e) \, P_{el,\max} \\ 0 & \text{otherwise} \end{cases} \tag{5.6}$$

Since the steam extraction occurs only during off-peak hours when the BWSMR's electrical power output falls below a specific threshold, namely, $(1 - \delta_e)$ of the maximum generator capacity power, where $\delta_e$ represents the reduction percentage in the BWSMR's electrical generation. In such cases, the ES is a fraction $\alpha_e$ of the steam mass flow between the HPT and LPT stages $\dot{m}_{HPT-LPT}$; otherwise, no steam is extracted.

To ensure stable turbine operation, the following constrain guarantee that the ES rate of change is slower than the steam turbine's ramp-up or ramp-down rate:

$$\left| \frac{d\dot{m}_{DHN}}{dt} \right| \leq \gamma \left| \frac{d\dot{m}_{MSI}}{dt} \right| \tag{5.7}$$

Finally, the ES mass flow rate balance is represented here by:

$$\dot{m}_{DHN} = \dot{m}_{HX1} + \dot{m}_{HX2} + \dot{m}_{\text{waste}} \tag{5.8}$$

#### 5.1.3.4 Thermal Energy Storage Control

A TES-based control strategy is proposed here to manage the charging and discharging processes depending on the reactor's surplus thermal power and the DHN demand. In this case, it is assumed that the TES is charged during off-peak hours when electrical demand is low, provided that its temperature stays within a safe operating range. A minimum temperature threshold of 80°C is maintained to ensure sufficient temperature difference between the TES and the DHN return water, which is necessary to achieve effective heat transfer through HX3 and deliver water at the required supply temperature. At the same time, an upper limit is enforced to avoid the risk of water boiling inside the storage tank, ensuring safe and stable operation. This can be represented as follows:

$$\text{TES}_{\text{mode}} = \begin{cases} \text{Charge} & \text{if } P_{el} \leq (1-\delta)\, P_{el,\max} \\ & \textit{and } 80°C \leq T_{\text{TES}} \leq 95°C \\ \text{Discharge} & \text{otherwise} \end{cases} \tag{5.9}$$

#### 5.1.3.5 Centralized Control of Heat Pumps

The centralized HPs proposed control system regulates the electrical power input based on the DHN-supplied water temperature difference error $\Delta T_{sup}$. The control strategy applies a stepwise adjustment of power levels to efficiently maintain temperature stability. The relationship between $\Delta T_{sup}$ and the electrical power input $P_{HPe}$ for parallel central HPs can be defined as follows:

$$P_{HPe} = \begin{cases} P_{HP1} & \text{if } \Delta T_{sup} \leq 0.5 \\ P_{HP1} + P_{HP2} & \text{if } 0.5 < \Delta T_{sup} \leq 1 \\ \vdots & \\ P_{HP1} + P_{HP2} + \cdots + P_{HPn} & \text{if } \Delta T_{sup} > 3 \end{cases} \tag{5.10}$$

## 5.2 Results and Discussion

In this section, a comprehensive overview of the BWRX-300 cogeneration system, which is planned for deployment at Darlington NPP, is provided, focusing on its performance from both electrical and thermal perspectives. Thus, first, the electrical behavior of the BWRX-300 cogeneration plant is examined, analyzing how steam extraction affects the system's dynamics. Second, the use of ES to supply thermal power to a nearby community in Darlington via a DHN is investigated. Finally, different approaches to supplying thermal loads in this community are compared, focusing on the utilization of ES-based DHN with central HPs and TES versus meeting thermal demands exclusively through the current trend of using distributed HPs. These simulations are carried out using MATLAB/Simulink [131].

Figure 5.2 illustrates the schematic of the BWRX-300 cogeneration system studied here. The reactor generates saturated steam at $P_{\text{sat}}$ and $T_{\text{sat}}$, which is then regulated by the MSI valve to drive the turbine for power generation. A governor droop mechanism controls the turbine operation to regulate the system frequency. In turbine-leading mode, the BP valve diverts excess steam to the condenser.

The steam turbine via a generator supplies power to the Ontario's grid. The BWRX-300 plant is assumed here to have a governor droop to contribute to frequency control, and has excitation control to maintain terminal voltage. A portion of the ES after reheating is directed to supply the DHN during a 4-hour period at night, when electricity demand is 62.4%, so that ES used to heat the return water and charge the TES yields the required 10 MW of thermal power for the DHN. Over the remaining 20 hours, the TES system discharges stored thermal energy to maintain the heating supply, ensuring continuous operation when excess steam is unavailable. When the TES cannot fully meet the DHN thermal demand, central HPs are used to provide the required thermal power for reliable heating throughout the day.

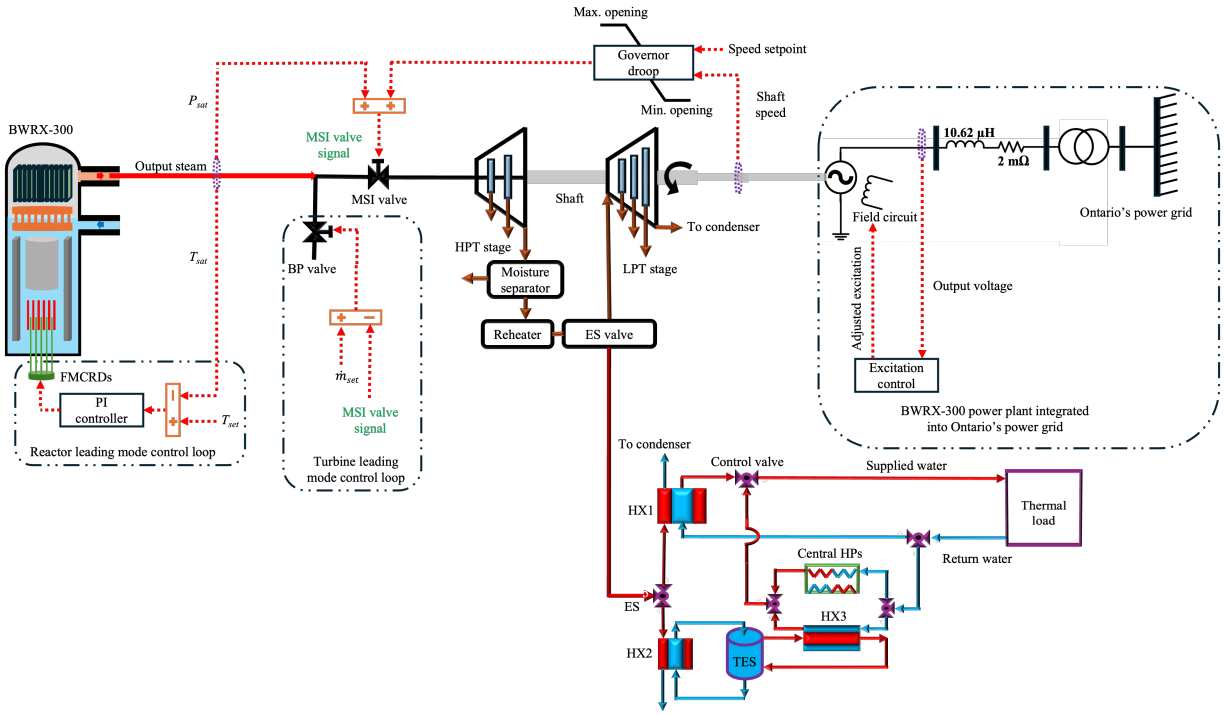



Figure 5.2: Schematic of BWRX-300-based CHP.

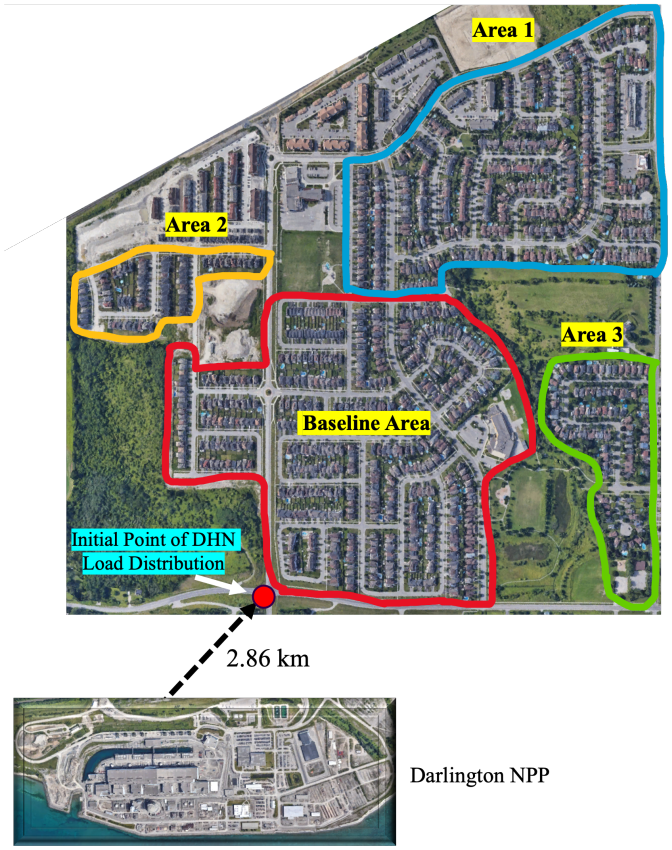
### 5.2.1 DHN Near Darlington NPP

Figure 5.3a illustrates the proposed block-based approach to model the potential DHN near Darlington's NPP, so that the heating demands of nearby residential buildings can be met. The modeling begins with Block 1 (B1), which consists of 20 households of varying footprints shown in Table 5.1, with a total area of 0.0031 $km^2$. The SRLS tool [155] is used to evaluate the B1's heating demand, assuming each household has two floors, making the effective heating area twice the footprint. B1 serves as a reference to extend the DHN by incorporating additional blocks, forming the Baseline DHN Area, as shown in Figure 5.3a. This Baseline DHN Area consists of 20 blocks covering 0.2771 $km^2$, with the corresponding area of each block listed in Table 5.2.

To further expand the DHN coverage and fully utilize the BWRX-300's ES, the aggregated thermal demand is increased from 4.5 MW to 10 MW, which is accomplished by expanding the Baseline DHN Area. As a result, the total DHN coverage increases to 0.61 $km^2$, integrating three additional zones as shown in Figure 5.3b, which includes Area 1 corresponding to 0.2206 $km^2$ of a high-density residential in the northeast, a residential Area 2 of 0.0354 $km^2$ in the northwest, and Area 3 supplying heat to 0.0765 $km^2$ of buildings in the southeast. This expansion minimizes wasted steam and enhances energy efficiency.




(a)




(b)

Figure 5.3: DHN layout near Darlington NPP: (a) Baseline Area and (b) expanded areas.

Table 5.1: House Areas in B1

| House | Area [m²] | House | Area [m²] |
|---|---|---|---|
| H1 | 152.57 | H2 | 141.08 |
| H3 | 147.84 | H4 | 149.71 |
| H5 | 152.92 | H6 | 134.56 |
| H7 | 134.32 | H8 | 127.03 |
| H9 | 148.08 | H10 | 150.17 |
| H11 | 144.50 | H12 | 138.85 |
| H13 | 168.46 | H14 | 161.46 |
| H15 | 183.69 | H16 | 200.56 |
| H17 | 160.08 | H18 | 178.20 |
| H19 | 153.56 | H20 | 180.32 |

The piping losses in the DHN are modeled using two lumped sections:

- Section 1 corresponds to the actual DHN piping from the NPP to the initial point of DHN load distribution, with a pipe diameter of 300 mm and a length of 2.860 km.
- Section 2 represents lumped DHN piping for the studied region, so that the piping thermal losses correspond to 7.7% of the total demand, which is a typical value for existing DHNs [156], and is influenced by factors such as piping diameters and length, as well as insulation quality and operational conditions.

Table 5.2: Block Areas in the Baseline DHN

| Block | Area [km²] | Block | Area [km²] |
|---|---|---|---|
| B1 | 0.0111 | B2 | 0.0111 |
| B3 | 0.0093 | B4 | 0.0202 |
| B5 | 0.0262 | B6 | 0.0252 |
| B7 | 0.0191 | B8 | 0.0148 |
| B9 | 0.0108 | B10 | 0.0186 |
| B11 | 0.0124 | B12 | 0.0336 |
| B13 | 0.0183 | B14 | 0.0133 |
| B15 | 0.0162 | B16 | 0.0080 |
| B17 | 0.0130 | B18 | 0.0116 |
| B19 | 0.0060 | B20 | 0.0118 |

### 5.2.2 Electrical Analysis

As indicated, the system operates so that the BWRX-300 reactor runs at full capacity for 20 h daily and then reduces its output to 62.4% capacity for the remaining 4 h, starting at midnight. Thus, as shown in Figure 5.4, electrical power generation undergoes a significant change at 400 s, which is controlled by a ramp-down of electrical output from 300 MW to 187.2 MW with a less than 80% reduction per minute. The total simulation period of 800 s suffices to effectively capture the dynamic behavior of the nuclear steam turbine under this varying dispatch condition, which is shown next to be feasible for the BWSMR considered.

As the electrical power generation decreases, surplus steam from the BWSMR becomes available. The ES is redirected to supply the DHN in the Darlington community studied here, effectively utilizing the steam that would otherwise be wasted. Figure 5.5 illustrates how the surplus steam increases from 0 to 228 kg/s, starting at 400 s. The ES control system is designed to operate with a slower response than the turbine's ramp up/down limits to maintain stability. Notably, the BP valve flow rate remains at zero, signifying that all surplus steam is efficiently diverted to the DHN, thereby maximizing operational efficiency and reducing energy wastage.

It is assumed here that the reactor operates in a turbine-leading control mode, which

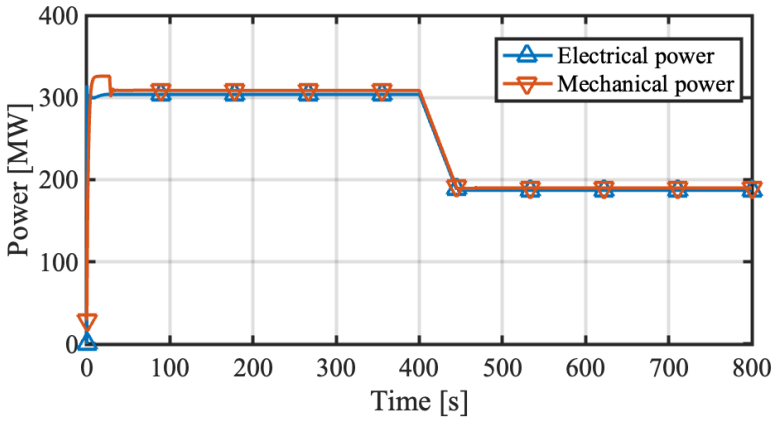



Figure 5.4: Dynamic response of electrical and mechanical power output of the BWRX-300 power plant during dispatch transitions.

corresponds to the reactor maintaining constant thermal power output while adjusting its operation based on turbine control valves. As discussed in Chapter 4, this mode of operation ensures stable reactor pressure and temperature, significantly reducing thermal stress on the reactor components and extending their operational lifespan. Thus, despite the assumed fluctuations in electrical output, Figure 5.6 shows that steam pressure and temperature in the reactor remain stable. This stability is achieved through precise control mechanisms that buffer the reactor from rapid changes, ensuring continuous operation at full capacity without subjecting the reactor components to damaging thermal cycling. This shows the relevance of modeling the BWSMR dynamics in some detail, as proposed in this thesis, so that the feasibility of the considered operating conditions can be analyzed.

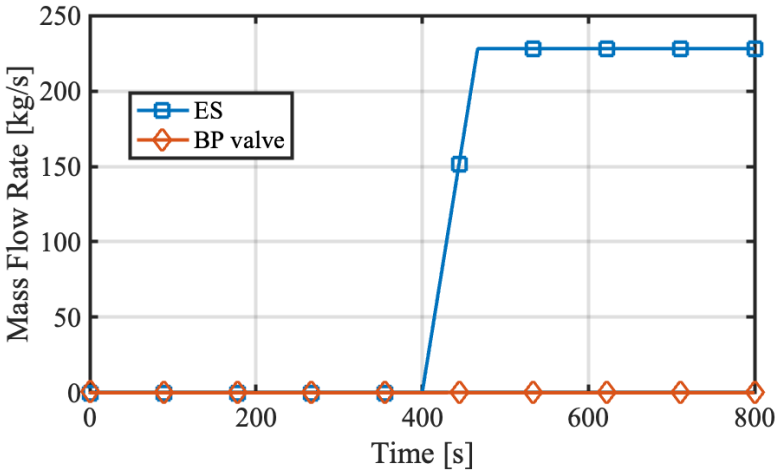



Figure 5.5: ES and BP valve mass flow rates during dispatch reduction in the BWRX-300 power plant.

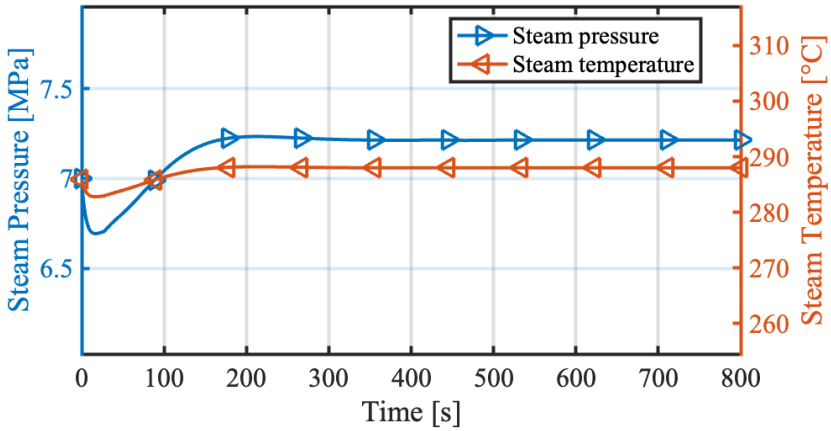



Figure 5.6: Stability of steam pressure and temperature in the BWRX-300 reactor under fluctuating dispatch conditions.

### 5.2.3 Thermal Analysis

A household thermal performance is illustrated in Figure 5.7, which tracks temperatures within its various rooms over the first three days of January 2024 [123]. The results reveal that indoor temperatures are maintained consistently at setpoint levels, even as outdoor conditions fluctuate.

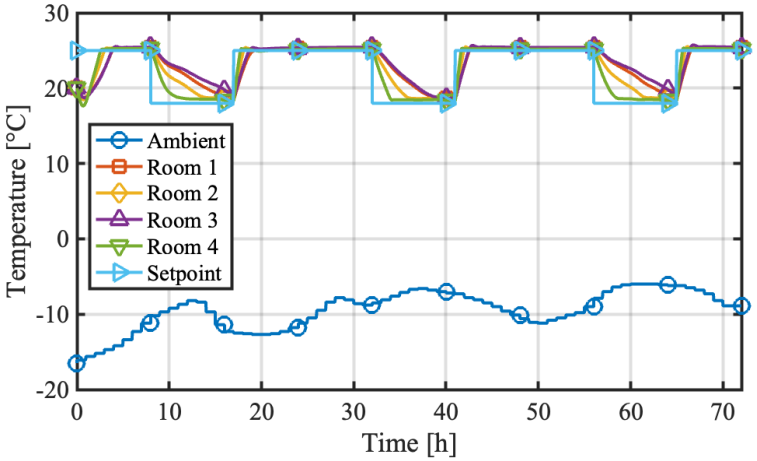



Figure 5.7: Temperature profiles of four rooms in a household supplied by the DHN.

Figure 5.8 illustrates the DHN water supply and return temperatures, with the supply temperature being regulated at approximately 80°C. Temperature fluctuations occur during system startup phases and when TES energy is insufficient to meet demand. During these periods, the central aggregated HP is activated to maintain a continuous and reliable heat supply, temporarily causing temperature dips.

The thermal demand dynamics depicted in Figure 5.9 show how a central aggregated HP responds to changes in ambient temperature, ensuring uninterrupted heating by dynamically adjusting its output based on real-time thermal demands. Figure 5.10 illustrates the changes in TES temperature and energy over time. Thus, note that during the first day, the TES fluctuations are less noticeable due to the initial system startup, where most of the mass flow rate is directed to heat the DHN return water through HX1. This results in rapid charging and discharging cycles within narrow temperature limits compared to the following two days. However, on the subsequent two days, the TES temperature increases steadily from 80°C to its maximum limits of 95°C. When the TES temperature drops below 80°C, the TES stops discharging, and the central HPs take over to maintain the required thermal supply. Figure 5.11 depicts the mass flow rate of the ES, clearly showing its distribution between two primary HXs, with HX1 dedicated to directly heating the DHN return water and HX2 dedicated to charging the TES.

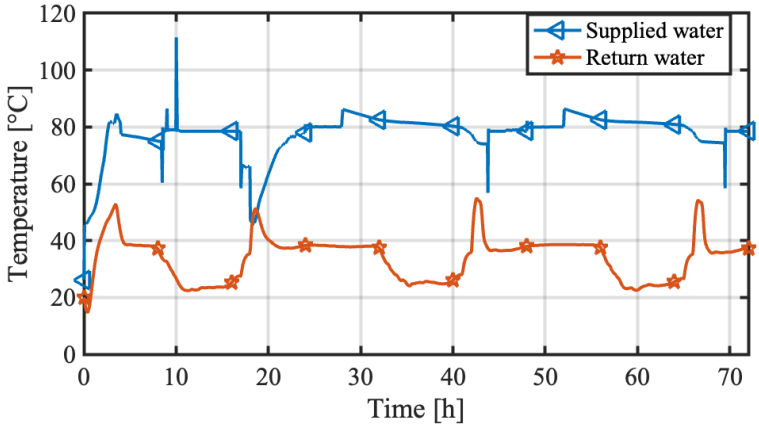



Figure 5.8: DHN supply and return water temperatures variation.

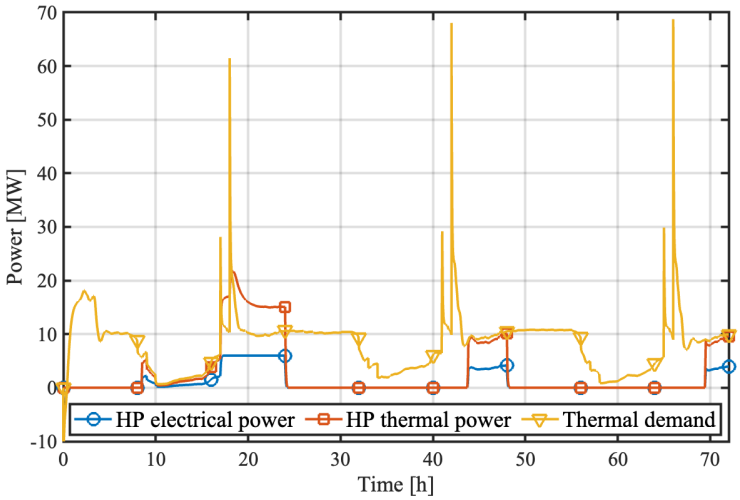



Figure 5.9: Thermal power demand and central aggregated HP operation under different ambient temperature conditions.

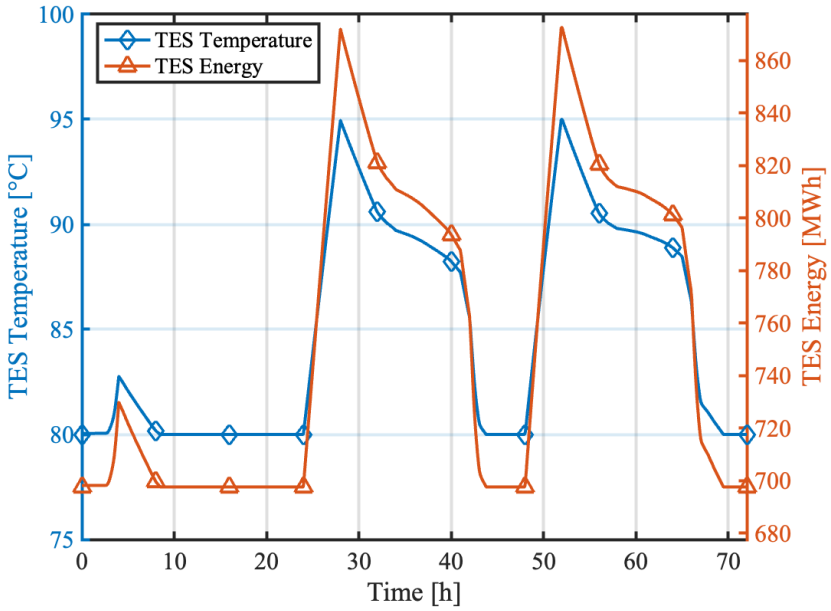



Figure 5.10: TES temperature and energy variation during charging and discharging cycles.

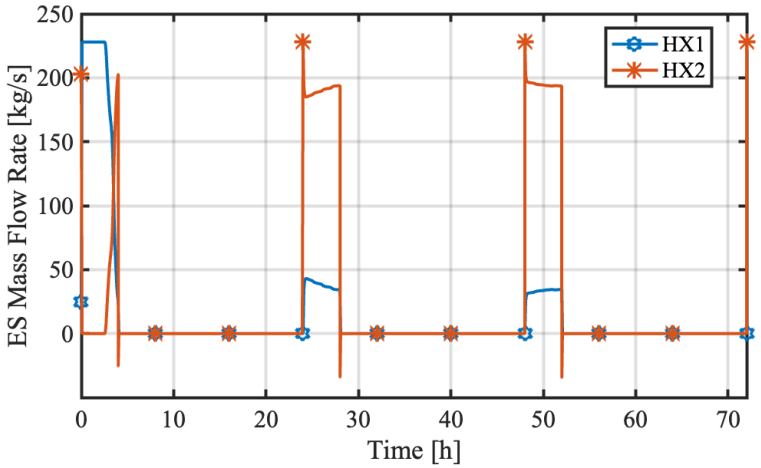
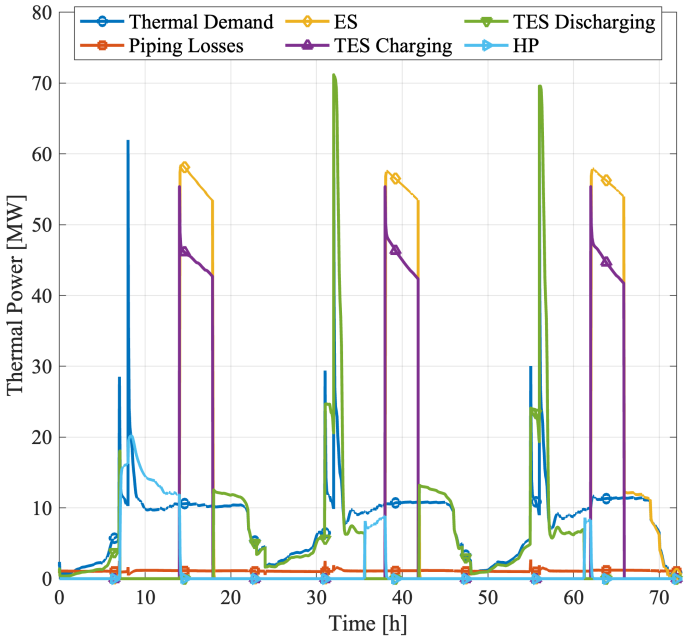


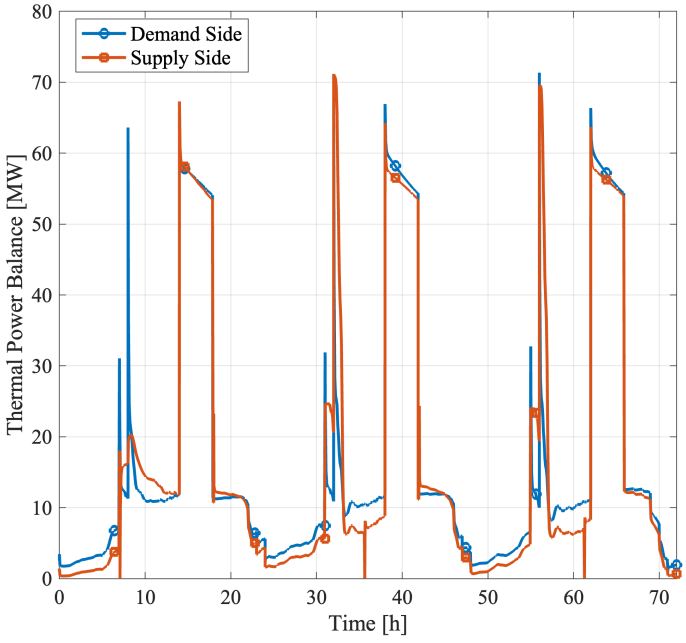

Figure 5.11: Mass flow rate of ES directed to the DHN and TES under varying dispatch conditions.

Figures 5.12 and 5.13 depict the thermal power and energy profiles, along with their respective energy balances, over the same 72 h operating period. Figure 5.12a shows the thermal power contributions from the supply sources, i.e., the ES, TES discharging, and HP, to meet the thermal demand, piping losses, and charge the TES. The ES, available during the 4 h night period, as discussed previously, is used to charge the TES and supply the thermal demand and piping losses, and when the ES is not available, the TES discharging and central HPs operate sequentially to ensure continuity of the thermal supply. Figure 5.12b compares the instantaneous thermal power balance between the total supply and demand. Note the close tracking between supply and demand over time, showing proper coordination among the proposed BWSMR-based DHN system components.

Moreover, Figure 5.13a illustrates the cumulative thermal energy contributions of each component over the 72 h period, illustrating the total energy delivered or stored. Note the thermal energy of the ES, when available, is utilized to charge the TES, supply the thermal demand, and compensate for piping losses. Otherwise, the TES discharges and provides the required thermal demand. When the TES energy is insufficient, the HPs provides the required energy. Finally, Figure 5.13b shows the cumulative thermal energy balance between supply and demand, illustrating the overlap between the two curves as expected from energy balance principles.Note that the small deviations are due to transient conditions or control transitions, but at the end, both values are essentially the same, as expected.

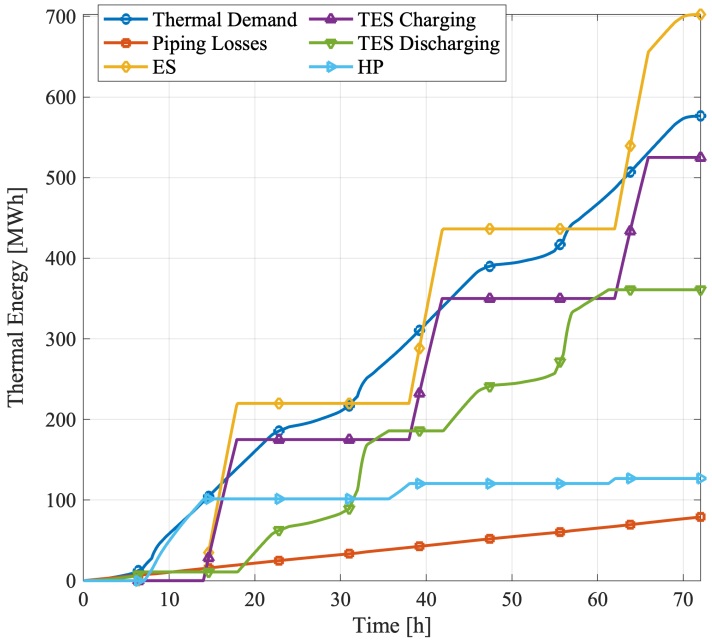



(a)

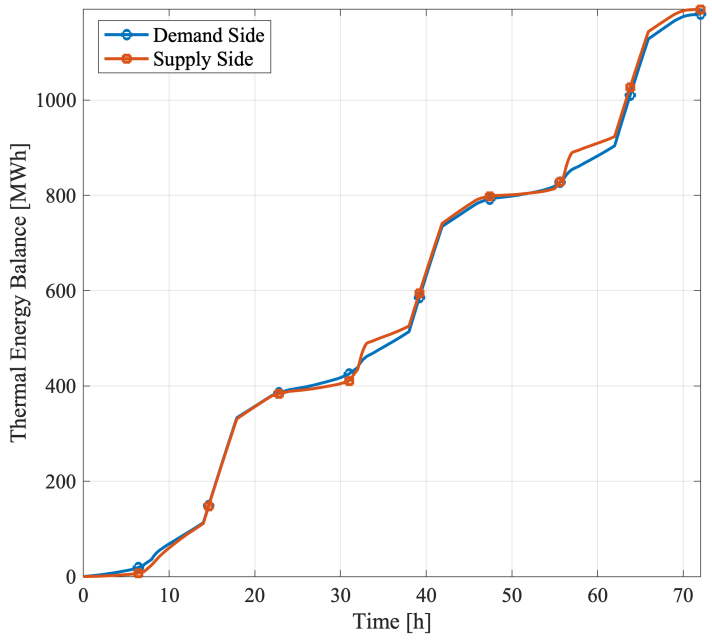



(b)

Figure 5.12: Thermal power profiles: (a) Power components and (b) power balance.




(a)




(b)

Figure 5.13: Thermal Energy profiles: (a) Energy components and (b) energy balance.

### 5.2.4 Distributed HPs

An additional study is conducted to compare the BWSMR-based DHN system with an alternative setup based on HPs, with one aggregated HP for each of the 20 blocks in the Baseline Area, which are reasonably assumed to linearly scale up for the expanded Areas 1 to 3. These HPs supply the same thermal loads under the same operating conditions discussed in Section 5.2.3.

Figure 5.14 displays the temperature profiles of four rooms of a household located near the Darlington NPP. Figure 5.15 illustrates the total aggregated electrical power consumption and thermal power supply of the distributed HPs. Figure 5.16 compares the total electrical energy consumption of the central HPs integrated with the BWSMR-based DHN system against the distributed HPs. These figures show significant energy savings, with the central aggregated HP consuming approximately 75 MWh over the three-day study period, while the distributed HPs require around 221 MWh during the same period. The latter represents nearly three times the energy usage compared to the centralized system.

Figure 5.17 compares the cumulative thermal demand energy supplied over the 72 h period by the BWSMR-based DHN system and the distributed HPs. Note that both configurations meet the same total thermal demand, with closely overlapping curves throughout the time horizon. The slight difference that can be observed at certain intervals, with the distributed HPs supplying marginally less cumulative thermal energy, is primarily due to the distributed HP configuration's limited ability to maintain temperature setpoints across all indoor rooms, resulting in slightly less heat demand. Specifically, the distributed HP case assumes one HP per household, with the control based on a single room's temperature, leading to uneven heating, which is common in residential buildings. In contrast, the BWSMR-based DHN supplies heat through dedicated radiators to each room individually, enabling precise temperature regulation across all zones. Nevertheless, the depicted results confirm that both systems effectively fulfill the thermal demand over the studied period.

It is important to highlight that the simulation results for both the BWRX-300-based cogeneration system and the associated DHN model show the expected behavior across both electrical and thermal systems. Thus, the BWRX-300 response to dispatch transitions, including ramp-down events and steam extraction, aligns with expected dynamics for SMRs operating in turbine-leading mode, as shown in Figures 5.4–5.6. The thermal response for the TES, HPs, and DHN water loops, illustrated in Figures 5.8–5.10, also match the proposed control logic and properly reflect the thermal inertia effects. The presented results are consistent with the DHN behavior discussed in Chapter 3 and the BPS dynamics presented in Chapter 4, and are further validated by the thermal power and energy balance

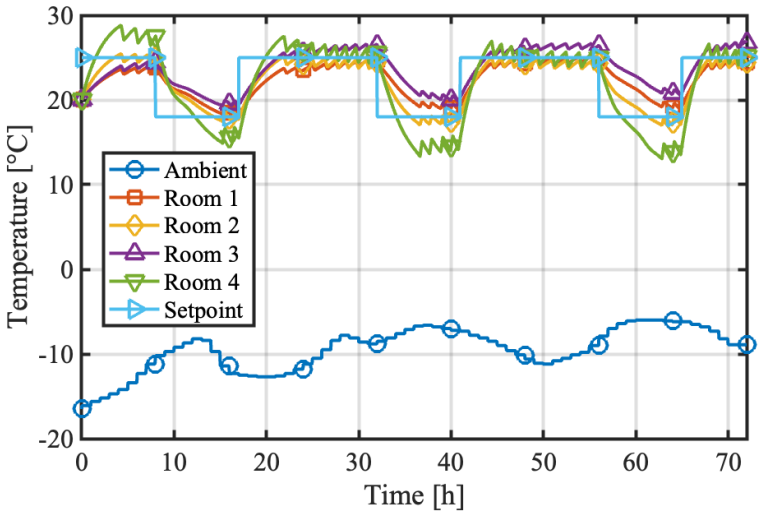



Figure 5.14: Temperature profiles of different household rooms supplied by the distributed HPs.

studies shown in Figures 5.12 and 5.13, which demonstrate close tracking between thermal supply and demand. Furthermore, note that the BPS model used for co-simulation is based on the real IESO base-case data, which is routinely used for power system stability studies in Ontario, ensuring the reliability of the presented power system studies. However, for the Darlington DHN itself, no real-world operational data is available, as this system does not yet exist. Nevertheless, the alignment of the simulation outcomes with expected physical and control behavior supports the validity of the proposed models and controls.

The presented results highlight the superior energy efficiency of the BWSMR-based DHN system. The centralized approach not only reduces overall energy consumption, but also enhances operational reliability.

## 5.3 Summary

This chapter proposed a comprehensive dynamic model for a BWSMR-based DHN cogeneration system, demonstrating the feasibility of utilizing SMRs for thermal energy supply. The developed models and controls in this work, which was submitted for publication in [157], properly capture the interactions between BWSMR, EPN, DHN, TES, HPs, and HXs, incorporating thermal delays, piping heat losses, and transient dynamics. The extended broader multi-timescale analysis enables an in-depth evaluation of short-term

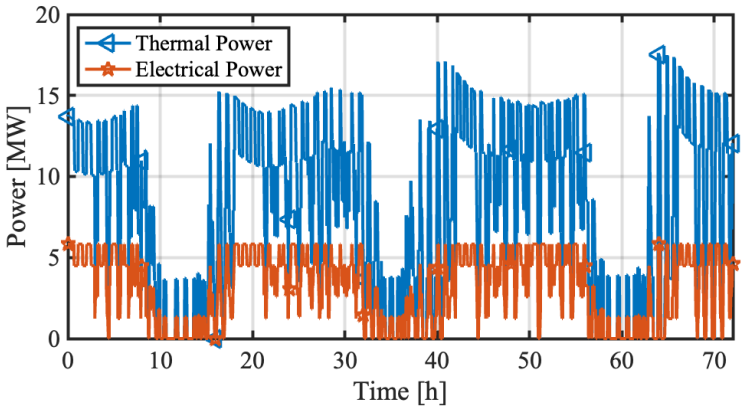



Figure 5.15: Aggregated electrical and thermal power of the distributed HPs.

stability and long-term cogeneration operation, addressing gaps in previous studies. The proposed TES and HP control mechanisms facilitates efficient thermal energy management by adjusting the steam extraction, TES discharge, and HP activation based on demand conditions.

The proposed model was used to study the application of a BWRX-300 SMR in the Ontario's BPS for heating purposes through a DHN deployed in Darlington region. The results demonstrated the feasibility of this application, which compared to a system that relies solely on distributed HPs, it was shown to significantly reduce electrical energy consumption, highlighting that integrating BWSMR-based DHN with TES and central HPs reduced electrical demand, significantly enhancing system sustainability and flexibility.

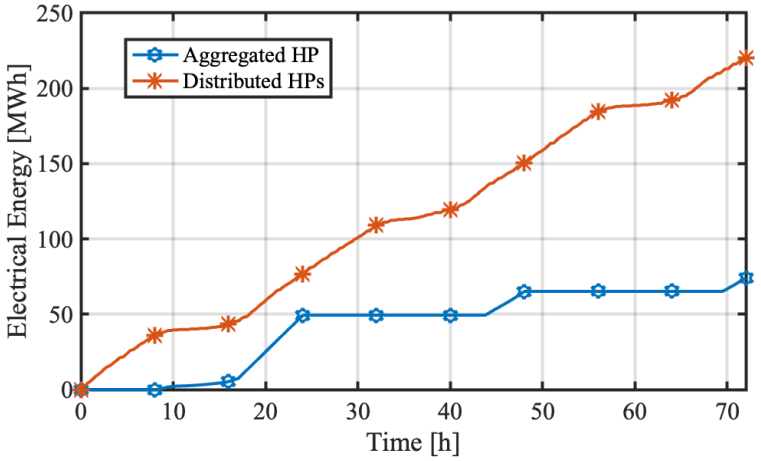



Figure 5.16: Total electrical energy consumption comparison between the central and distributed HPs over three days.

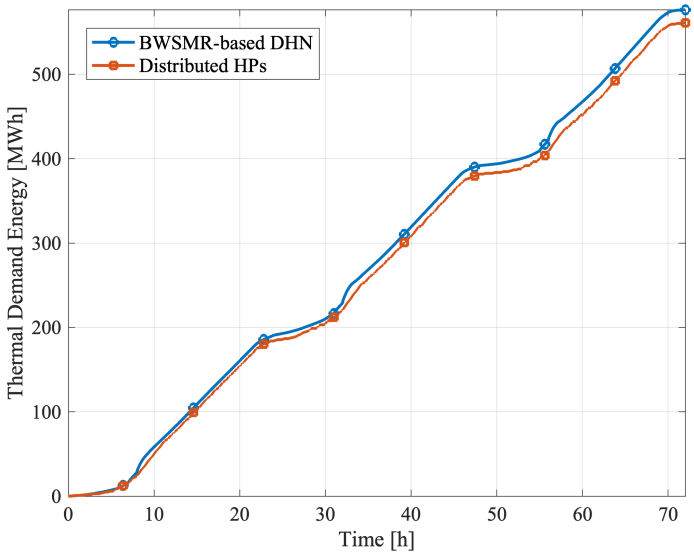



Figure 5.17: Comparison of cumulative thermal demand energy supplied by the BWSMR-based DHN and distributed HPs over a 72 h period.

# Chapter 6

# Conclusion and Future Work

## 6.1 Summary and Conclusions

This thesis focused on proposing dynamic models and control strategies for integrated energy systems to support the transition toward zero-emission solutions, with a thorough review of the relevant state of the art in IEHS dynamic modeling and control, SMR modeling for power system dynamics and control studies, and SMR cogeneration modeling and control. Thus, the thesis started by identifying the key research gaps, which were properly and clearly outlined to be addressed throughout the subsequent chapters.

Chapter 2 provided a comprehensive qualitative background review of the key systems examined in this thesis. The chapter began with a discussion of MGs, where it highlighted their architecture, components, dynamic modeling, and hierarchical control strategies. It then examined DHNs, outlining their historical development, main components, energy sources, and control hierarchies, with an emphasis on modeling approaches that captured thermal losses and delays. This chapter also introduced IEHSs as a potential solution for energy sector decarbonization, supported by coordinated control between electrical and thermal subsystems. The chapter then concluded with an overview of SMRs, particularly BWSMRs, where it discussed their natural circulation design and control, and turbine operation. This included the modeling of steam extraction and integration with TES for DHN applications, within the broader context of cogeneration systems based on NPPs, which were also briefly covered. These foundational concepts and modeling principles laid the groundwork for the detailed dynamic modeling and control studies presented in Chapters 3 through 5.

In Chapter 3, detailed dynamic modeling and control of IEHSs in isolated MGs were

developed and validated, with a focus on remote northern communities. The design and modeling of a DHN to provide space heating in these communities were discussed in detail, based on the utilization of waste heat energy from DGU exhaust systems. In this context, the developed dynamic model enabled the analysis of specific insulation requirements for DHN piping in remote areas due to their low linear heat density, which is an analysis that is not feasible using existing static models. The dynamic IEHS model of the DHN and EPN, including HPs, was also presented. This model incorporated both primary and secondary frequency control strategies to provide power reserves for frequency regulation in isolated MGs, supporting the integration of variable RES while leveraging the significant TES capacity of DHNs. Finally, the feasibility and benefits of using an integrated DHN+EPN IEHS to meet both thermal and electrical demands in remote communities were demonstrated through dynamic simulations and by comparing the integrated system with an ETS-based approach. The results showed the effective use of the DHN for satisfying thermal requirements and regulating EPN frequency in isolated MGs with high RES penetration. The proposed models and controls of IEHSs in Chapter 3 have been published in [141].

Chapter 4 presented and justified the development of a comprehensive dynamic model for BWSMR power plants, incorporating key components such as the reactor, steam turbine, power system, and steam flow controls relevant to power system dynamic and control studies. The primary objective of this work, which has been submitted for publication in [154], was to provide a proper physics-based model of BWSMR operation under typical conditions relevant for power grid studies. The model included essential dynamic phenomena such as pressure variations and two-phase drift velocity, which enhanced the fidelity and reliability of the simulations. The proposed dynamic models were tested and validated using simulations of a simple generator-load system and Ontario's BPS.

Two operational modes for primary frequency control, i.e, reactor-leading and turbine-leading, were compared. The results demonstrated the superior performance of the turbine-leading mode in regulating frequency, confirming that the BWSMR power plant could effectively manage load variations through dynamic steam flow and pressure control. These findings validated the BWSMR's frequency regulation capability and confirmed its suitability for integration into existing power systems.

The chapter also demonstrated the practical application of the proposed BWSMR model in Ontario's BPS, emphasizing that despite the advantages of SMRs, grid operators must account for the challenge of reduced system inertia when replacing conventional reactors with SMRs. Additionally, the chapter highlighted that the thermal model developed for BWSMR power plants enabled the study of their potential to deliver both electricity and heating in integrated energy systems. The model allowed to represent steam extraction

between high-pressure and low-pressure turbine sections at appropriate temperature and pressure levels for the DHN and TES integration studies represented in Chapter 5.

Finally, chapter 5 proposed a comprehensive dynamic model for a BWSMR-based DHN cogeneration system and demonstrated the feasibility of using SMRs for thermal energy integration. The developed models and control strategies, which were submitted for publication in [157], accurately captured the interactions among the BWSMR, EPN, DHN, TES, HPs, and HXs, while incorporating thermal delays, piping heat losses, and transient dynamics. An extended broader multi-timescale analysis enabled an in-depth evaluation of both short-term stability and long-term cogeneration operation, addressing limitations found in previous studies. The proposed TES and HP control mechanisms facilitated efficient thermal energy management by adjusting steam extraction, TES discharge, and HP activation according to thermal demand.

The proposed model was applied to evaluate the integration of a BWRX-300 SMR into Ontario's BPS for providing heating via a DHN in the Darlington region. The results demonstrated the feasibility of this approach. Compared to a system relying solely on distributed HPs, the BWSMR-based DHN, integrated with TES and central HPs, significantly reduced electrical energy consumption, thereby enhancing overall system sustainability and operational flexibility.

## 6.2 Contributions

Based on the identified research gaps, the key contributions of this thesis are summarized next.

### 6.2.1 IEHS Modeling in MGs

- Developed dynamic models to assess the feasibility and challenges of utilizing diesel engine exhaust waste heat to supply a DHN in remote MGs, considering soil constraints, extreme climatic conditions, insulation strategies, and optimal HP sizing to meet variable thermal loads based on weather, EPN characteristics, and consumer demand.

- Designed a demand response control strategy for HPs to provide frequency regulation reserves in the EPN of isolated MGs.

- Demonstrated the benefits of integrating variable RESs through DHNs in remote MGs, using a simulated DHN model and a real EPN case study to compare centralized DHNs and decentralized ETSs in supplying thermal loads and supporting grid stability via HP or ETS demand response.

### 6.2.2 SMR Modeling

- Developed and justified an enhanced BWSMR dynamic model incorporating pressure variations and two-phase drift velocity to improve simulation accuracy for proper dynamic and control studies.
- Proposed a novel equation linking reactor pressure changes to steam turbine mass flow rate to properly represent turbine dynamics in transient studies.
- Evaluated reactor-leading and turbine-leading strategies for frequency control, highlighting their impact on system stability.
- Validated the BWSMR model in the Ontario BPS to demonstrate its practical application in large-scale power systems.

### 6.2.3 SMR-based DHN Modeling

- Developed a cogeneration system model integrating a BWSMR with a DHN, distinct from existing IPWR-based models.
- Represented thermal losses, transport delays, and time-varying heating demands for realistic BWSMR-based DHN operation.
- Integrated electrical and thermal transients to capture the interdependencies within the cogeneration system.
- Demonstrated the role of TES and HPs in utilizing excess SMR thermal energy during low electric demand, enhancing operational flexibility.
- Applied an extended broader multi-timescale dynamic analysis to develop robust and adaptive control strategies.
- Applied the proposed models and control strategies to a potential BWSMR-based DHN in Darlington, Ontario, confirming their feasibility and effectiveness.

## 6.3 Future Work

The following directions for future work can enhance the research presented in this thesis:

- Expand dynamic IEHS models to include domestic hot water delivery through DHNs, enhancing their value in remote and urban communities, since this load constitutes a substantial share of household thermal consumption and affects overall DHN sizing and operation.
- Develop an EMS for the proposed IEHS, enhancing operational flexibility and efficiency in both MGs and BPSs, since an integrated EMS is essential for optimizing the coordination of thermal and electrical subsystems, especially under variable RES generation and demand profiles, thus supporting optimal and reliable operation.
- Perform techno-economic analyses of IEHS to evaluate long-term viability, cost-effectiveness, and environmental impact compared to traditional heating systems, exploring their economic feasibility for both MGs and BPSs. This is needed to provide critical insights into the practical deployment potential of IEHS solutions, guiding investment decisions and policy development based on quantitative performance indicators.

# References


[1] "Net-zero emissions by 2050." Available online: `https://www.canada.ca/en/services/environment.html`.

[2] M. E. Javanmard, Y. Tang, Z. Wang, and P. Tontiwachwuthikul, "Forecast energy demand, CO2 emissions and energy resource impacts for the transportation sector," *Applied Energy*, vol. 338, p. 120830, 2023.

[3] M. Arriaga, C. A. Cañizares, and M. Kazerani, "Northern lights: Access to electricity in Canada's Northern and remote communities," *IEEE Power and Energy Magazine*, vol. 12, no. 4, pp. 50–59 rblack, 2014.

[4] S. Werner, "International review of district heating and cooling," *Energy*, vol. 137, pp. 617–631, 2017.

[5] L. Frison, M. Kollmar, A. Oliva, A. Bürger, and M. Diehl, "Model predictive control of bidirectional heat transfer in prosumer-based solar district heating networks," *Applied Energy*, vol. 358, p. 122617 rred, 2024.

[6] J. Coady and J. Duquette, "Quantifying the impacts of biomass driven combined heat and power grids in northern rural and remote communities," *Renewable and Sustainable Energy Reviews*, vol. 148, p. 111296, 2021.

[7] A. M. Hendricks, J. E. Wagner, T. A. Volk, D. H. Newman, and T. R. Brown, "A cost-effective evaluation of biomass district heating in rural communities," *Applied Energy*, vol. 162, pp. 561–569, 2016.

[8] H. Elsaraf, M. Jamil, and B. Pandey, "Techno-economic design of a combined heat and power microgrid for a remote community in Newfoundland Canada," *IEEE Access*, vol. 9, pp. 91548–91563 rred, 2021.

[9] J. K. Nøland, M. Hjelmeland, L. B. Tjernberg, and C. Hartmann, "The race to realize small modular reactors: Rapid deployment of clean dispatchable energy sources," *IEEE Power and Energy Magazine*, vol. 22, no. 3, pp. 90–103, 2024.

[10] W. Xie, J. Atherton, J. Bai, F. Farazi, S. Mosbach, J. Akroyd, and M. Kraft, "A nuclear future? small modular reactors in a carbon tax-driven transition to clean energy," *Applied Energy*, vol. 364, p. 114732, 2024.

[11] G. Asuega, G. Locatelli, and D. C. Invernizzi, "Techno-economic analysis of advanced small modular nuclear reactors," *Applied Energy*, vol. 334, p. 120669, 2023.

[12] Y. Liu, G. Huang, J. Chen, X. Zhang, X. Zheng, and M. Zhai, "Development of an optimization-aided small modular reactor siting model–a case study of saskatchewan, canada," *Applied Energy*, vol. 305, p. 117867, 2022.

[13] Independent Electricity System Operator (IESO), "Regional planning progress update." [Online]. Available: `https://www.ieso.ca/Get-Involved/Regional-Planning/GTA-and-Central-Ontario/GTA-East`, Feb. 2025.

[14] B. Poudel and R. Gokaraju, "Small modular reactor (SMR) based hybrid energy system for electricity and district heating," *IEEE Transactions on Energy Conversion*, vol. 36, no. 4, pp. 2794–2802, 2021.

[15] R. Li and V. Mahalec, "Greenhouse gas emissions reduction by cross-sector integration of energy systems: Optimal sizing of integrated entities," *Energy Conversion and Management*, vol. 248, p. 114788, 2021.

[16] B. Poudel and R. Gokaraju, "Optimal operation of SMR-RES hybrid energy system for electricity and district heating," *IEEE Transactions on Energy Conversion*, vol. 36, no. 4, pp. 3146–3155, 2021.

[17] T. Korpela, J. Kaivosoja, Y. Majanne, L. Laakkonen, M. Nurmoranta, and M. Vilkko, "Utilization of district heating networks to provide flexibility in CHP production," *Energy Procedia*, vol. 116, pp. 310–319, 2017.

[18] F. Iov, M. Khatibi, and J. D. Bendtsen, "On the participation of power-to-heat assets in frequency regulation markets—A Danish case study," *Energies*, vol. 13, no. 18, p. 4608, 2020.

[19] T. B. Harild Rasmussen, Q. Wu, and M. Zhang, "Primary frequency support from local control of large-scale heat pumps," *International Journal of Electrical Power & Energy Systems*, vol. 133, p. 107270, 2021.

[20] J. W. Craig, E. L. Miller, J. Benowitz, M. Manson, T. Dumitru, and C. W. Hoiland, "Application of low temperature thermochronology for exploration of blind geothermal systems: A case study from the Kigluaik fault system and Pilgrim Hot Springs, northwestern Alaska," *PROCEEDINGS, 49th Workshop on Geothermal Reservoir Engineering Stanford University, Stanford, California, 2024 rblack*, 2024.

[21] C. Yang and Z. Li, "Distributed conditional-distributionally robust coordination for an electrical power and flexibility-enhanced district heating system," *Applied Energy*, vol. 347, p. 121491, 2023.

[22] D. E. Olivares, A. Mehrizi-Sani, A. H. Etemadi, C. A. Cañizares, R. Iravani, M. Kazerani, A. H. Hajimiragha, O. Gomis-Bellmunt, M. Saeedifard, R. Palma-Behnke, *et al.*, "Trends in microgrid control," *IEEE Transactions on Smart Grid*, vol. 5, no. 4, pp. 1905–1919, 2014.

[23] E. Saloux and J. A. Candanedo, "Model-based predictive control to minimize primary energy use in a solar district heating system with seasonal thermal energy storage," *Applied Energy*, vol. 291, p. 116840, 2021.

[24] A. Boldrini, J. J. Navarro, W. Crijns-Graus, and M. van den Broek, "The role of district heating systems to provide balancing services in the European Union," *Renewable and Sustainable Energy Reviews*, vol. 154, p. 111853, 2022.

[25] X. Sheng and L. Duanmu, "Electricity consumption and economic analyses of district heating system with distributed variable speed pumps," *Energy and Buildings*, vol. 118, pp. 291–300, 2016.

[26] J. Yang, N. Zhang, A. Botterud, and C. Kang, "On an equivalent representation of the dynamics in district heating networks for combined electricity-heat operation," *IEEE Transactions on Power Systems*, vol. 35, no. 1, pp. 560–570, 2019.

[27] J. Zheng, Z. Zhou, J. Zhao, and J. Wang, "Integrated heat and power dispatch truly utilizing thermal inertia of district heating network for wind power integration," *Applied Energy*, vol. 211, pp. 865–874, 2018.

[28] W. Zheng, Y. Hou, and Z. Li, "A dynamic equivalent model for district heating networks: Formulation, existence and application in distributed electricity-heat operation," *IEEE Transactions on Smart Grid*, vol. 12, no. 3, pp. 2685–2695, 2021.

[29] S. Zhang, W. Gu, S. Lu, S. Yao, S. Zhou, and X. Chen, "Dynamic security control in heat and electricity integrated energy system with an equivalent heating network model," *IEEE Transactions on Smart Grid*, vol. 12, no. 6, pp. 4788–4798, 2021.

[30] P. Wang, Y. Fu, X. Wei, and F. Zhao, "Simulation study of frequency control characteristics of a generation III+ nuclear power plant," *Annals of Nuclear Energy*, vol. 115, pp. 502–522, 2018.

[31] G. Ablay, "A modeling and control approach to advanced nuclear power plants with gas turbines," *Energy Conversion and Management*, vol. 76, pp. 899–909, 2013.

[32] H. Gao, C. Wang, and W. Pan, "A detailed nuclear power plant model for power system analysis based on PSS/E," in *2006 IEEE PES Power Systems Conference and Exposition*, pp. 1582–1586, IEEE, 2006.

[33] H. Wang, S. Mu, G. Li, Z. Yang, J. Yang, F. P. G. Marquez, X. Zhou, Y. Ma, and Z. Chen, "Modeling and operation strategy of nuclear power plant with electric heat storage in the ancillary service market," *Nuclear Engineering and Design*, vol. 415, p. 112686, 2023.

[34] J. March-Leuba, D. G. Cacuci, and R. B. Perez, "Nonlinear dynamics and stability of boiling water reactors: Part 1–qualitative analysis," *Nuclear Science and Engineering*, vol. 93, no. 2, pp. 111–123, 1986.

[35] J. March-Leuba, D. G. Cacuci, and R. B. Perez, "Nonlinear dynamics and stability of boiling water reactors: Part 2–quantitative analysis," *Nuclear Science and Engineering*, vol. 93, no. 2, pp. 124–136, 1986.

[36] M. Polo-Labarrios, L. Franco-Pérez, L. Quezada-Téllez, and G. Fernández-Anaya, "Local dynamic analysis in boiling water reactor," *Annals of Nuclear Energy*, vol. 137, p. 107084, 2020.

[37] D. Hennig, "A study on boiling water reactor stability behavior," *Nuclear Technology*, vol. 126, no. 1, pp. 10–31, 1999.

[38] G. D. Prasad and M. Pandey, "Stability analysis and nonlinear dynamics of natural circulation boiling water reactors," *Nuclear Engineering and Design*, vol. 238, no. 1, pp. 229–240, 2008.

[39] J. Fleck, "The dynamic behaviour of boiling water reactors," *Journal of Nuclear Energy Part A: Reactor Science*, vol. 11, no. 2-4, pp. 114–130, 1960.

[40] A. N. Nahavandi and R. F. von Hollen, "A space-dependent dynamic analysis of boiling water reactor systems," *Nuclear Science and Engineering*, vol. 20, no. 4, pp. 392–413, 1964.

[41] P. Girijashankar, G. Srikantiah, and M. Pai, "Dynamic simulation of a boiling water nuclear reactor," *Annals of Nuclear Energy*, vol. 3, no. 2-3, pp. 133–145, 1976.

[42] "Darlington New Nuclear Project: BWRX-300 Preliminary Safety Analysis Report." https://www.opg.com/document/2022/BWRX-300_Preliminary_Safety_Analysis_Report.pdf.

[43] A. Huning, J. Rader, and P. Ramuhalli, "Development of a BWR system fault simulator using TRANSFORM/Modelica," technical Report, Oak Ridge National Laboratory (ORNL), Oak Ridge, TN (United States), 2022.

[44] G. Trundle, "Reliability assessment of passive ICS in an SMR as part of the PSA analysis," master's thesis, KTH Royal Institute of Technology, 2023.

[45] A. Pomogaev, "BWRX-300 isolation condenser system analysis," master's thesis, Lappeenranta–Lahti University of Technology LUT, 2022.

[46] K. Kulkowski, M. Grochowski, K. Duzinkiewicz, and A. Kobylarz, "Nuclear power plant steam turbine—Modeling for model based control purposes," *Applied Mathematical Modelling*, vol. 48, pp. 491–515, 2017.

[47] B. Poudel, K. Joshi, and R. Gokaraju, "A dynamic model of small modular reactor based nuclear plant for power system studies," *IEEE Transactions on Energy Conversion*, vol. 35, no. 2, pp. 977–985, 2019.

[48] International Atomic Energy Agency, "Nuclear cogeneration for climate change mitigation and sustainable development goals," Tech. Rep. IAEA-TECDOC-2056, 2021. [Online]. Available: https://www-pub.iaea.org/MTCD/publications/PDF/TE-2056web.pdf.

[49] J. Vujić, R. M. Bergmann, R. Škoda, and M. Miletić, "Small modular reactors: Simpler, safer, cheaper? ," *Energy*, vol. 45, no. 1, pp. 288–295, 2012.

[50] G. Locatelli, A. Fiordaliso, S. Boarin, and M. E. Ricotti, "Cogeneration: An option to facilitate load following in small modular reactors," *Progress in Nuclear Energy*, vol. 97, pp. 153–161, 2017.

[51] E. Pursiheimo and T. J. Lindroos, "Optimal investment analysis for heat pumps and nuclear heat in decarbonised Helsinki metropolitan district heating system," *Energy Storage and Saving*, vol. 1, pp. 80–92, 2022.

[52] A. Teräsvirta and J. Hyvärinen, "Nuclear engineering and design nuclear heat supply system for a small district heating reactor," *Nuclear Engineering and Design*, vol. 426, p. 113389, 2024.

[53] S. W. Kang and M.-S. Yim, "Multi-objective optimization application for a coupled light water small modular reactor-combined heat and power cycle (cogeneration) systems," *Nuclear Engineering and Technology*, vol. 56, no. 5, pp. 1654–1666, 2024.

[54] H. A. S. Abushamah, O. Burian, D. Ray, and R. Škoda, "Integration of district heating systems with small modular reactors and organic rankine cycle including energy storage: Design and energy management optimization," *Energy Conversion and Management*, vol. 322, p. 119138, 2024.

[55] D. Michaelson and J. Jiang, "Review of integration of small modular reactors in renewable energy microgrids," *Renewable and Sustainable Energy Reviews*, vol. 152, p. 111638, 2021.

[56] S. W. Kang and M.-S. Yim, "Coupled system model analysis for a small modular reactor cogeneration (combined heat and power) application," *Energy*, vol. 262, p. 125481, 2023.

[57] J. Saari, M. Kozlova, H. Suikkanen, E. Sermyagina, J. Hyvärinen, and J. S. Yeomans, "Global sensitivity analysis of nuclear district heating reactor primary heat exchanger and pressure vessel optimization," *Energy*, vol. 312, p. 133393, 2024.

[58] A. Cagnano, E. De Tuglie, and P. Mancarella, "Microgrids: Overview and guidelines for practical implementations and operation," *Applied Energy*, vol. 258, p. 114039, 2020.

[59] F. Kanellos, A. I. Tsouchnikas, N. Hatziargyriou, *et al.*, "Micro-grid simulation during grid-connected and islanded modes of operation," in *International Conference on Power Systems Transients*, vol. 6, 2005.

[60] S. Parhizi, H. Lotfi, A. Khodaei, and S. Bahramirad, "State of the art in research on microgrids: A review," *IEEE Access*, vol. 3, pp. 890–925, 2015.

[61] B. Wang and G. Verbič, "Stability analysis of low-voltage distribution feeders operated as islanded microgrids," *IEEE Transactions on Smart Grid*, vol. 12, no. 6, pp. 4681–4689, 2021.

[62] S. Chakraborty and M. G. Simoes, "Experimental evaluation of active filtering in a single-phase high-frequency ac microgrid," *IEEE Transactions on Energy Conversion*, vol. 24, no. 3, pp. 673–682, 2009.

[63] T. Sels, C. Dragu, T. Van Craenenbroeck, and R. Belmans, "Electrical energy storage systems: existing systems versus newest systems—an overview," in *Proc. Int. Conf. Power Generation Sustainable Develop.(AIM)*, pp. 215–220, Citeseer, 2001.

[64] E. Planas, J. Andreu, J. I. Gárate, I. M. De Alegría, and E. Ibarra, "AC and DC technology in microgrids: A review," *Renewable and Sustainable Energy Reviews*, vol. 43, pp. 726–749, 2015.

[65] V. C. Gungor, D. Sahin, T. Kocak, S. Ergut, C. Buccella, C. Cecati, and G. P. Hancke, "Smart grid technologies: Communication technologies and standards," *IEEE Transactions on Industrial Informatics*, vol. 7, no. 4, pp. 529–539, 2011.

[66] W. Liu, W. Gu, W. Sheng, X. Meng, Z. Wu, and W. Chen, "Decentralized multi-agent system-based cooperative frequency control for autonomous microgrids with communication constraints," *IEEE Transactions on Sustainable Energy*, vol. 5, no. 2, pp. 446–456, 2014.

[67] D.-J. Lee and L. Wang, "Small-signal stability analysis of an autonomous hybrid renewable energy power generation/energy storage system part I: Time-domain simulations," *IEEE Transactions on Energy Conversion*, vol. 23, no. 1, pp. 311–320, 2008.

[68] N. Pogaku, M. Prodanovic, and T. C. Green, "Modeling, analysis and testing of autonomous operation of an inverter-based microgrid," *IEEE Transactions on Power Electronics*, vol. 22, no. 2, pp. 613–625, 2007.

[69] N. L. Soultanis, S. A. Papathanasiou, and N. D. Hatziargyriou, "A stability algorithm for the dynamic analysis of inverter dominated unbalanced LV microgrids," *IEEE Transactions on Power Systems*, vol. 22, no. 1, pp. 294–304, 2007.

[70] M. Ahmed, L. Meegahapola, A. Vahidnia, and M. Datta, "Stability and control aspects of microgrid architectures–a comprehensive review," *IEEE Access*, vol. 8, pp. 144730–144766, 2020.

[71] Y. Li, D. M. Vilathgamuwa, and P. C. Loh, "Design, analysis, and real-time testing of a controller for multibus microgrid system," *IEEE Transactions on Power Electronics*, vol. 19, no. 5, pp. 1195–1204, 2004.

[72] F. Katiraei and M. R. Iravani, "Power management strategies for a microgrid with multiple distributed generation units," *IEEE Transactions on Power Systems*, vol. 21, no. 4, pp. 1821–1831, 2006.

[73] M. N. Marwali, J.-W. Jung, and A. Keyhani, "Control of distributed generation systems-part II: Load sharing control," *IEEE Transactions on Power Electronics*, vol. 19, no. 6, pp. 1551–1561, 2004.

[74] N. Altin and S. E. Eyimaya, "A review of microgrid control strategies," in *2021 10th International Conference on Renewable Energy Research and Application (ICRERA)*, pp. 412–417, IEEE, 2021.

[75] B. Rezaie and M. A. Rosen, "District heating and cooling: Review of technology and potential enhancements," *Applied Energy*, vol. 93, pp. 2–10, 2012.

[76] C. Philibert, "The present and future use of solar thermal energy as a primary source of energy," *International Energy Agency*, pp. 1–16, 2005.

[77] B. Wei, S.-L. Wang, and L. Li, "Fuzzy comprehensive evaluation of district heating systems," *Energy Policy*, vol. 38, no. 10, pp. 5947–5955, 2010.

[78] A. R. Mazhar, S. Liu, and A. Shukla, "A state of art review on the district heating systems," *Renewable and Sustainable Energy Reviews*, vol. 96, pp. 420–439, 2018.

[79] B. Skagestad and P. Mildenstein, *District heating and cooling connection handbook*. NOVEM, Netherlands Agency for Energy and the Environment, 2002.

[80] H. Gadd and S. Werner, "Daily heat load variations in Swedish district heating systems," *Applied Energy*, vol. 106, pp. 47–55, 2013.

[81] I. del Hoyo Arce, S. H. López, S. L. Perez, M. Rämä, K. Klobut, and J. A. Febres, "Models for fast modelling of district heating and cooling networks," *Renewable and Sustainable Energy Reviews*, vol. 82, pp. 1863–1873, 2018.

[82] J. Duquette, A. Rowe, and P. Wild, "Thermal performance of a steady state physical pipe model for simulating district heating grids with variable flow," *Applied Energy*, vol. 178, pp. 383–393, 2016.

[83] A. Lake, B. Rezaie, and S. Beyerlein, "Review of district heating and cooling systems for a sustainable future," *Renewable and Sustainable Energy Reviews*, vol. 67, pp. 417–425, 2017.

[84] Y. Wang, S. You, H. Zhang, X. Zheng, S. Wei, Q. Miao, and W. Zheng, "Operation stability analysis of district heating substation from the control perspective," *Energy and Buildings*, vol. 154, pp. 373–390, 2017.

[85] W. Zheng, H. Lu, M. Zhang, Q. Wu, Y. Hou, and J. Zhu, "Distributed energy management of multi-entity integrated electricity and heat systems: A review of architectures, optimization algorithms, and prospects," *IEEE Transactions on Smart Grid*, 2023.

[86] A. Martens, "The energetic feasibility of chp compared to the separate production of heat and power," *Applied Thermal Engineering*, vol. 18, no. 11, pp. 935–946, 1998.

[87] M. A. Sayegh, P. Jadwiszczak, B. Axcell, E. Niemierka, K. Bryś, and H. Jouhara, "Heat pump placement, connection and operational modes in European district heating," *Energy and Buildings*, vol. 166, pp. 122–144, 2018.

[88] H. Lund, S. Werner, R. Wiltshire, S. Svendsen, J. E. Thorsen, F. Hvelplund, and B. V. Mathiesen, "4th Generation District Heating (4GDH): Integrating smart thermal grids into future sustainable energy systems," *Energy*, vol. 68, pp. 1–11, 2014.

[89] A. Shakeel, D. Chong, and J. Wang, "Load forecasting of district heating system based on improved FB-Prophet model," *Energy*, vol. 278, p. 127637, 2023.

[90] M. Zhang, Q. Wu, J. Wen, Z. Lin, F. Fang, and Q. Chen, "Optimal operation of integrated electricity and heat system: A review of modeling and solution methods," *Renewable and Sustainable Energy Reviews*, vol. 135, p. 110098, 2021.

[91] Q. Yang, T. Yang, and W. Li, *Smart power distribution systems: control, communication, and optimization.* Academic Press, 2018.

[92] C. Shao, Y. Ding, J. Wang, and Y. Song, "Modeling and integration of flexible demand in heat and electricity integrated energy system," *IEEE Transactions on Sustainable Energy*, vol. 9, no. 1, pp. 361–370, 2017.

[93] A. S. Gaur, D. Z. Fitiwi, and J. Curtis, "Heat pumps and our low-carbon future: A comprehensive review," *Energy Research & Social Science*, vol. 71, p. 101764, 2021.

[94] H. Averfalk, P. Ingvarsson, U. Persson, M. Gong, and S. Werner, "Large heat pumps in swedish district heating systems," *Renewable and Sustainable Energy Reviews*, vol. 79, pp. 1275–1284, 2017.

[95] P. A. Østergaard and A. N. Andersen, "Booster heat pumps and central heat pumps in district heating," *Applied Energy*, vol. 184, pp. 1374–1388, 2016.

[96] S. Zhang, W. Gu, S. Yao, S. Lu, S. Zhou, and Z. Wu, "Partitional decoupling method for fast calculation of energy flow in a large-scale heat and electricity integrated energy system," *IEEE Transactions on Sustainable Energy*, vol. 12, no. 1, pp. 501–513, 2020.

[97] J. Dancker and M. Wolter, "Improved quasi-steady-state power flow calculation for district heating systems: A coupled newton-raphson approach," *Applied Energy*, vol. 295, p. 116930, 2021.

[98] B. van der Heijde, M. Fuchs, C. R. Tugores, G. Schweiger, K. Sartor, D. Basciotti, D. Müller, C. Nytsch-Geusen, M. Wetter, and L. Helsen, "Dynamic equation-based thermo-hydraulic pipe model for district heating and cooling systems," *Energy Conversion and Management*, vol. 151, pp. 158–169, 2017.

[99] X. Xiong and X. Wu, "Coordinated control of heat-power integrated energy system using zone model predictive control with variable zone width," *Applied Thermal Engineering*, vol. 217, p. 119270, 2022.

[100] Z. Wu, W. S. Yang, S. Shi, and M. Ishii, "A core design study for a small modular boiling water reactor with long-life core," *Nuclear Technology*, vol. 193, no. 3, pp. 364–374, 2016.

[101] A. Halimi and K. Shirvan, "Impact of core power density on economics of a small integral pwr," *Nuclear Engineering and Design*, vol. 385, p. 111488, 2021.

[102] "BWRX-300 General Description." `https://www.gevernova.com/content/dam/gepower-new/global/en_US/images/gas-new-site/en/bwrx-300/005N9751_Rev_BWRX-300_General_Description.pdf`.

[103] M. Furuya, F. Inada, and T. Van der Hagen, "Flashing-induced density wave oscillations in a natural circulation BWR—Mechanism of instability and stability map," *Nuclear Engineering and Design*, vol. 235, no. 15, pp. 1557–1569, 2005.

[104] Y. Wang, W. Chen, L. Zhang, X. Zhao, Y. Gao, and V. Dinavahi, "Small modular reactors: An overview of modeling, control, simulation, and applications," *IEEE Access*, vol. 12, pp. 39628–39650, 2024.

[105] M. Jaskólski, A. Reński, and T. Minkiewicz, "Thermodynamic and economic analysis of nuclear power unit operating in partial cogeneration mode to produce electricity and district heat," *Energy*, vol. 141, pp. 2470–2483, 2017.

[106] K. Sadeghi, S. H. Ghazaie, E. Sokolova, E. Fedorovich, and A. Shirani, "Comprehensive techno-economic analysis of integrated nuclear power plant equipped with various hybrid desalination systems," *Desalination*, vol. 493, p. 114623, 2020.

[107] M. Lipka and A. Rajewski, "Regress in nuclear district heating. the need for rethinking cogeneration," *Progress in Nuclear Energy*, vol. 130, p. 103518, 2020.

[108] A. Wilson, W. J. Nuttall, and B. A. Glowacki, "A methodology for techno-economic evaluation of asymmetric energy storage systems: A nuclear energy case study," *Progress in Nuclear Energy*, vol. 147, p. 104127, 2022.

[109] A. A. Al Kindi, M. Aunedi, A. M. Pantaleo, G. Strbac, and C. N. Markides, "Thermo-economic assessment of flexible nuclear power plants in future low-carbon electricity systems: Role of thermal energy storage," *Energy Conversion and Management*, vol. 258, p. 115484, 2022.

[110] I. Calero, C. A. Cañizares, K. Bhattacharya, and R. Baldick, "Duck-curve mitigation in power grids with high penetration of PV generation," *IEEE Transactions on Smart Grid*, vol. 13, no. 1, pp. 314–329, 2022.

[111] C. A. Thilker, P. Bacher, H. G. Bergsteinsson, R. G. Junker, D. Cali, and H. Madsen, "Non-linear grey-box modelling for heat dynamics of buildings," *Energy and Buildings*, vol. 252, p. 111457, 2021.

[112] H. V. Larsen, H. Pálsson, B. Bøhm, and H. F. Ravn, "Aggregated dynamic simulation model of district heating networks," *Energy Conversion and Management*, vol. 43, no. 8, pp. 995–1019, 2002.

[113] J. M. G. Lopez, E. Pouresmaeil, C. A. Canizares, K. Bhattacharya, A. Mosaddegh, and B. V. Solanki, "Smart residential load simulator for energy management in smart grids," *IEEE Transactions on Industrial Electronics*, vol. 66, no. 2, pp. 1443–1452, 2018.

[114] S. Lim, S. Park, H. Chung, M. Kim, Y.-J. Baik, and S. Shin, "Dynamic modeling of building heat network system using Simulink," *Applied Thermal Engineering*, vol. 84, pp. 375–389, 2015.

[115] C. S. Brown, N. J. Cassidy, S. S. Egan, and D. Griffiths, "Thermal and economic analysis of heat exchangers as part of a geothermal district heating scheme in the Cheshire Basin, UK," *Energies*, vol. 15, no. 6, p. 1983, 2022.

[116] T. L. Bergman, T. L. Bergman, F. P. Incropera, D. P. Dewitt, and A. S. Lavine, *Fundamentals of heat and mass transfer*. John Wiley & Sons, 2011.

[117] A. Maiboom, X. Tauzia, and J.-F. Hétet, "Experimental study of various effects of Exhaust Gas Recirculation (EGR) on combustion and emissions of an automotive direct injection diesel engine," *Energy*, vol. 33, no. 1, pp. 22–34, 2008.

[118] M. Aghbashlo, M. Tabatabaei, E. Khalife, B. Najafi, S. M. Mirsalim, A. Gharehghani, P. Mohammadi, A. Dadak, T. R. Shojaei, and Z. Khounani, "A novel emulsion fuel containing aqueous nano cerium oxide additive in diesel–biodiesel blends to improve diesel engines performance and reduce exhaust emissions: Part ii–exergetic analysis," *Fuel*, vol. 205, pp. 262–271, 2017.

[119] C. rredBorgnakke and R. E. Sonntag, *Fundamentals of thermodynamics*. John Wiley & Sons, 2020 rblack.

[120] M. Capone, E. Guelpa, and V. Verda, "Optimal installation of heat pumps in large district heating networks," *Energies*, vol. 16, no. 3, p. 1448, 2023.

[121] A. W. M. van Schijndel, *Integrated heat air and moisture modeling and simulation*. PhD thesis, 2007.

[122] T. Törnros, B. Resch, M. Rupp, and H. Gündra, "Geospatial analysis of the building heat demand and distribution losses in a district heating network," *ISPRS International Journal of Geo-Information*, vol. 5, no. 12, p. 219, 2016.

[123] "PVWatts calculator.." Available online: `https://pvwatts.nrel.gov/pvwatts.php`.

[124] "Census of population.." Available online: `https://www12.statcan.gc.ca/census-recensement/index-eng.cfm`.

[125] "What is Thermos?." Available online: `https://www.thermos-project.eu/thermos-tool/what-is-thermos/`.

[126] "Geology Soil Geochem Surv Rpt." Available online: `https://www.geologyontario.mines.gov.on.ca/`.

[127] L. Zhang, Z. Wang, X. Yang, L. Jin, Q. Zhang, and W. Hu, "Thermo-economic analysis for directly-buried pipes insulation of district heating piping systems," *Energy Procedia*, vol. 105, pp. 3369–3376, 2017.

[128] N. H. Abu-Hamdeh, A. I. Khdair, and R. C. Reeder, "A comparison of two methods used to evaluate thermal conductivity for some soils," *International Journal of Heat and Mass Transfer*, vol. 44, no. 5, pp. 1073–1078, 2001.

[129] "rredCaterpillar Inc., 3512 diesel generator sets electric power." `https://www.wpowerproducts.com/wp-content/uploads/2020/08/CM20181219-11054-44856.pdf` rblack.

[130] D. Jakubek, P. Ocłoń, M. Nowak-Ocłoń, M. Sułowicz, P. S. Varbanov, and J. J. Klemeš, "Mathematical modelling and model validation of the heat losses in district heating networks," *Energy*, vol. 267, p. 126460, 2023.

[131] "Simscape Electrical." Available online: `https://www.mathworks.com/help/sps/`.

[132] M. Farrokhabadi, C. A. Cañizares, and K. Bhattacharya, "Frequency control in isolated/islanded microgrids through voltage regulation," *IEEE Transactions on Smart Grid*, vol. 8, no. 3, pp. 1185–1194, 2015.

[133] M. A. De Brito, L. P. Sampaio, G. Luigi, G. A. e Melo, and C. A. Canesin, "Comparative analysis of MPPT techniques for PV applications," in *IEEE International Conference on Clean Electrical Power (ICCEP)*, pp. 99–104, 2011.

[134] M. Arriaga and C. Cañizares, "Overview and analysis of data for microgrid at Kasabonika Lake First Nation (KLFN)," Hatch Project Confidential Report, University of Waterloo, Tech. Rep, 2015.

[135] B. V. Solanki, C. A. Cañizares, and K. Bhattacharya, "Practical energy management systems for isolated microgrids," *IEEE Transactions on Smart Grid*, vol. 10, no. 5, pp. 4762–4775, 2018.

[136] P. S. Sauter, B. V. Solanki, C. A. Canizares, K. Bhattacharya, and S. Hohmann, "Electric thermal storage system impact on northern communities' microgrids," *IEEE Transactions on Smart Grid*, vol. 10, no. 1, pp. 852–863, 2017.

[137] W. Devia, K. Agbossou, and A. Cardenas, "An evolutionary approach to modeling and control of space heating and thermal storage systems," *Energy and Buildings*, vol. 234, p. 110674, 2021.

[138] B. Y. Bedouani, A. Moreau, M. Parent, and B. Labrecque, "Central electric thermal storage (ETS) feasibility for residential applications: Part 1. numerical and experimental study," *International Journal of Energy Research*, vol. 25, no. 1, pp. 53–72, 2001.

[139] W. Mendieta and C. A. Cañizares, "Primary frequency control in isolated microgrids using thermostatically controllable loads," *IEEE Transactions on Smart Grid*, vol. 12, no. 1, pp. 93–105, 2020.

[140] D. Curtis and B. Singh, "Northern Microgrid Project–A Concept," in *World Energy Congress,* Montreal, Canada, 2010.

[141] M. Abuelhamd and C. A. Cañizares, "Dynamic model of integrated electricity and district heating for remote communities," *Applied Energy*, vol. 376, p. 124337, 2024.

[142] K. Kunitomi, A. Kurita, Y. Tada, S. Ihara, W. W. Price, L. M. Richardson, and G. Smith, "Modeling combined-cycle power plant for simulation of frequency excursions," *IEEE Transactions on Power Systems*, vol. 18, no. 2, pp. 724–729, 2003.

[143] J. March-Leuba, *Dynamic behavior of boiling water reactors: a dissertation*. PhD thesis, 1984.

[144] P. Coddington and R. Macian, "A study of the performance of void fraction correlations used in the context of drift-flux two-phase flow models," *Nuclear Engineering and Design*, vol. 215, no. 3, pp. 199–216, 2002.

[145] C. Cai, I. Mudawar, H. Liu, and X. Xi, "Assessment of void fraction models and correlations for subcooled boiling in vertical upflow in a circular tube," *International Journal of Heat and Mass Transfer*, vol. 171, p. 121060, 2021.

[146] M. R. A. Ali, *Lumped Parameter, State Variable Dynamic Models for U-Tube Recirculation Type Nuclear Steam Generators*. Doctoral dissertation, The University of Tennessee, 1976.

[147] W. J. Garland and B. Hand, "Simple functions for the fast approximation of light water thermodynamic properties," *Nuclear Engineering and Design*, vol. 113, no. 1, pp. 21–34, 1989.

[148] A. Chaibakhsh and A. Ghaffari, "Steam turbine model," *Simulation Modelling Practice and Theory*, vol. 16, no. 9, pp. 1145–1162, 2008.

[149] Q. K. Nguyen, K. H. Jung, G. N. Lee, S. B. Suh, and P. To, "Experimental study on pressure distribution and flow coefficient of globe valve," *Processes*, vol. 8, no. 7, p. 875, 2020.

[150] Powertech Labs Inc., "DSATools™ Power System Analysis Software," 2024. https://www.powertechlabs.com/dsatools.

[151] "Safety Evaluation by the Office of Nuclear Reactor Regulation." https://www.nrc.gov/docs/ML2017/ML20176A449.pdf.

[152] J. H. Chow and J. J. Sanchez-Gasca, *Power system modeling, computation, and control*. John Wiley & Sons, 2020.

[153] "Grid connection requirements." Available online: https://www.ieso.ca/-/media/files/ieso/document-library/engage/esag/esag-20200826-Chapter4-Grid-Connection-Requirements-Appendices. Accessed on: Jul. 2025.

[154] M. Abuelhamd, C. A. Cañizares, D. Sohm, E. Ahmed, and I. El-Samahy, "Dynamic modeling and practical application of boiling water small modular reactor power plants," *IEEE Transactions on Energy Conversion*, pp. 1–10, submitted May 2025.

[155] I. Calero, C. A. Canizares, K. Bhattacharya, and R. Baldick, "Duck-curve mitigation in power grids with high penetration of pv generation," *IEEE transactions on Smart Grid*, vol. 13, no. 1, pp. 314–329, 2021.

[156] J. Danielewicz, B. Śniechowska, M. Sayegh, N. Fidorów, and H. Jouhara, "Three-dimensional numerical model of heat losses from district heating network pre-insulated pipes buried in the ground," *Energy*, vol. 108, pp. 172–184, 2016.

[157] M. Abuelhamd, C. A. Cañizares, D. Sohm, E. Ahmed, and I. El-Samahy, "Modeling and control of a boiling water small modular reactor cogeneration system for district heating applications," *IEEE Transactions on Smart Grid*, pp. 1–10, submitted March 2025.